Università degli studi di Padova

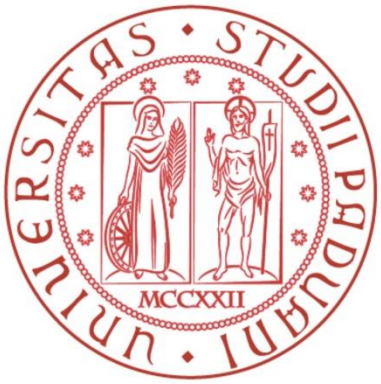

Dipartimento di Biologia

Corso di Laurea Magistrale in Scienze della Natura

Qual è il ruolo dell'anatomia dello xilema nei processi di embolizzazione e ripristino della conducibilità idraulica degli elementi vascolari?

Any role of xylem anatomy in hydraulic vulnerability and recovery?

Relatore: Prof. Nicoletta La Rocca - Dip. di Biologia

Correlatore: Dott. Giai Petit - Dip. di Territorio e Sistemi Agro-Forestali (TeSAF), Università degli Studi di Padova

Correlatore: Prof. Andrea Nardini – Dip. di Scienze della Vita, Università degli Studi di Trieste

Laureando: Luca Da Sois

Anno Accademico 2017/2018

Table of contents

Summary

Introduction

Climate changes

"Climate changes" refer to a global alteration of climate patterns such as the rising of the overall mean surface temperature (Hansen et al. 2010) and the variation of precipitation regimes (Salzmann et al. 2014). These changes are impacting forest ecosystems (Allen et al. 2010; Bonan 2008; Ernakovich et al. 2014) reshaping forest cover worldwide (Hansen et al. 2013). Higher temperatures lead to a faster soil drying up, limiting forest productivity (Boisvenue and Running 2006) and increasing forest dieback rates worldwide (Allen et al. 2010; Birdsey and Pan 2011). It is therefore of primary importance to understand trees and forests potential acclimatization to the changing climate and predict the impacts that will be generated by future environmental conditions to forest ecosystems (Hansen et al. 2013; O'Brien et al. 2017).

Tree structure and function

Trees have three main organs: roots, leaves and trunk, where xylem is present and is involved in sap transport. There are two types of cells specialised in transporting high water amounts at high efficiency called tracheary elements: tracheids and vessel elements (Crivellaro and Schweingruber 2015). Both cell types are dead at maturity and form hollow tubes through water can flow at relatively little resistance (Taiz and Zeiger 2006). Fibres confer hardness and flexibility to the wood. Parenchyma cells are alive at maturity and play key functions in different metabolically active processes (Hilaire et al. 2001; Yadeta and Thomma 2013; Secchi et al. 2017; Venturas et al. 2017) and can be in direct contact with vessels thus exchanging water and solutes with them (Hacke 2015). Water inside vascular elements is present in a metastable state and moves due to a potential gradient. During drought conditions, water tension inside the xylem increases, rising the risk of embolism formation and therefore vessel cavitation reducing xylem water transport. Xylem resistance to cavitation is expressed by the P_{50}, that is the water potential at which xylem loses 50% of its conductivity and is frequently accompanied by the Hydraulic Safety Margin (HSM) (Nardini et al. 2013) that corresponds to the difference between the regulation of daily minimum stem water potential (ψ_{min}) under non-extreme conditions and the P_{50} (Meinzer et al. 2009). While gymnosperms tend to have a generally wide HSM, angiosperms tend to have a very narrow or even negative HSM (Choat et al. 2012) being exposed to embolism formation and potentially facing long-term reductions in productivity. According to the "refilling theory", plants are able to restore the hydraulic conductance by mobilizing the sugars (non-structural

carbohydrates) carried by the phloem and stored in parenchyma cells (Nardini et al. 2011).

Working hypothesis

The aim of this work is to investigate if there are some anatomical features linked to the tolerance of plants to cavitation. Hypothetically, vulnerable species should rely on efficient refilling mechanisms to recover from embolism formation and therefore have high parenchyma amount. This would allow them to store and utilise non-structural carbohydrates more effectively throughout the xylem.

Materials and methods

A database was built up composed of anatomical (axial parenchyma (PA_A), radial parenchyma (PA_R), total parenchyma amount (PA_{AR}), xylem area (X_a), fibres area (F_a), volume of wood occupied by vessels (V_a), mean conduit area (MC_a), conduit density (C_d), theoretical hydraulic conductivity (K_S)), hydraulic (P_{50}), and qualitative traits (angiosperms vs. gymnosperms (A vs. G), evergreenness vs. deciduousness (E vs. D), climbers vs. self-supporting (C vs. S)).

Dataset construction

Three main groups were developed in my dataset: a first group (group 1) with data coming from literature (N=107) (Choat et al. 2012; Morris et al. 2016), a second group (group 2) combining hydraulic data coming from literature with anatomical measurements made on my own (N=74) and a third group (group 3) made of hydraulic and anatomical measurements made on my own (N=14).

Anatomical analyses

Branch segments were collected and microsections were obtained using a rotary microtome LEICA RM 2245 (Leica Biosystems, Nussloch, Germany), decoloured with a solution of water and bleach (1% in distilled water), stained with a solution of Safranin and AstraBlue (1% and 0.5% in distilled water respectively), permanently fixed on microscope slides with Eukitt (BiOptica, Milano, Italy) and covered by a glass cover. Images from the micro-sections were acquired using a D-sight slide scanner (Menarini, Florence, Italy). The estimate of parenchyma fraction was performed by analysing images with Fiji Is Just ImageJ version 2.0.0 (Schneider et al. 2012) doing manual editing. Cross-sectional images were also analysed with ROXAS 3.0.139 ® (von Arx and Carrer 2014) for the estimate of the other anatomical traits.

Hydraulic analyses

Branches were excised at predawn and the maximum vessel length (VL_{max}) was estimated with the air injection method (Jacobsen et al. 2012). For assessing vulnerability curves branch segments at least longer than VL_{max} were chosen (Ennajeh et al. 2011a) and connected to a hydraulic apparatus (Xyl'em, Bronkhorst, France), perfused with a filtered poly-ionic solution enriched with $10\ mmol L^{-1}\ KCl$ (Savi et al. 2017), flushed, mounted on a double-ended pressure sleeve (PMS Instruments, OR, USA) and the percentage loss of conductivity (PLC), at different applied pressures P_x, was assessed. P_{50} was estimated by drawing vulnerability curves fitting PLC on P_x data using RStudio version 1.1.423 and the packages Rcmdr version 2.2-4 and fitplc version 1.1-7 (Duursma and Choat 2017).

Statistical analyses

The relationships between P_{50} and PA_{AR} (group 1, 2, 3), P_{50} and F_a, P_{50} and MC_a, C_d and MC_a (group 2, 3) were assessed with log_{10}-transformed data to comply with assumptions of normality and homoscedasticity (Zar 1999; Zuur 2010). The relationships between P_{50} and C_d, P_{50} and V_a, F_a and PA_{AR} (group 2, 3) were fitted using linear regressions. The comparability of the slopes of the regressions found for the same relationships between variables in different dataset groups was verified with One-way ANOVA tests. These analyses were performed using RStudio version 1.1.423.

Results

$PA_{AR} \sim P_{50}$

I found: (i) a positive trend between PA_{AR} and P_{50} in angiosperms ($R^2 = 0.17$, $F = 29.39$, $DF = 139$, $p < 0.001$) with species having a higher P_{50} (i.e., less negative) producing a bigger amount of parenchyma cells in the xylem; (ii) no clear trend between PA_{AR} and P_{50} in gymnosperms ($R^2 = 0.030$, $F = 2.606$, $DF = 51$, $p > 0.05$).

$PA_{AR} \sim P_{50}$, $F_a \sim P_{50}$, $V_a \sim P_{50}$

I found in angiosperms: (i) a negative trend between F_a and P_{50} ($R^2 = 0.24$, $F = 23.4$, $DF = 71$, $p < 0.001$) with species having a higher P_{50} producing a lower amount of fibres in the xylem; (ii) no clear trend between V_a and P_{50} ($R^2 = 0.015$, $F = 2{,}101$, $DF = 71$, $p > 0.05$).

$F_a \sim PA_{AR}$

F_a and PA_{AR} are inversely related in angiosperms ($R^2 = 0.73$, $F = 193.3$, $DF = 71$, $p < 0.001$).

C_d ~ MC_a

C_d and MC_a are inversely related in angiosperms (R^2 = 0.79, F = 261.5, DF = 69, p < 0.001).

C_d ~ P_{50}, MC_a ~ P_{50}

I found in angiosperms: (i) a negative trend between C_d and P_{50} (R^2 = 0.29, F = 30.2, DF = 70, p < 0.001) with species having a higher P_{50} producing a lower number of vessels per unit area; (ii) a positive trend between MC_a and P_{50} (R^2 = 0.25, F = 30.2, DF = 70, p < 0.001) with species having a higher P_{50} (i.e., less negative) producing bigger vessels.

Discussion

More vulnerable angiosperm species would rely on a more efficient xylem refilling mechanism by producing a higher parenchyma amount in the wood. The greater xylem parenchyma volume would allow to both exchange NSC more efficiently (Plavcová and Jansen 2015) and storage a greater NSC amount (Plavcová et al. 2016). Parenchyma tissues do not seem to have an important role in xylem embolism reversal in gymnosperms. It was shown that gymnosperms present a great parenchyma amount at leaf level therefore allowing them to repair xylem embolism in the distal portions (Johnson et al. 2012), where tension is highest (Petit et al. 2018), thus preventing xylem embolism formation. Angiosperm species presenting a lower vulnerability to embolism have a higher amount of fibres. This result may explain why, in many studies (Lens et al. 2013; Rosner 2017) species that are less vulnerable to cavitation were found to have a higher wood density (i.e., that is mainly due to the high amount of fibres) even if is not directly linked to plant hydraulic functioning (Lachenbruch and McCulloh 2014). Species with narrower and denser vessels were found to have a lower vulnerability to embolism, in line with many other studies (Martinez-Cabrera et al. 2009; Christman et al. 2012).

Conclusions

The hydraulic vulnerability to embolism (P_{50}) is strongly related with xylem anatomical structures and with conduits properties in particular. Wider and therefore less dense vessels determine a higher vulnerability of xylem to embolism (i.e., P_{50} less negative). Angiosperms therefore tend to produce a greater amount of living cells that would allow to both storage a greater amount of non-structural carbohydrates and utilize them more efficiently throughout the xylem, relying on more efficient refilling mechanism as to compensate for the low safety of the water transport system.

1 Introduction

1.1 Climate changes

For "climate changes" we refer to a global alteration of climate patterns. This modification is evident from the mid-20th century onwards. In fact, there is scientific evidence that since the end of '800, the global mean annual surface temperature (GMST) (Figure 1.1) has increased of $0.8°C$ (Hansen et al. 2010). It may appear to be a non-significant variation compared to the global variation of $-5.4°C$ during the last Glacial Maximum (Stute et al. 1995) 20.000 years ago. Notwithstanding, the effects of this global temperature increase are clearly visible worldwide. There are ongoing gradual changes such as the oceans level rise due to the melting of the polar ice caps, but also abrupt changes as great heat waves and devastating storms. Of great concern is also the observation of the reduction of the Atlantic meridional overturning circulation (Bryden et al. 2005; Cunningham et al. 2007; Bryden et al. 2014) that carries warm waters from the Gulf of Mexico (therefore known also as Gulf Stream) to the North and Norwegian Seas, mitigating the climate of ocean facing regions in Northern Europe. Its reduction may dramatically change heat fluxes in the Atlantic Ocean and lead to a climate cooling in Northern Europe.

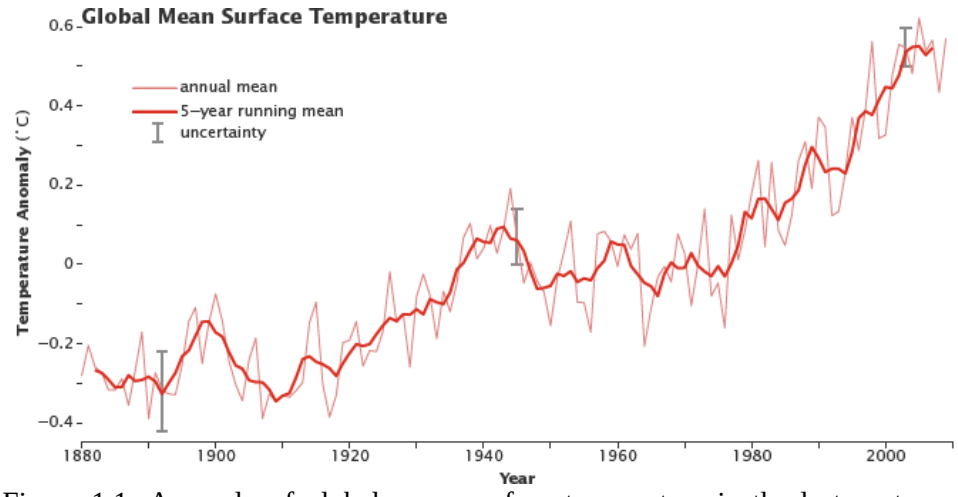

Figure 1.1: Anomaly of global mean surface temperature in the last century. It has increased of $0.8°C$ since 1880 (from https://earthobservatory.nasa.gov/).

These changes are due to the rapid human population and economic growth leading to a constant increase of greenhouse gasses (GHG) emission (IPCC 2014) in the atmosphere (Figure 1.2). These molecules are able to absorb infrared radiation. By increasing their concentration in the atmosphere, the natural greenhouse effect grows in intensity causing a rise in the GMST.

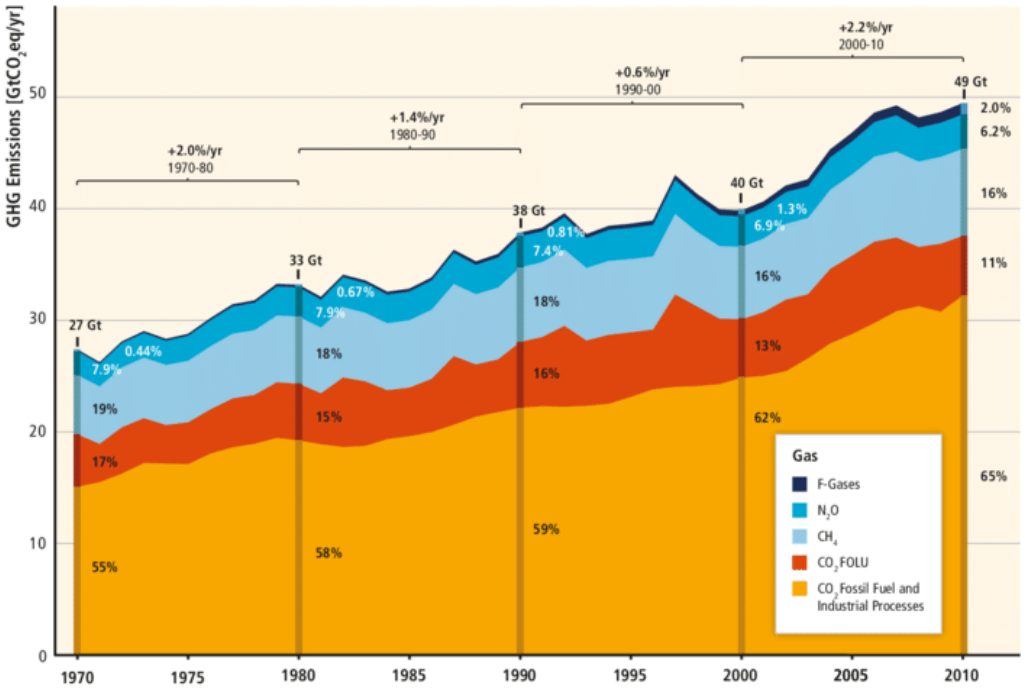

Figure 1.2: Total annual anthropogenic GHG emissions by groups of gases in the period 1970-2010 (from IPCC 2014).

The Intergovernmental Panel on Climate Change (IPCC) proposed four atmospheric greenhouse concentration growth trajectories, used for climate modelling research, to predict future temperature rise expressed using Representative Concentration Pathways (RPCs) (IPCC 2014). According to these models, global temperature will increase between $0.3°C$ (RCP 2.6) to $4.8°C$ (RCP 8.5) by 2100. As a result, we will assist worldwide to both a change of mean and variance of surface temperatures and to a modification of precipitations intensity and distributions (called precipitation regimes) (Figure 1.3) (Salzmann et al. 2014) causing huge impacts on ecosystems, biodiversity and life on Earth as a whole.

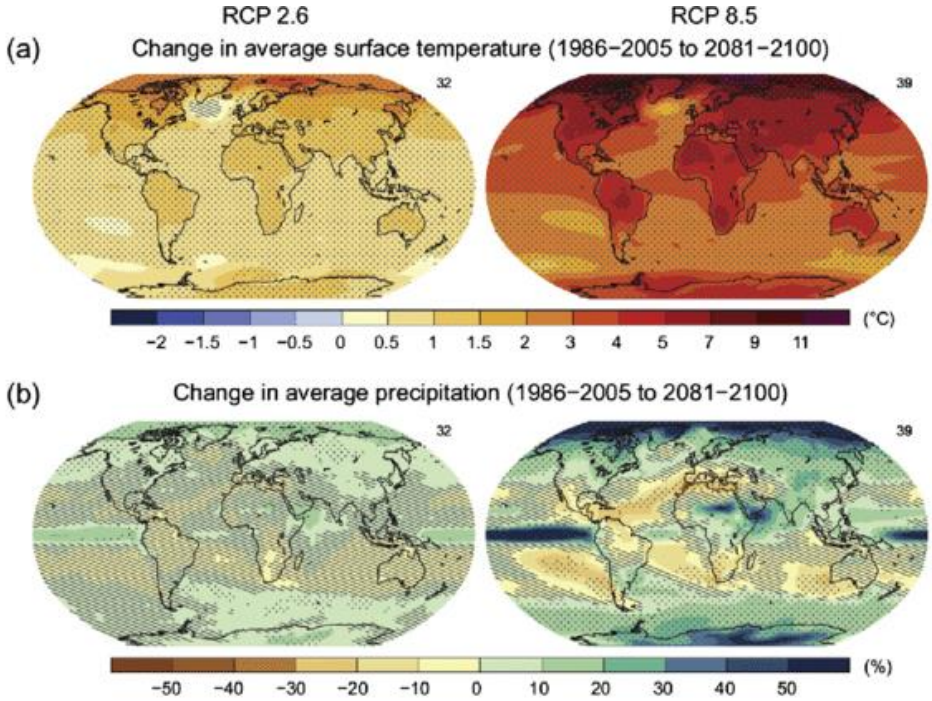

Figure 1.3: Changes in average surface temperature and precipitation expected by the end of the century according to RCP 2.6 and RCP 8.5 (from Salzmann et al. 2014).

1.1.1 Tree mortality

Due to climate changes, we are assisting to an increase in frequency and severity of heat and drought events. These occurrences are highly impacting forest ecosystems both in warm and dry environments (i.e., Mediterranean regions) and in wetter ones (i.e., Tropical forest) (Bonan 2008; Allen et al. 2010; Ernakovich et al. 2014) therefore reshaping forest cover worldwide (Menzel and Fabian 1999; Peng et al. 2011; Hansen et al. 2013; Reichstein et al. 2013). Trees are put under physiological stress, exacerbated by other climate-mediated processes such as insects-outbreaks and wildfires (Allen et al. 2010). In these conditions, the water shortage becomes a limiting factor reducing forest productivity and therefore tree growth (Boisvenue and Running 2006). Higher temperatures lead to a faster soil drying up. The water available to roots between the soil particles called "capillary water" (Figure 1.4) therefore decreases, and water and nutrient uptake from roots becomes more difficult. However, trees need to keep high evapo-transpiration regimes at the leaf level and therefore experience the so called "hydraulic stress" (HS) increasing their mortality risk (Figure 1.5). As a result, we are assisting to a speed up of forest dieback rates worldwide (Figure 1.6) (Allen et al. 2010;

Birdsey and Pan 2011) but the understanding on ultimate mechanism leading to tree mortality under drought is still lacking (Mitchell et al. 2013).

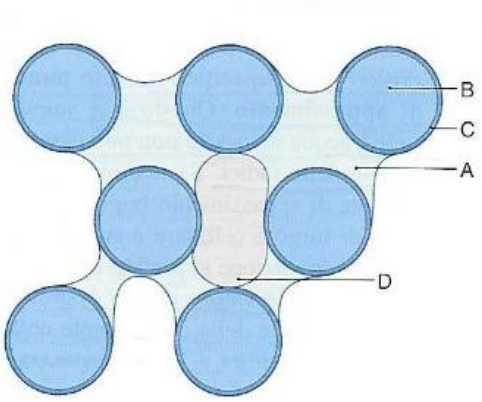

Figure 1.4: Sketch showing water hold due to capillarity (A) from the soil particles (B) and hygroscopic water (C). Interstitial air of the soil (D) is also shown. (from Rascio et al. 2012).

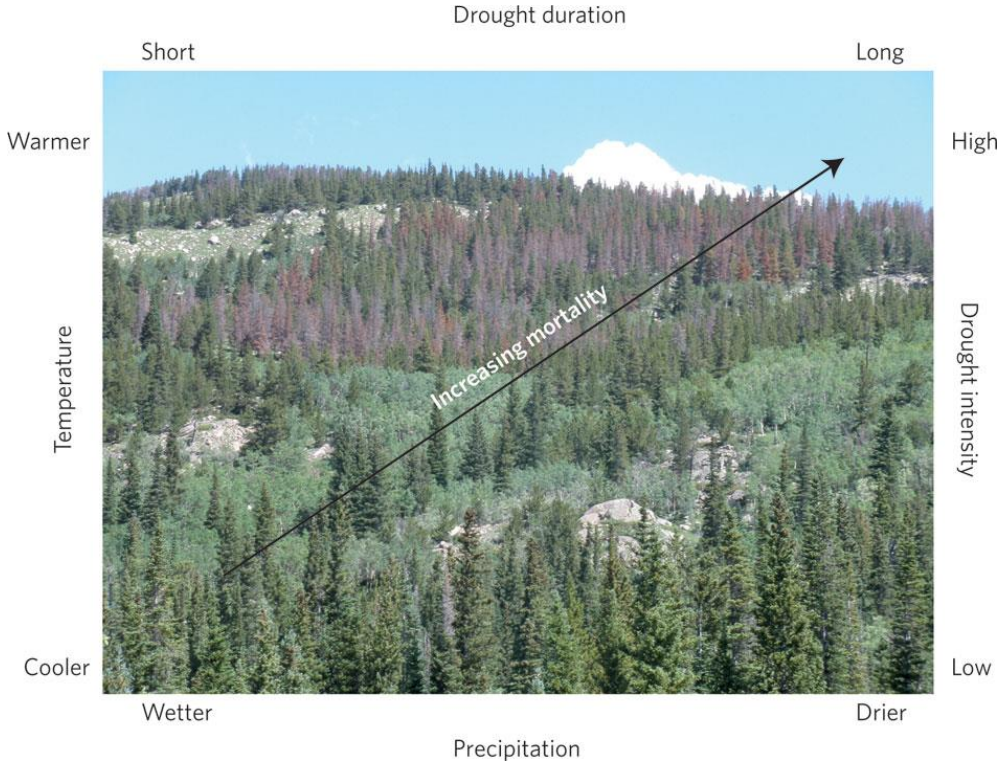

Figure 1.5: Conceptual schematic showing how tree mortality might vary with temperature, drought duration and intensity, and precipitation (from Birdsey and Pan 2011).

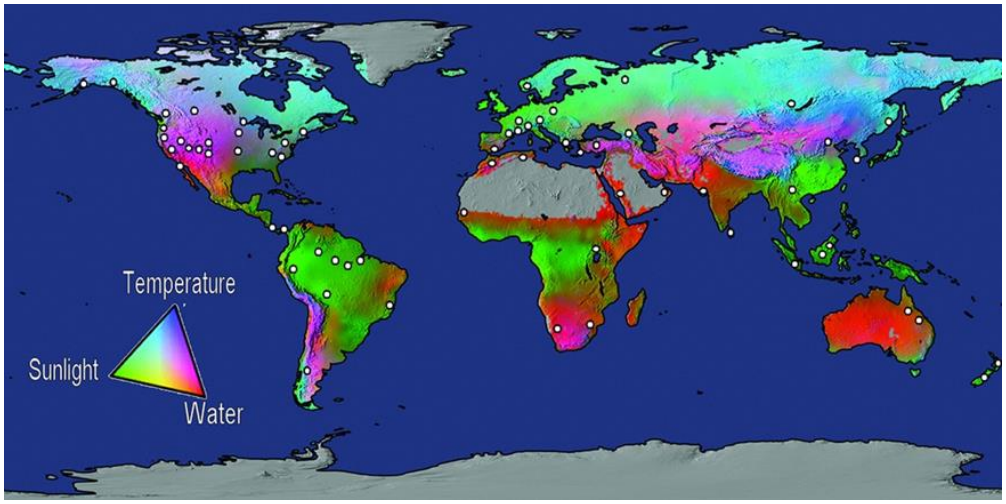

Figure 1.6: White dots indicate documented localities with forest mortality related to climatic stress from drought and high temperatures. Background map shows potential environmental limits to vegetation net primary production (Boisvenue and Running 2006). Drought and heat-driven forest mortality often is documented in relatively dry regions (red/orange/ pink), but also occurs outside these regions (from Allen et al. 2010).

The larger trees, covering a key role as biomass storage in forests (Slik et al. 2013) present greater sensitivity to drought than small trees potentially exacerbating feedbacks to climate change (Bennett et al. 2015; Prendin et al. 2018a).

Forests are of primary importance as carbon sink (Birdsey and Pan 2011), biodiversity hotspots, play other important functions (i.e., forest dynamics, hydrology, surface energy fluxes) (Bonan 2008) and are of great economic value (Hanewinkel et al. 2013). It is therefore of primary importance to understand trees and forests potential acclimatization strategies to the changing climate (Jump and Penuelas 2005; Awad et al. 2012; De Micco and Aronne 2012) and predict the impacts that will be generated by future environmental conditions to forest ecosystems (Anderegg et al. 2013; O'Brien et al. 2017).

1.2 Tree structure and function

Trees have three main organs: roots, trunk and leaves (Figure 1.7) (Rece et al. 2014). Roots are situated in the soil and are therefore involved in the underground processes such as the absorption of water and nutrients from the soil. At the same

time, roots anchor the tree structure, work as nutrient storage and interact with other organisms living in the soil like bacteria (*Rizobium* sp.), fungi (mycorrhizae) and many others. The remaining two organs are present aboveground. The trunk is composed of two main elements: the xylem and the phloem. The xylem is involved in transporting sap from the roots to the leaves and confers mechanical support to the tree structure. The phloem is involved in the transport of water and nutrients both upwards and downwards. Its main function consists in carrying the nutrients from the storage/production site (e.g. roots/leaves) to the place where these elements will be utilised (i.e., metabolically active living cells). On top of the tree, we find leaves carrying out most of the tree's photosynthetic processes. Photosynthesis converts the carbon dioxide and water into sugars and oxygen as is shown below:

$$6CO_2 + 6H_2O \xrightarrow{Sunlight} C_6H_{12}O_6 + 6O_2 \qquad \text{Eq. 1.1}$$

In the leaves takes also place the evapotranspiration (Lack and Evans 2001): water carried by the xylem goes back to the atmosphere via stomatal apertures (Figure 1.8) present in the lower leaf margins.

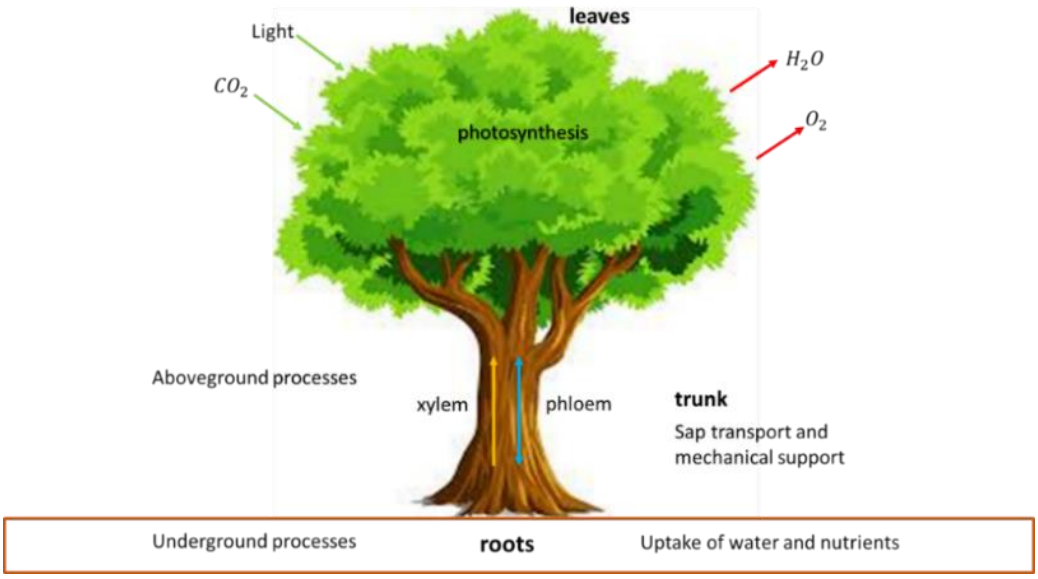

Figure 1.7: Concise scheme showing tree's organs and relative functions.

Figure 1.8: SEM image showing an open stoma (A) and closed one (B) of *Lavandula dentata* L. (2000x) (modified from https://fineartamerica.com/featured/stomata-of-lavendula-dentata-sem-power-and-syred.html).

In order to grow a plant needs to maintain a positive carbon balance, meaning that the fixed carbon due to photosynthetic processes must be higher than the carbon consumed due to respiration (Mitchell et al. 2014; Petit et al. 2016). In other words, a given leaf mass must provide the necessary carbon resources to sustain the maintenance of the living tissues in a given xylem mass. In parallel, above- and belowground xylem must ensure coupling water flow and leaf transpiration requirements (Mencuccini 2014; Nardini and Luglio 2014; Petit et al. 2016; Sterck and Zweifel 2016; Kiorapostolou et al. 2018) and therefore optimal leaf functioning (Mencuccini and Comstock 1999; Martínez-Vilalta et al. 2014; Price et al. 2014).

1.2.1 Xylem anatomy

A trunk can be observed in three different planes of section (Figure 1.9): it is possible to make transverse (also called cross-sections), tangential and radial sections.

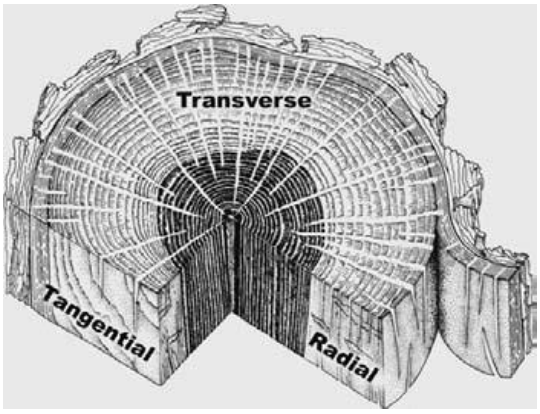

Figure 1.9: Illustration of the three planes of section. Note that for the tangential plane of section, only the right-hand portion of the cut is perpendicular to the rays. Due to the curvature of the rings, the left portion of the cut is out of plane (from Wiedenhoeft 2012).

Having a look at a stained trunk in cross-section (Figure 1.10), we can easily distinguish the xylem, occupying the inner part of the section, from the outer bark that was not considered in this study.

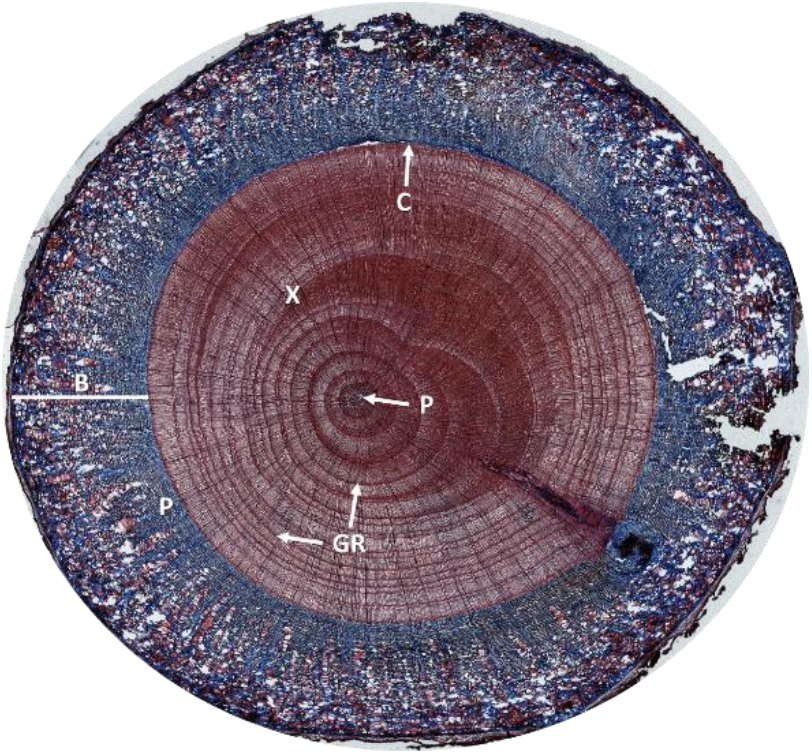

Figure 1.10: Trunk cross-section of *Chamaecyparis lawsoniana* (A.Murray bis) Parl. (100x). The pith (P) is situated in the very centre of the section. All around it, the xylem (X) with the annual growth rings (GR) is present. The bark (B) occupies the outer part of the trunk and, within it, the phloem is shown. Between the xylem and the phloem, we find the cambium (C).

Xylem appears to be made of different rings one inside the other. Each ring represent one-year of growth due to the cambium cells reproduction and differentiation (Speranza and Calzoni 1996; Wiedenhoeft 2012). The visible rings are the effect of the production of wood, within a single year, with different densities: less dense in spring (light red) and denser at the end of the summer (dark red) called early and late-wood respectively(Mauseth et al. 2006; Wiedenhoeft 2012). Under favourable conditions (i.e., good water availability), a tree will produce wider annual rings while dryer years will result in thinner ones (Figure 1.11) (Kozlowski et al. 1991; Arend and Fromm 2007; Friedrichs et al. 2008; Brienen et al. 2010).

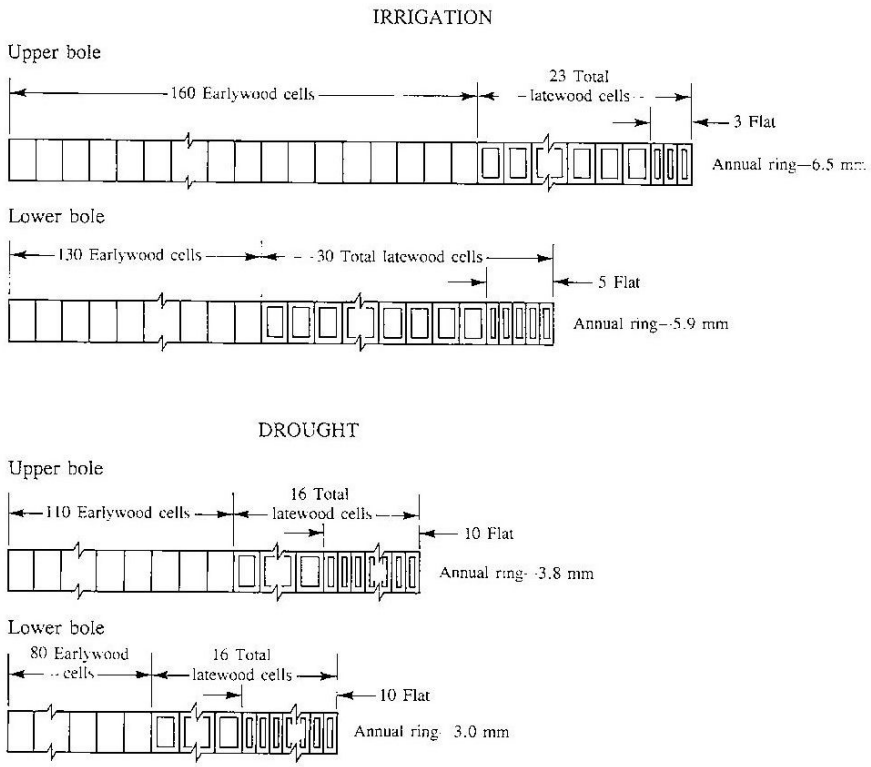

Figure 1.11: Difference in width of tracheids and in proportion of latewood in xylem rings of red pine (*Pinus resinosa* Aiton) grown with irrigation and under water stress. Also note differences between upper and lower bole (from Kozlowski et al. 1991).

There are two different kinds of wood called softwood and hardwood (Figure 1.12). These categories correspond to two different evolutionary groups of spermatophytes (plants producing seeds): the gymnosperms (i.e., conifers, cycads, gnetophytes and *Ginkgo biloba* L.) and the angiosperms (flowering plants)

respectively (Akkemik and Yaman 2012). In the temperate portion of the Northern Hemisphere, softwoods are generally needle-leaved evergreen trees such as pine (*Pinus* sp.) and spruce (*Picea* sp.), whereas hardwood are typically broadleaved, deciduous trees such as maple (*Acer* sp.) and birch (*Betula* sp.) (Wiedenhoeft 2012). Nevertheless, exceptions are present like *Larix decidua* Mill. (softwood, needle-leaved, deciduous) and *Magnolia grandiflora* L. (hardwood, broadleaved, evergreen). Despite what one might conclude based on the names, not all softwoods have soft, lightweight wood, nor do all hardwoods have hard, heavy wood (Wiedenhoeft 2012).

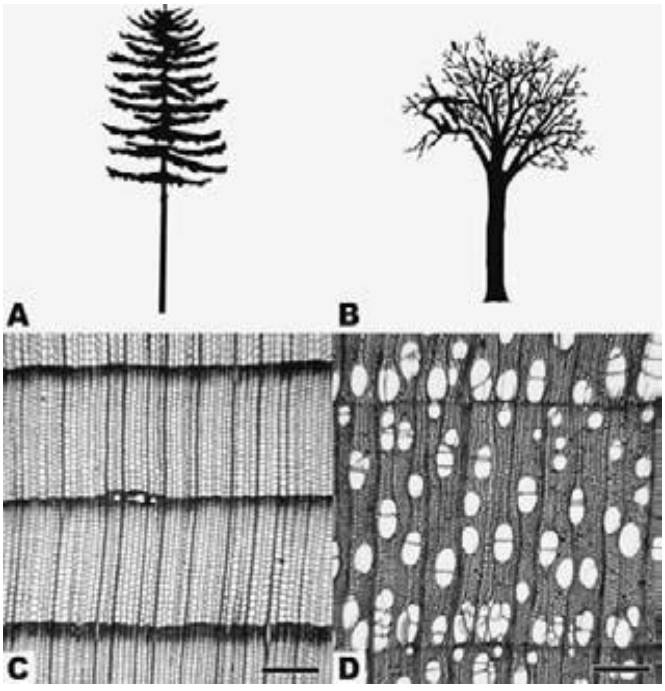

Figure 1.12: Softwood and hardwood. (A) The general form of a generic softwood tree. (B) The general form of a generic hardwood tree. (C) Transverse section of *Pseudotsuga menziesii* (Mirb.) Franco, a typical softwood. The three round white spaces are resin canals. (D) Transverse section of *Betula alleghaniensis* Britton, a typical hardwood. The many large, round white structures are vessels, the characteristic feature of a hardwood. Scale bars = 300 μm (from Wiedenhoeft 2012).

There are two types of cells that are specialised in the transport of high water amounts at high efficiency for long distances called tracheary elements: tracheids and vessel elements (Crivellaro and Schweingruber 2015). Both cell types are dead at maturity and form hollow tubes through water can flow at relatively little resistance (Taiz and Zeiger 2006).

Tracheids are elongated, spindle-shaped cells, arranged in overlapping vertical files (Figure 1.13 A). Water flows due to the numerous lateral wall apertures called “pits”. Pits of one conduit are typically located close to an adjoined tracheid forming pit pairs having a porus layer called pit membrane (Angyalossy et al. 2016) (Figure 1.14 A, D, E). Tracheids are both present in angiosperms and gymnosperms. Anyway, in conifers the pit membranes present a central thickening called “torus” (Figure 1.14 C) that can act as a valve to close the pit (Figure 1.13 C) preventing gas bubbles from spreading into neighbouring tracheids (Delzon et al. 2010) (see chapter 1.2.3). In all other plants, pit membranes are lacking of torus (Venturas et al. 2017) (Figures 1.13 D, 1.14 B) but, by having very small pores, they act again as barriers against gas bubbles movement (Taiz and Zeiger 2006). Tracheids account also for structural support and confer elasticity to the wood.

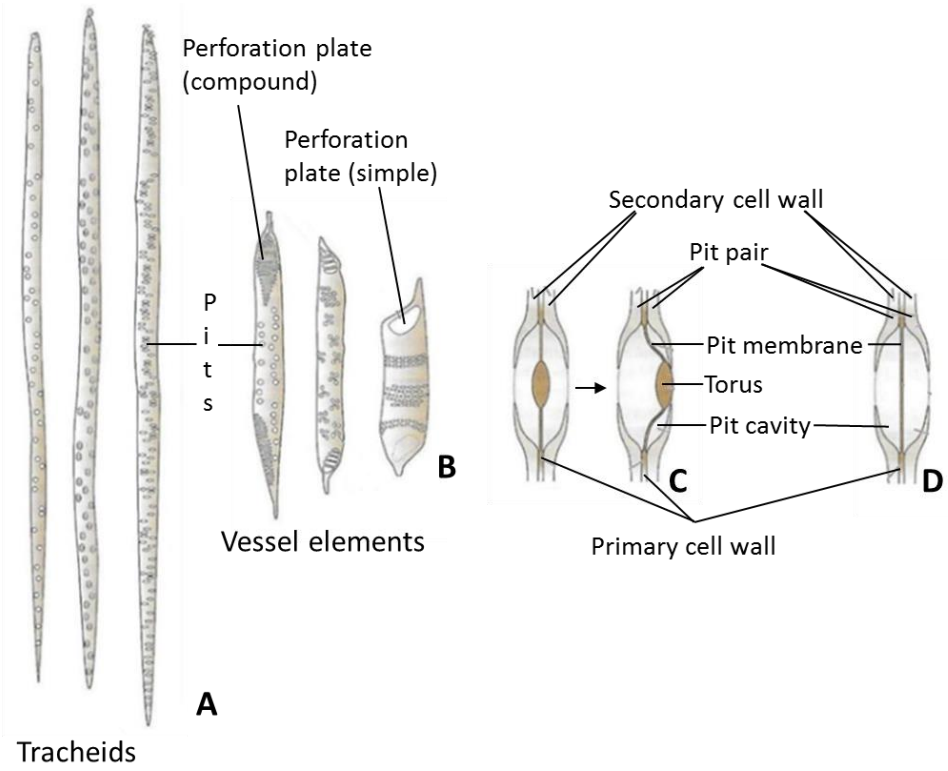

Figure 1.13: Tracheary elements and their interconnections. (A) Tracheids and (B) vessel elements. Both present numerous pits on the lateral walls. (C) Coniferous bordered pit with the torus cantered in the pit cavity (left) and lodged to one side of the cavity (right). (D) Pit membrane of angiosperms and other non coniferous plants (modified from Taiz and Zeiger 2006).

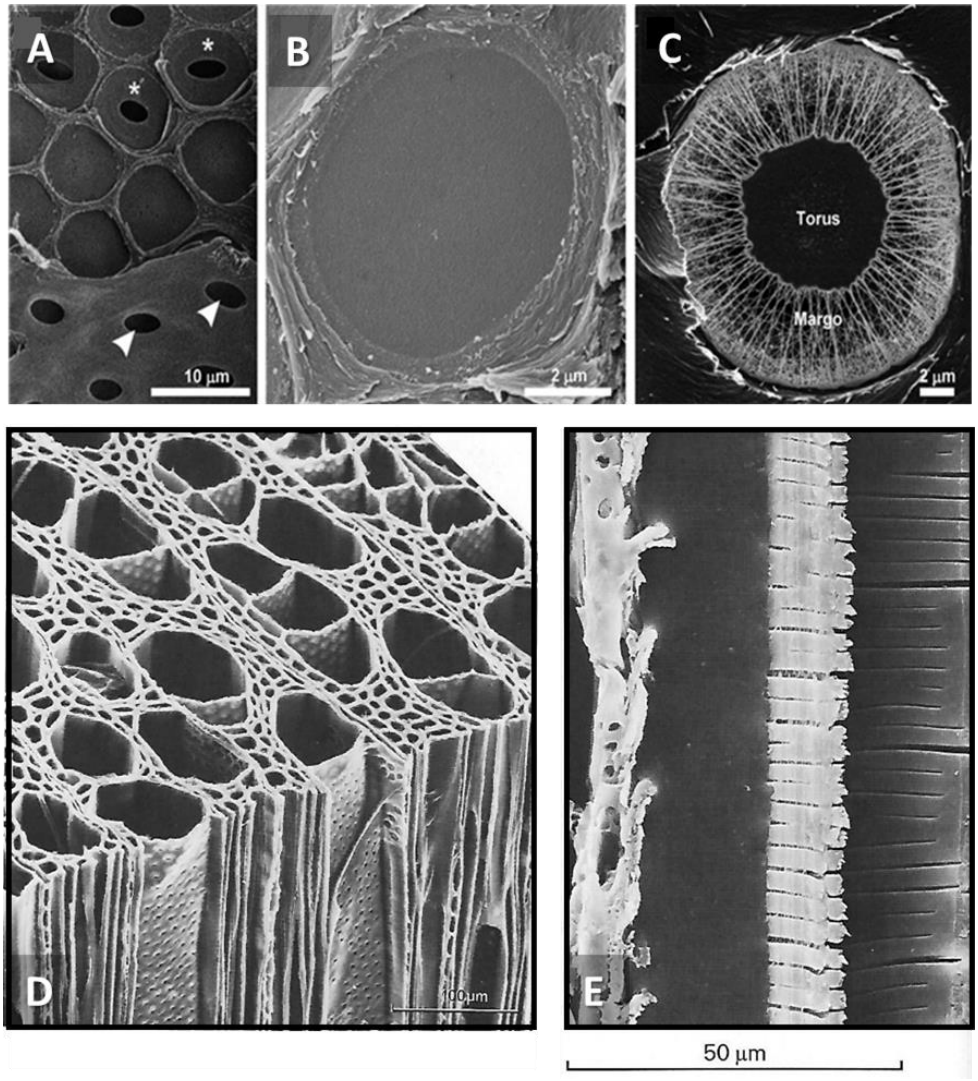

Figure 1.14. Inter-conduit pit field and pit membranes: (A) Inter-vessel pit field in a hybrid poplar stem (*Populus trichocarpa* x *deltoides*). The pits in the upper third of the image have their membranes removed (asterisks); the pits in the center have their membrane but the pit border facing the viewer is removed; the pits on the lower third of the image show the pit apertures from the other side of the vessel wall (arrowheads). (B) Surface view of pit membrane of an angiosperm (*Acer platanoides* L.) with fairly small and homogeneous pores. (C) Pit membrane of a conifer (*Picea glauca* (Moench) Voss) root tracheid showing the typical torus-margo structure (from Venturas et al. 2017). (D) Block of wood of *Populus grandidentata* Michx. showing intervessel pitting on the walls between the two vessels whenever they run parallel. (E) Pores of the vessel-to-vessel pit apertures (from Zimmermann 1983).

Vessel elements tend to be shorter and wider than tracheids and have perforated end-walls forming a "perforation plate" at each end of the cell (Figure 1.13 B, 1.15 A, B). They also have pits on their lateral walls but, differently from tracheids, the perforated end walls allow vessel members to be stacked end-to-end

forming a larger conduit called "vessel". Vessels are therefore multicellular conduits varying in length both within and between species (Zimmermann 1983; Jacobsen et al. 2012). Maximum vessel length (see chapter 2.5.2) can range from few centimetres (i.e., *Carpinus orientalis* Mill.) to one or more meters (i.e., lianas). The vessel members present at the extreme ends of vessels lack perforations in their end walls and communicate with the neighbouring vessels via pit pairs (Figure 1.21). Vessels are only present in angiosperms.

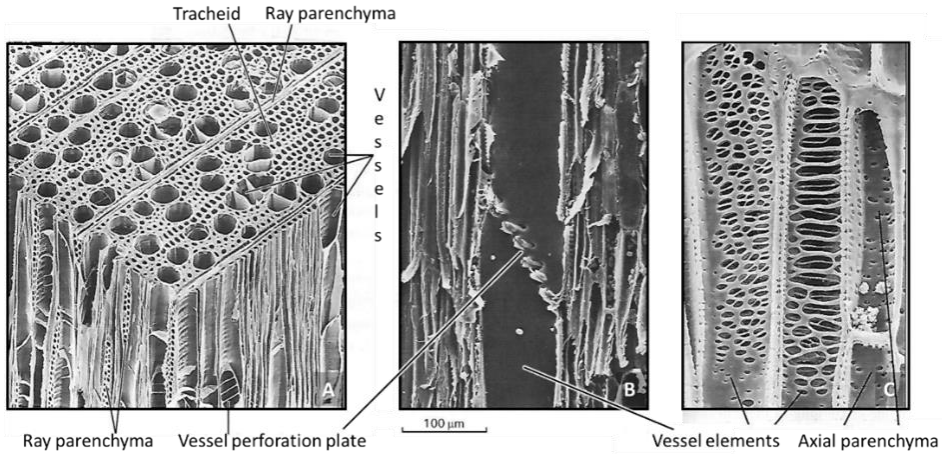

Figure 1.15: SEM images: (A) Wood block of *Liriodendron tulipifera* L. (110x) (modified from Mauseth et al. 2003). (B) Longitudinal micro-sections of *Rhapis excelsa* (Thunb.) Henry showing scalariform perforation plates connecting two vessel members vertically (modified from Zimmermann 1983). (C) Axial parenchyma cells adjacent to the vessels (700x) (modified from Mauseth et al. 2003).

In angiosperms' xylem there is another cell type dead at maturity called "fibre". This cell type is thick walled and present a narrow lumen (Figure 1.16 A). Fibres confer hardness and flexibility to the wood depending on their abundance and cell wall thickness.

The cells that are alive at maturity are called "parenchyma cells" and are present in both angiosperms and gymnosperms. Parenchyma cells can be distinguished into two different groups: "axial" parenchyma cells, oriented along the length of the trunk (parallel to the vessels) (Figure 1.16 B), and "radial" parenchyma cells, radially organised in "rays" (for it is also called "ray parenchyma") (Figure 1.16D) from the pith to the bark (perpendicularly to the vessels). Parenchyma cells play key functions in different metabolically active processes such as starch storage (Secchi et al. 2017; Venturas et al. 2017), temporary water storage

(Mauseth et al. 2006) and defence against pathogens (Hilaire et al. 2001; Yadeta and J. Thomma 2013). Some parenchyma cells (both axial and radial) are in direct contact with vessels (Figure 1.15 C) and can exchange water and solutes (i.e., sugars also called "non-structural carbohydrates") with them (Plavcová and Jansen 2015). Therefore, parenchyma cells create a network for short distance transport of water and solutes within the xylem (i.e., between vessels) and between xylem and phloem (Salleo et al. 2004; Nardini et al. 2011; Brodersen and McElrone 2013). The Pith (Figure 1.10), being also made of parenchyma cells, is part of this network (Plavcová and Jansen 2015). Other functions of parenchyma cells will be further discussed in chapter 1.2.3.

Wood is therefore composed of conduits, parenchyma cells and fibres (only present in angiosperms). A change of the percentage amount of these three tissues may affect the wood density (WD) (Martinez-Cabrera et al. 2011) (i.e., generally denser wood with an increase of fibres amount).

I will now describe the cytological differences of the previously mentioned wood cell types as they appear in stained micro-sections coloured with Safranin and AstraBlue (see chapter 2.4.1) observed with an optical microscope. While Safranin colours the lignified cell walls of red, AstraBlue confers the blue colour to the cellulose. Generally, vessel elements, tracheids and fibres therefore appear red because of the abundance of lignin in their cell's walls while parenchyma cells generally appear blue for the prevalence of cellulose in their wall.

Seen in cross-section, vessel elements present thick walls and big lumina (Figure 1.16 A) compared to the other wood elements. Fibres generally are again thick walled but have a very narrow lumen. (Figure 1.16 A). Tracheids appear similar to fibres in terms of wall thickness but present a wider and clearly visible lumen (Figure 1.16 C). Parenchyma cells are thin-walled and can be distinguished by the other dead xylem elements for having an intact protoplast. Radial parenchyma is organised in uni- bi- or multiseriate rays (composed of a single, two or many lines of cells packed together respectively) radially disposed and elongated along the pith to the bark direction (Figure 1.16 A, C). Axial parenchyma cells appear rather circular (being axially elongated) and can again be organised as single cells or in groups (Figure 1.16 A, C).

Seen in tangential sections, vessel elements are longitudinally elongated (Figure 1.16 B). Fibres also are longitudinally elongated but are shorter, smaller and more compactly organised (Figure 1.16 B) so that their lumina can hardly be seen. Tracheids appear again as elongated cells. They are fusiform, and clearly present a lumen but on average smaller than vessels' (Figure 1.16 D). Radial parenchyma cells generally are circular on a tangential section and can be distinguished for their peculiar organisation in in rays (Figure 1.16 B, D). Axial parenchyma is longitudinally elongated, rectangular shaped (Figure 1.16 B) and frequently disposed adjacent to vessel elements. When axial parenchyma is scanty, it can hardly be seen in tangential sections (Figure 1.16 D).

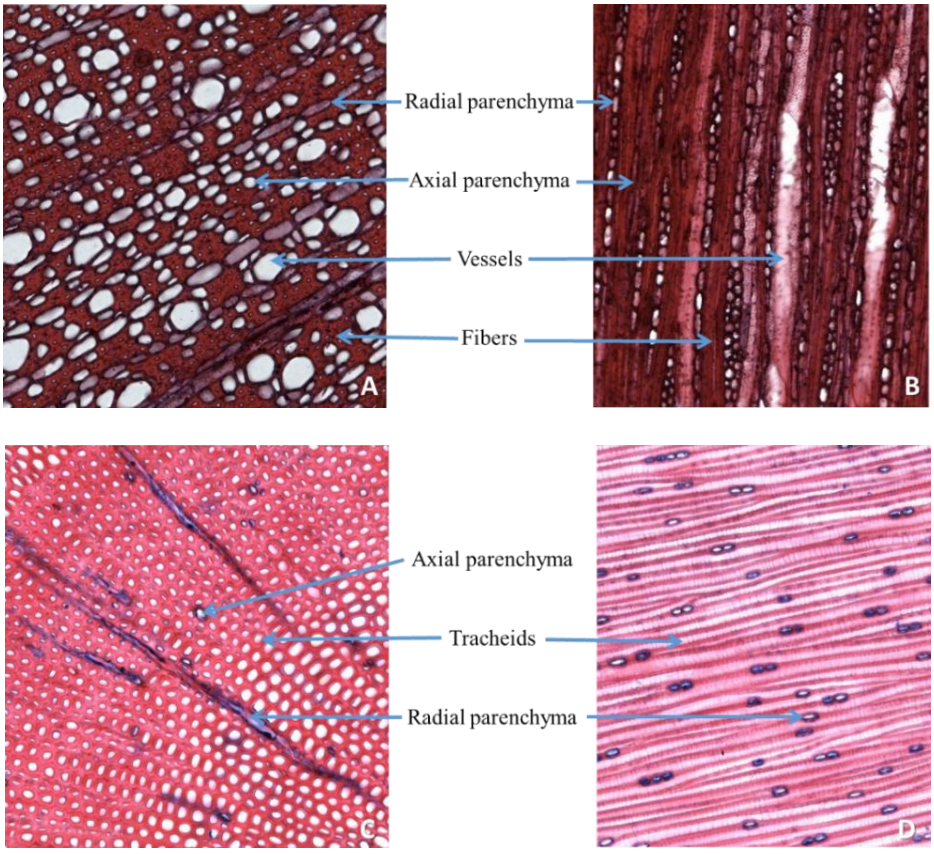

Figure 1.16: Xylem images of: *Myrtus communis* L. (angiosperm) seen in cross section (A, 100x) and tangential section (B, 40x). Parenchyma, vessels and fibres are shown from both points of view; *Taxus baccata* L. (gymnosperm) seen in cross section (C, 100x) and tangential section (D, 40x). Radial parenchyma and tracheids are shown from both points of view. Axial parenchyma is scanty and can only be observed in cross-section (C).

1.2.2 Tree water relations

The concept of water potential

We define as "chemical potential" (μ) a quantitative expression of free energy associated with the molecules of a chemical species. It indicates, from a thermodinamically point of view, the potential for performing work. Hystorically, plant physiologists have most used a related parameter called "water potential" (ψ_{H_2O} or P_{H_2O}) (Slatyer 1958) defined as the chemical potential of water (μ_{H_2O}) divided by its partial molar volume (V_{H_2O}):

$$\psi_{H_2O} = \frac{\mu_{H_2O}}{V_{H_2O}} \qquad \text{Eq. 1.2}$$

The ψ_{H_2O} is the energy needed, per volume unit, to move water in a system reversibly and isothermically from an initial point to a reference point (Rascio et al. 2012). In other words, it is a measure of the free energy of water per unit volume (Taiz and Zeiger 2006). ψ_{H_2O} can be expressed as pressure unit:

$$\psi_{H_2O} = \frac{Jmol^{-1}}{m^3 mol^{-1}} = \frac{Nm}{m^3} = Nm^{-2} = Pa \qquad \text{Eq. 1.3}$$

In general, water molecules move from a higher to a lower ψ_{H_2O}. This chemical property is very useful to describe the processes regulating the water transport in plants and is commonly used to explain the mechanism of sap ascent in the xylem.

The ascent of sap

In plant's xylem water is carried from the roots to the leaves (see chapter 1.2). Since the 18th century, scientists have been investigating how this may happen. For species like *Sequoia sempervirens* (D.Don) Endl., *Sequoiadendron giganteum* (Lindl.) J.Buchholz and *Eucalyptus regnans* F.Muell. (Figure 1.17), that can grow up to around 100 m tall, the ascent of sap from the roots to the leaves would require to win the effect of gravity of $0.01\ MPa\ m^{-1}$ (Koch et al. 2004) (that is 10^3 higher than the pressure present in common car's tyres). Where is this energy coming from? The answer was formulated in "the cohesion tension theory of the sap ascent" (C-T) (Dixon and Joly 1894). According to C-T theory, water movement is not due to an active metabolic process but to a difference of water

potential between the roots and the leaves. Water at the top of a tree develops a negative hydrostatic pressure (i.e., tension) generated by the evaporation of water molecules during leaf transpiration (Figure 1.18) (Koch et al. 2004). This tension is transmitted down the continuous water columns through the xylem conduits thanks to the cohesion properties of water, and transmitted to the roots. Water is therefore pulled through the xylem. Although this theory triggers much debates even nowadays (Canny 1995; Tyree 1997; Steudle 2001; Wheeler and Stroock 2008), C-T remains the more robust explanation of water transport in plants.

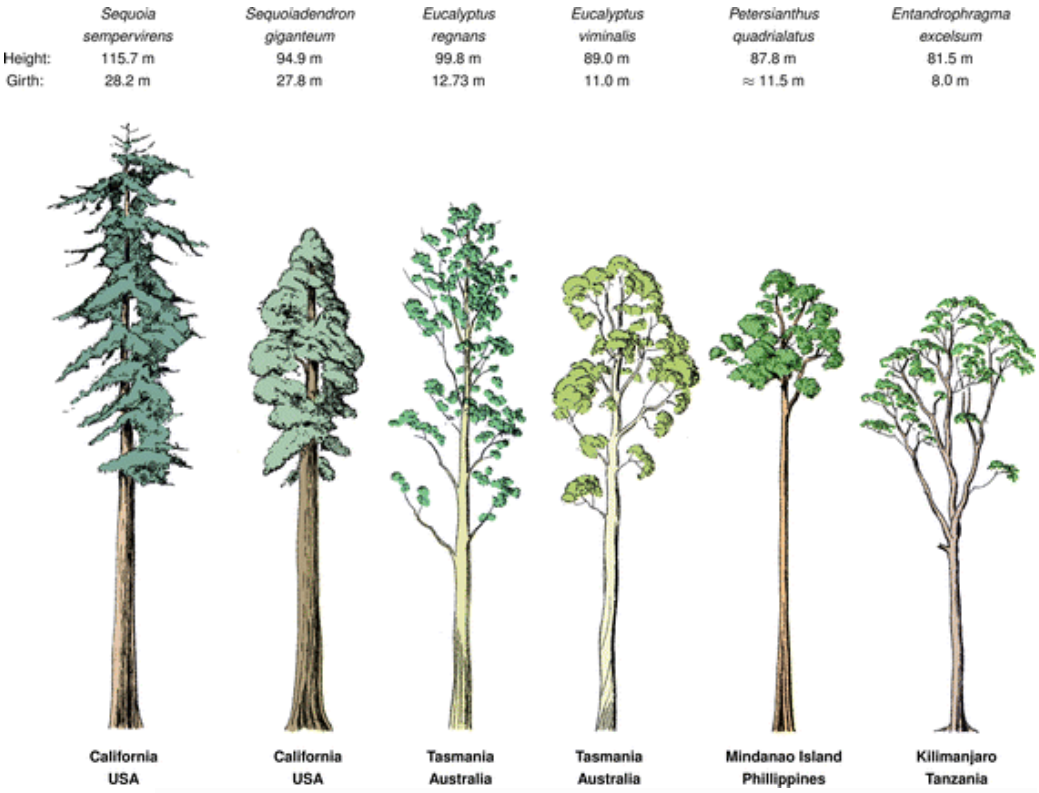

Figure 1.17: The height, girth, and locations of some of the world's tallest tree species (from Hemp et al. 2017).

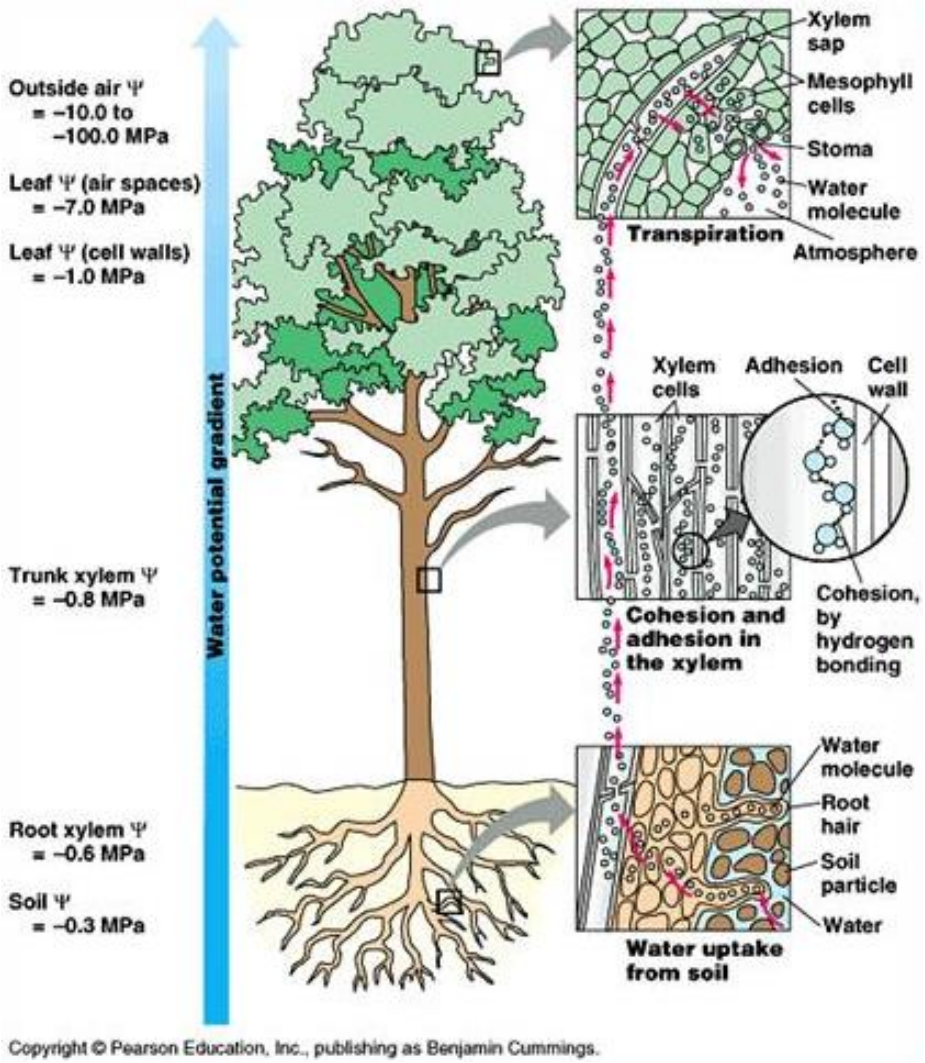

Figure 1.18: Schematic of water movement in the soil-plant-atmosphere continuum. Water moves following the potential gradient from the soil to the atmosphere trough the plant. Water evapo-transpiration at leaf level generates negative water potentials that spread to the roots through the xylem conduits.

Xylem tension is in direct relation to the abundance of hygroscopic water in the soil (Figure 1.19). In fact, when soil is fully hydrated the soil water potential (ψ_{soil}) is higher (i.e., less negative) and water absorption and transport requires less tension to be developed throughout the water columns. When soil dries out, ψ_{soil} becomes more negative meaning that, in order to pull water, the ψ_{H_2O} gradient in the xylem needs to be more negative (Figure 1.20) (Kozlowski et al. 1991). A plant can control the xylem tension by opening and closing the stomata at the leaf level (Figures 1.8, 1.19). When the stomata are open, the water evaporation is higher and therefore the water demands generates greater xylem

tensions. When the stomata are closed, the transpiration rates decreases and the xylem tension is reduced.

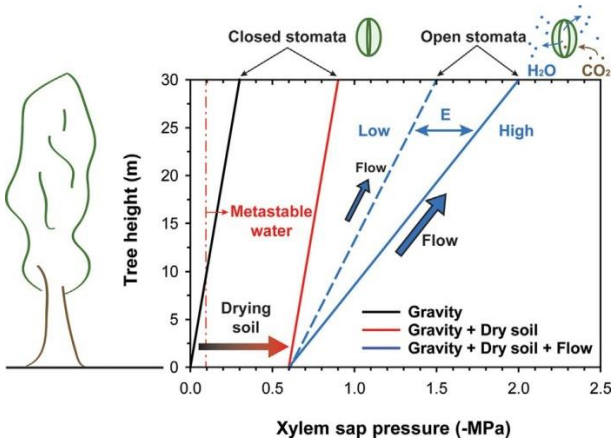

Figure 1.19. Pressure gradients in a tree. When soil is fully hydrated and stomata are closed the pressure gradient of the stationary, hanging water column balances gravitational force (black line). As soil dries the starting point of the pressure gradient is more negative but the slope is unchanged as long as there is no flow (red line). When plants open their stomata the slope of the pressure gradient within the plant increases due to friction (solid blue line) and transpiration (E) is proportional to the plant's hydraulic conductance and its soil to leaf pressure drop. Plants can actively control this frictional pressure drop by adjusting their stomatal aperture to vary E (e.g., the dashed blue line is the pressure drop for Low E whereas the solid blue line for High E). Water is transported in a metastable liquid state because the boiling point is only 0.099 MPa (red dashdot line, assuming 101.3 kPa atmospheric pressure and 20 °C temperature). The metastable liquid realm is reached by the gravity gradient alone at >10 m height for plants in wet soil (from Venturas et al. 2017).

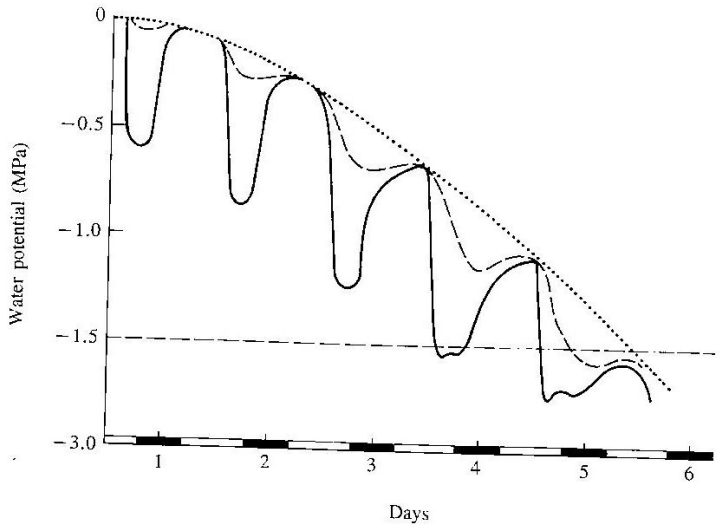

Figure 1.20: Diagram showing probable daily changes in leaf (—) and root (---) water potential of a transpiring plant rooted in dry soil (...). The dark bars indicate darkness (modified from Kozlowski et al. 1991).

1.2.3 Hydraulic stress

Cavitation

The large tensions generated inside the xylem requires plants to face two great physiological challenges.

First, the water under tension transmits an inward force to the walls of the xylem. If the cell walls were weak or pliant, they would collapse under the influence of this tension (Taiz and Zeiger 2006), seemingly to try inhaling air from a straw closed on the other side, so that aspiring tension makes the straw's structure to collapse. Plants overcome this problem by building thick walled vascular elements (see chapter 1.2.1).

A second challenge is that water under tension is in a physically metastable state. When the hydrostatic pressure in liquid water becomes equal to its saturated vapour pressure, the water undergoes a phase change (it boils) (Taiz and Zeiger 2006). This phenomenon can be experimentally observed by placing a glass of water in a vacuum chamber. Surprisingly, water inside the xylem generally lies below the vapour pressure threshold of $0.002\ MPa$ (at $20°C$) that would make water boil. The persistence of liquid water in the xylem despite the presence of a thermodynamically lower energy state (i.e., the vapour state) is due to the cohesion and adhesion of water, making the activation energy for water liquid to vapour phase change very high. Moreover, the structure of the xylem minimize the presence of nucleating sites providing this activation energy (Taiz and Zeiger 2006).

The most important nucleating sites are gas bubbles of sufficient size that the inward force resulting from surface tension is less than the outward force due to the negative pressure of the liquid phase. Bubbles will therefore start expanding until reaching a critical sixe for expansion that will lead it to fill the entire conduit. This phenomenon is called cavitation. Gas filled (embolized) conduits do not allow water to flow anymore through them. Water therefore has to detour through other water-filled vessels (Figure 1.21). During hydraulic stress (see chapter 1.1.1), under water shortage conditions, water tension inside the xylem increases and the air can be pulled through microscopic pores in the xylem cell walls

(Vilagrosa et al. 2012). This phenomenon is called “air seeding” (Taiz and Zeiger 2006). Pit membranes, (see chapter 1.2.1), that are the most permeable regions of xylem wall, normally prevent the spread of gas between conduits but, when exposed to air on one side, they can serve as sites for air entry. This happens when the pressure difference overcomes either the capillary forces of air-water interfaces within the cellulose microfibril matrix of angiosperm’s pits (Figure 1.13 D), or by dislodging the torus in coniferous pit membranes (Figure 1.13 C, 1.22) (Delzon et al. 2010). Moreover, air bubbles can form in conduits due to the freeze-thaw of water inside the conduits (Hacke and Sperry 2001). In fact, air has a lower solubility in ice than in water (figure 1.23) (Davis et al. 1999).

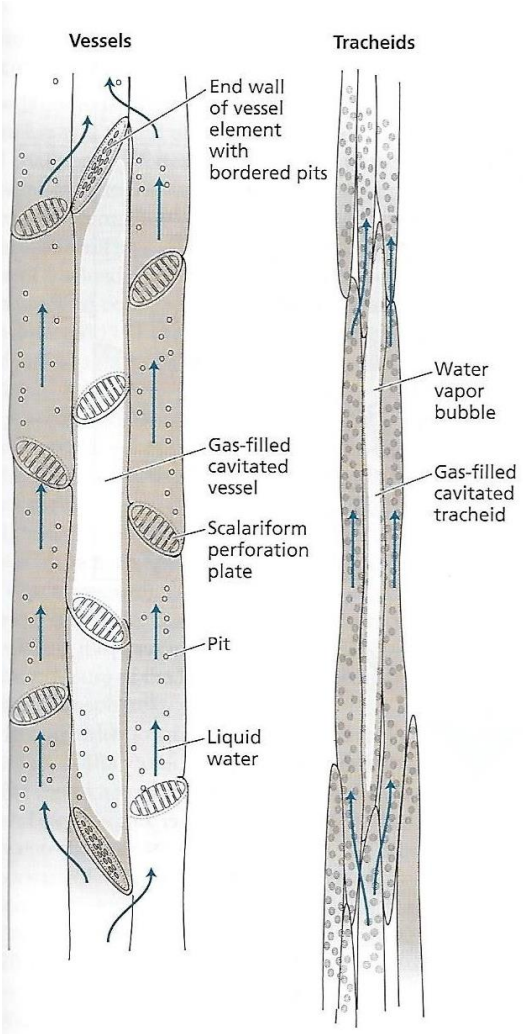

Figure 1.21: Vessel (left) and tracheids (right). Cavitation blocks water movement because of the formation of gas filled (embolized) conduits. Water can detour around the blocked conduits by moving to the adjacent tracheary elements via pits (from Taiz and Zeiger 2006).

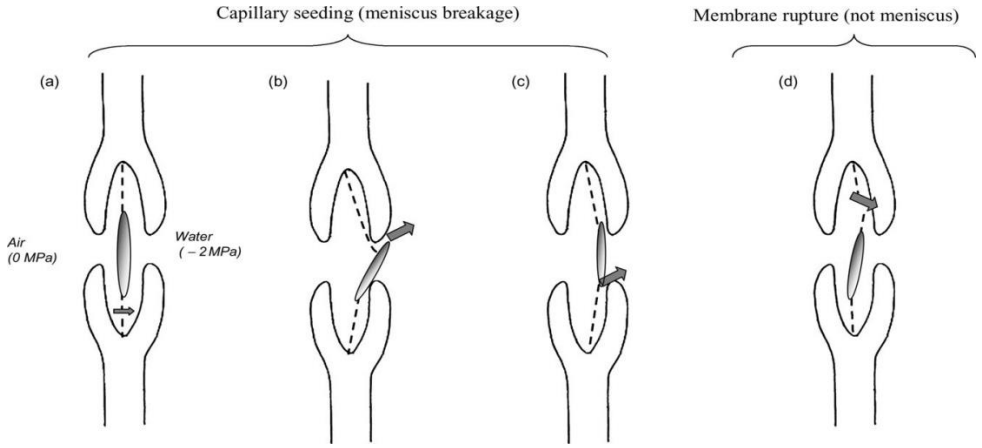

Figure 1.22: Different hypotheses of air-seeding through a conifer bordered pit membrane: (a) margo capillary-seeding, by capillary rupture of an air/water meniscus through pores in the margo when torus aspiration does not occur; (b) margo stretch-seeding, by elastic stretching allowing the torus to be pulled out through the pit aperture or through membrane slippage that allows the torus to move off-center; (c) seal capillary-seeding, when the torus is not tightly sealed against the pit border (weak aspiration or poor air tightness of torus/pit aperture interface); and (d) margo rupture-seeding, by membrane breakage (from Delzon et al. 2010).

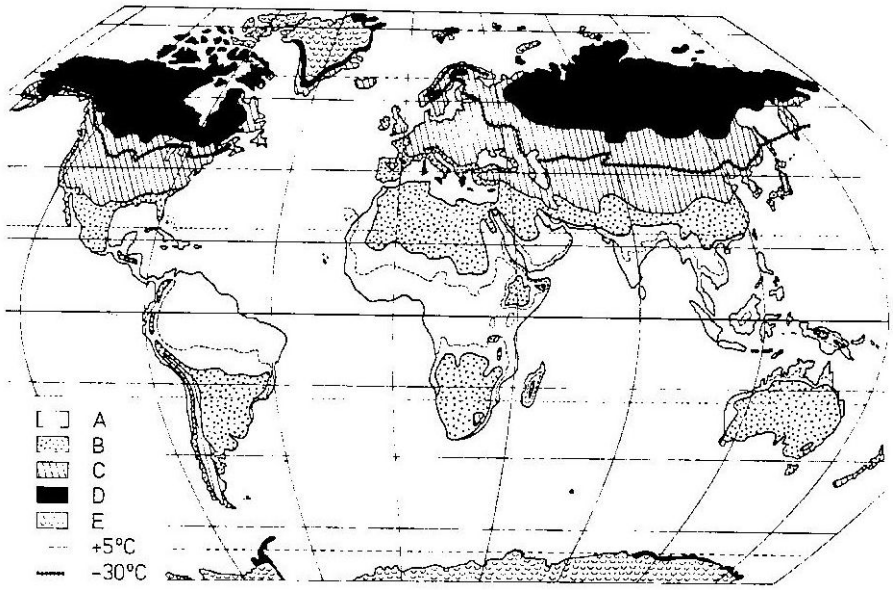

Figure 1.23: Occurrence of low temperatures and frosts on Earth. A, frost free zone; B, episode frosts down to -10°C; C, average annual minimum temperature between -10° and -40°C; D, average annual minimum temperature below -40°C; E, polar ice; --- +5°C minimum isotherm; … -30°C minimum isotherm (from Larcher 1983).

In conduits, the water flow rates increase with the 4th power of the transverse sectional area (Figure 1.24) (Heagen-Poiseuille law, Zimmermann 1983; Tyree and Ewers 1991).

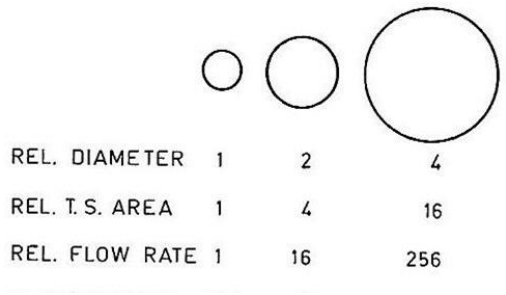

Figure 1.24: Relative diameter and transverse-sectional areas (T.S. Area) and relative flow rates in capillaries of different diameters (modified from Zimmermann 1983).

Smaller conduits can better cope with the water tensile metastable status due to the greater adhesive forces for a unit of water volume (Hacke et al. 2017). Xylem anatomy is therefore strongly related to both the total hydraulic safety and efficiency (Hacke and Sperry 2001; McCulloh et al. 2012), and to the plant performance under different water conditions (Kiorapostolou et al. 2018). In fact, a similar hydraulic conductivity could be obtained hypothetically by producing few wide conduits, reducing carbon costs but being more vulnerable to air seedling (Hacke et al. 2006) or by developing many small conduits, rising carbon costs but counting on a safer hydraulic apparatus.

In other words, on average tracheids are less efficient in water transport due to the small lumens and the many resistances to water flow but are safer from an hydraulic point of view, meaning that they are less likely to experience cavitation, accounting on pits for cell-to-cell water movement. Vessels are very efficient in water transport for the wide lumens where water can move faster, and the long pipes minimizing resistances to water movement, but are more likely to experience cavitation. We can therefore assume that vessels are adapted for working in a condition of good soil hydration while tracheids are reliable under water shortage conditions (Mauseth et al. 2003).

Empirical evidence demonstrates that plant architecture is shaped with a conduit lumen areas widening from the stem apex towards the base (Rosell et al. 2017) following a scaling pattern very similar between species in different environments (Anfodillo et al. 2013). Sapwood conductivity therefore increases from the stem apex towards the base (Petit et al. 2018) and from the pith to the bark for the effect on conduit size of longitudinal growth (Carrer et al. 2015). This general

architectural design implies that narrower and safer conduits (Hacke et al. 2006; Hacke et al. 2017) are present within a short distance from the apex and therefore close to the transpiring leaves, where tension is highest (Petit et al. 2018). Therefore, most of the total hydraulic resistance is confined in this region (Yang and Tyree 1993; Becker et al. 2000; Petit and Anfodillo 2009; Petit et al. 2010) making the apical anatomical features of particular importance for the whole plant conductance (Petit et al. 2011; Prendin et al. 2018a) as for hydraulic vulnerability (Prendin et al. 2018b).

Mechanisms inducing tree mortality

Tree mortality is driven by two different and co-occurring mechanisms called "carbon starvation" and "hydraulic failure" (McDowell 2011; McDowell et al. 2013; Pellizzari et al. 2016; Adams et al. 2017).

Carbon starvation occurs mainly during prolonged droughts periods. When plants are under hydraulic stress (see chapter 1.1.1) and the xylem tension becomes too negative (see chapter 1.2.2), the stomata close and the photosynthesis is reduced (Figure 1.25) (Fitter and Hay 2012). This strategy reduces xylem tension (Figure 1.19) and therefore xylem embolism formation minimizing the water loss at leaf level. By closing the stomata and reducing photosynthesis, a tree starts consuming its energy reservoirs (non-structural carbohydrates) for carrying on respiration processes:

$$C_6H_{12}O_6 + 6O_2 \rightarrow 6CO_2 + 6H_2O \qquad \text{Eq. 1.4}$$

If this negative carbohydrate balance lasts for too long, a tree depletes its stored non-structural carbohydrates and fails to maintain metabolism or defend against biotic agents literally starving to death (McDowell 2011).

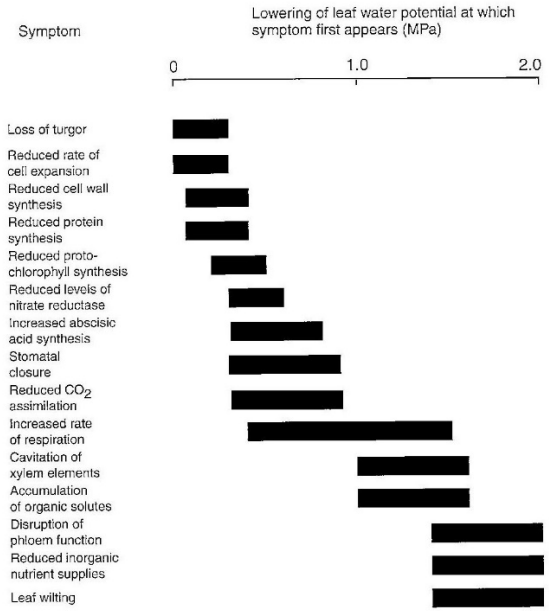

Figure 1.25: The influence of water stress on the physiology of mesophytic plants. The horizontal bars are guides to the level of stress at which the relevant symptoms first occur. The lowering of leaf water potential is in relation to a well-watered plant under mild evaporative demand (from Fitter and Hay 2012).

Hydraulic failure mostly occurs during intense drought events causing high xylem tensions and therefore widespread of embolism formation. Cavitation therefore breaks the continuous water transport pathway (also called Soil Plant Atmosphere Continuum (SPAC)) and reduces the xylem water transport capacity (conductance) (Figure 1.26) untill reaching a level leading a tree to desiccate for failed water transport (Figure 1.28) (McDowell et al. 2013).

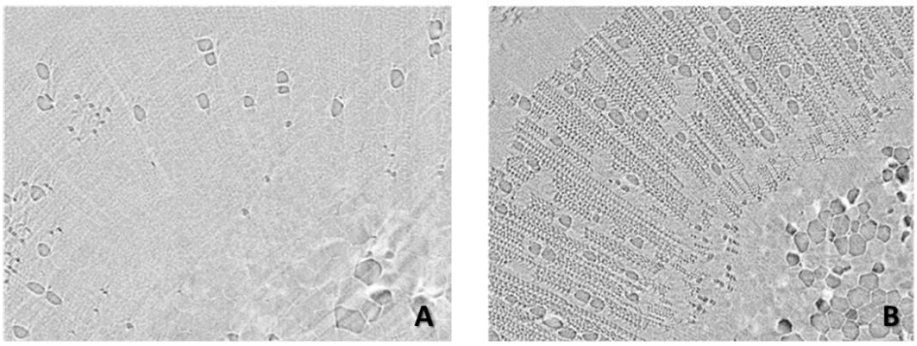

Figure 1.26 Direct visualization of xylem embolism by X-ray microtomography (microCT). *Laurus nobilis* L. shoots 30 cm in length were scanned at 8 cm from the shoot apex, and a two-dimensional cross-section was reconstructed. Functional (grey) and air-filled (black) xylem conduits can be seen. The figure shows the image reconstruction for: (a) stem with a xylem pressure (Ψxyl) of 0.11 MPa; and (b) a second shoot dehydrated to Ψxyl =3.3 MPa (from Nardini et al. 2017a).

Plant survival strategies under drought

In relation to leaf stomatal regulation response to different water soil potentials, plants are distributed along a continuum from isohydric to anisohydric species (Franks et al. 2007; Klein 2014; Martínez-Vilalta and Garcia-Forner 2017). Relatively isohydric species keep a constant midday leaf water potential (ψ_l) by a strict and conservative water-balance management, limiting the water loss by reducing stomatal conductance (g_s) (Sade et al. 2012) and therefore CO_2 assimilation (A_N). Relatively anisohydric species are able to lower their ψ_{leaf} during drought conditions keeping a certain degree of gas exchange (Attia et al. 2015), maintaining higher g_s and A_N and therefore being more productive under these conditions (Almeida-Rodriguezet al. 2010; McDowell 2011; Kumagai and Porporato 2012). These stomatal control models are supposedly linked to different survival strategies under drought. Relatively isohydric species preserve the transport system from xylem tensions potentially triggering xylem embolization, relying upon store carbon reserves to sustain respiration metabolism. They are therefore exposed to the risk of carbon starvation during prolonged drought for depleting their carbon sources (McDowell et al. 2008). Relatively anisohydric species not necessarily rely upon stored reserves to survive drought events (McDowell 2011) but keep an efficient water transport to sustain leaf transpiration and carbon assimilation (Brodribb 2009) taking the risk of experiencing cavitation events due to extreme xylem tensions leading to hydraulic failure under intense water deficit irrespective of their duration (Attia et al. 2015).

Xylem vulnerability

In order to describe the vulnerability of xylem to embolism, and therefore xylem resistance to cavitation, the most widely used parameter is the P_{50}, expressing the water potential at which xylem loses 50% of its conductivity. Being P_{50} a value of tension, it is negative. The more negative the value of P_{50}, the more resistant the system to xylem embolism. This parameter is assessed by generating hydraulic vulnerability curves (i.e., data fitting) (see chapter 2.5.3) and describes the relationship between xylem pressure and the Percentage Loss of Conductivity (PLC) (Figure 1.27). Vulnerability curves typically have a sigmoid shape with

loss of conductivity initially increasing gradually as xylem pressure decreases followed by an abrupt transition to a much steeper, nearly linear phase, ending with a more gradual phase as loss of conductivity approaches 100% (Meinzer et al. 2009). After reaching the value of P_{50}, plant is exposed to considerable risk of accelerated embolism leading to long-term reductions in productivity, tissue damage, and ultimately death.

P_{50} can be used to compare xylem vulnerability across species, within different parts of the same individual and within species across different environmental gradients (Pockman and Sperry 2000; Maherali et al. 2004; Maherali et al. 2006; Nardini et al. 2013; Anderegg 2015; Trueba et al. 2017).

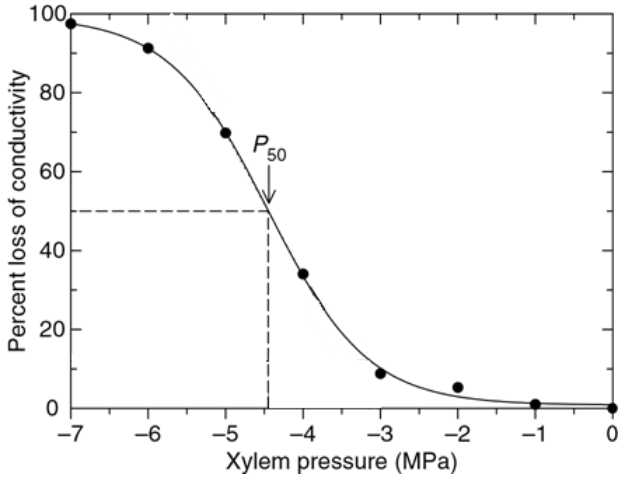

Figure 1.27: Typical xylem vulnerability curve showing the relationship between the percent loss of hydraulic conductivity and xylem pressure. The xylem pressures corresponding to 50% loss of conductivity (P_{50}) is shown (modified from Meinzer et al. 2009).

Hydraulic safety margin

Another important parameter used to assess xylem responses to embolism formation is the Hydraulic Safety Margin (HSM) (Nardini et al. 2013). It corresponds to the difference between the regulation of daily minimum stem water potential (ψ_{min}) under non-extreme conditions and the P_{50} (Meinzer et al. 2009). A species with a wide HSM tend to close the stomata before xylem cavitation event may occur, meaning that it is more resistant to embolism formation (Figure 1.28).

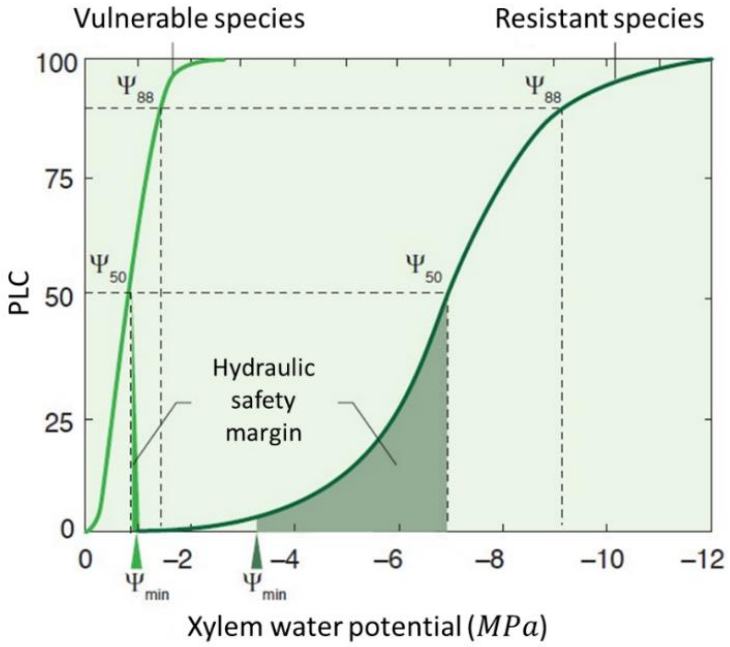

Figure 1.28: Comparison of the vulnerability curves of a vulnerable and a resistant species. The hydraulic safety margin is wider in the more resistant species. The ψ_{88}, potential at which xylem experiences 88% of conductivity loss is also shown. It is believed to be the threshold after which embolism is not reversible anymore and a plant will undergo hydraulic failure and death (modified from Rascio et al. 2017).

While gymnosperms tend to have a generally wide HSM (Figure 1.29), angiosperms tend to have a very narrow HSM ($1\,MPa$) (Choat et al. 2012). Anyway, gymnosperms are not immune to the threat of hydraulic failure as they generally live in semi-arid conditions where water becomes a limiting factor for woody plant growth. Some species in particular (Figure 1.29 top right) have a negative safety margin. It means that they tend to keep stomata open even when embolism formation is taking place in the stems therefore potentially facing long-term reductions in productivity. Being safety margins largely independent of mean annual precipitation, there is a global convergence in the vulnerability of forests to drought (see chapter 1.1.1), with all forest biomes equally vulnerable to hydraulic failure regardless of their current rainfall environment. (Choat et al. 2012).

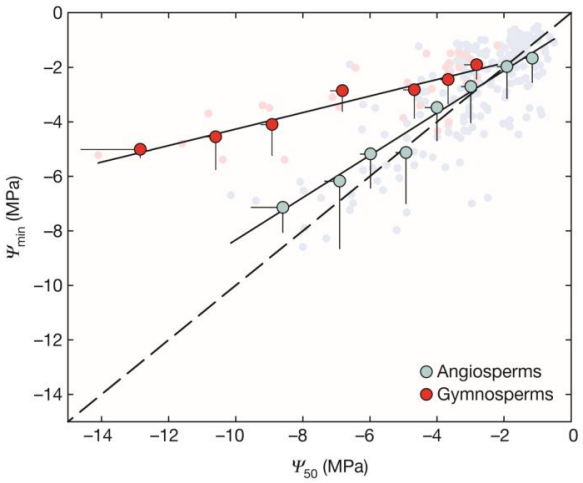

Figure 1.29: Minimum xylem pressure (ψ_{min}) as a function of embolism resistance (ψ_{50}) for 191 angiosperm and 32 gymnosperm species. The safety margin is the distance between each point and the 1:1 (dashed) line. Data were binned in 1.0 MPa increments for embolism resistance (ψ_{50}). Bins were pooled with the next lowest bin if they contained only one sample. Raw data are shown as smaller points behind binned data. Error bars, s.d. Regression lines shown were fitted to raw data (angiosperms, $R^2 = 0.57,\ p < 0.0001$; gymnosperms, $R^2 = 0.59,\ p < 0.0001$ (from Choat et al. 2012).

Moreover, there is general agreement that xylem architecture is bound to a threshold between the xylem transport efficiency and its hydraulic safety (Hacke and Sperry 2001; Pratt and Jacobsen 2017). Hypothetically, we would expect to have either species resistant to embolism with low transport efficiency or vulnerable species with high transport efficiency. Surprisingly, there are many species having both low safety and low efficiency (Figure 1.30 down left) (Gleason et al. 2016; Pratt and Jacobsen 2017: Torres-Ruiz et al. 2017).

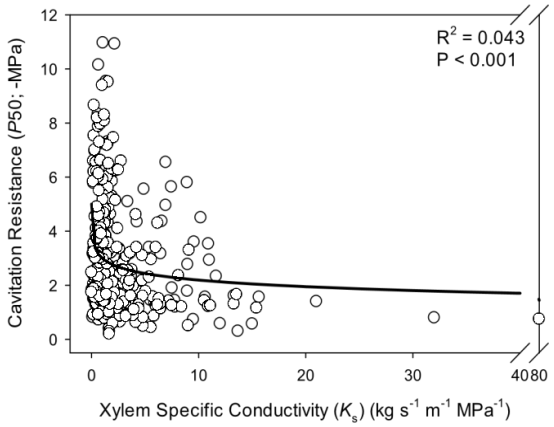

Figure 1.30: Plot of xylem safety (P_{50}) as a function of xylem efficiency expressed as xylem specific conductivity (K_s) of branches of angiosperms. Solid line is a best logarithmic fit (from Pratt and Jacobsen 2017).

These findings indicate that embolism formation is a very common process (Zwieniecki and Holbrook 1998; Domec et al. 2006). In order to avoid long-term reduction in productivity, plants should possess a mechanism to restore hydraulic conductance. This mechanism was proposed in the "refilling theory" that will be discussed in the next paragraph.

Refilling

According to the "refilling theory", plants are able to restore the hydraulic conductance by mobilizing the sugars (i.e., non-structural carbohydrates) carried by the phloem and stored in parenchyma cells (Nardini et al. 2011). The proposed refilling mechanism (see Figure 1.31) (Zwieniecki and Holbrook 2009) suggests that parenchyma cells (a) in contact with vessels release a small but steady amount of soluble carbohydrates into the xylem mobilizing their stored starch (b). Normally, these solutes are swept away by the transpiration stream (c). Their concentration remain therefore at a very low level. In cavitated vessels, solutes tend to accumulate instead (d), increasing the apoplastic solute concentration that triggers (e) signalling pathways (f) for refilling by regulating sugar and water transport through the membrane (g) and sugar metabolic activity (h). Solutes accumulation triggers water movement from xylem parenchyma cells into the vessels by establishing an osmotic gradient forming water droplets (i) with high osmotic activity. Vessel partially non-wettable walls prevent these droplets from being removed by the tension generated by other functional vessels (j). Moreover, condensation of water vapour coming from adjacent conduits provides additional water for refilling (k). The osmotic droplets grow and coalesce until the vessel is filled (l) and the embolus is removed both by compressing the gas until it dissolves into solution and by pushing it through small pores of the vessel walls in the intercellular spaces. The pit chamber acts like a check valve (m) until the lumen is filled, preventing contact with the highly wettable pit membranes. When the pressure in the lumen exceeds that of the entry threshold into the pit chambers, vessel reconnection occurs simultaneously among multiple bordered pits thanks to a hydrophobic layer within pit membranes.

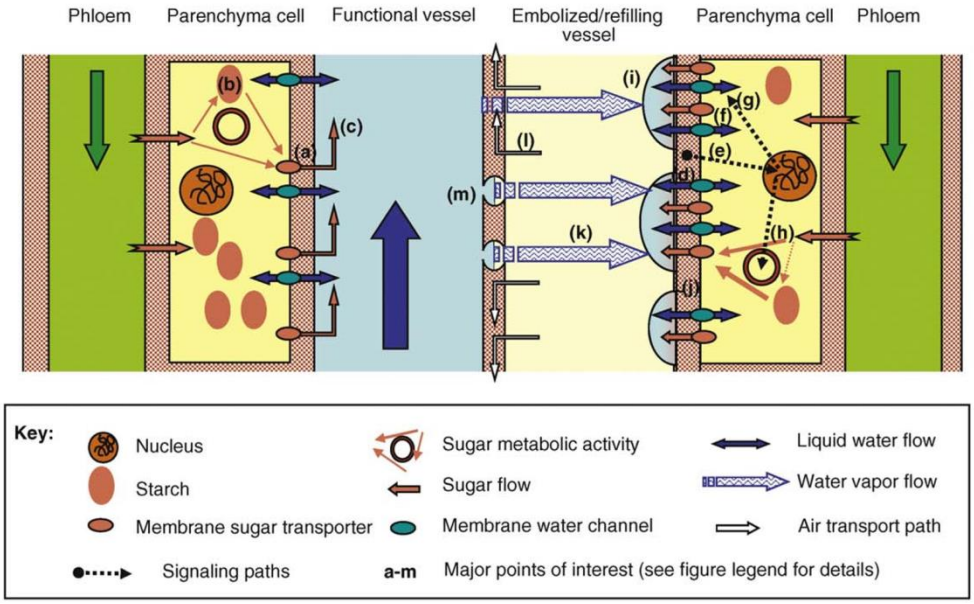

Figure 1.31: Embolism refilling scenario. See text for the description (from Zwieniecki and Holbrook 2009).

Though different papers are providing new evidences supporting this theory from the sensing of embolism formation inside vessels (Secchi and Zwieniecki 2011), to the influence of plant carbon status on plant performance during and after drought (Nardini et al. 2016; Nardini et al. 2017b) or the in vivo observations of vessels undergoing refilling (Figure 1.32) (Brodersen et al. 2010), still much debate on the mechanism of water plant embolism recovery is present nowadays (Clearwater and Clark 2003; Hacke and Sperry 2003; Sperry 2013; Wang et al. 2014; Nardini et al. 2017b).

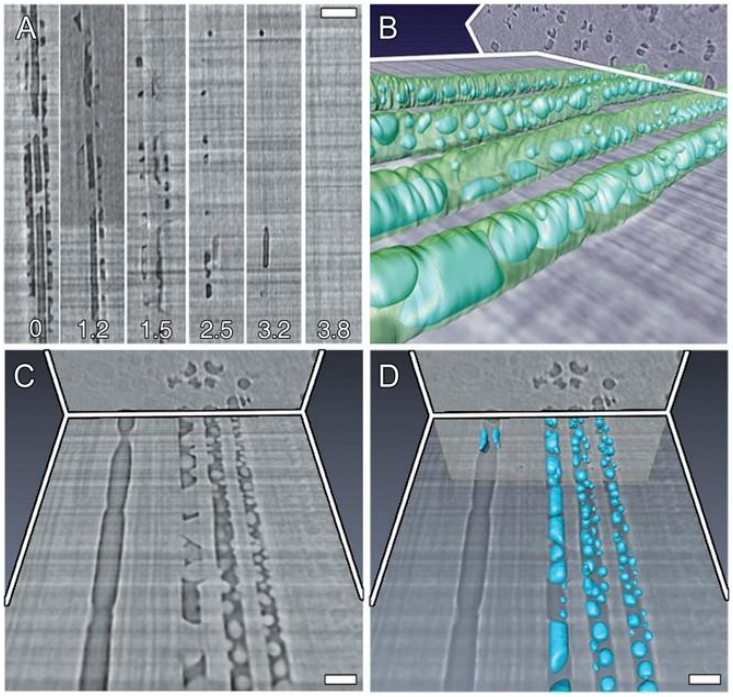

Figure 1.32: In vivo HRCT sections of a representative grapevine stem undergoing vessel refilling. Time-lapse longitudinal sections (A) showing the refilling of three adjacent vessels and the presence of water droplets on the inner vessel walls (hours indicated in each section). Bar = 200 mm. Trans-longitudinal section with vessel walls and droplets rendered in 3D (B). Trans-longitudinal section showing droplet details in four vessels at different stages of refilling (C), and the corresponding 3D volume rendering (D). Vessel on the far left shows evidence of failed refilling. Bars = 100 mm (from Brodersen et al. 2010).

1.3 Working hypothesis

The aim of this work is to investigate if there are some anatomical features linked to the tolerance of plants to cavitation. Hypothetically, vulnerable species (see chapter 1.2.3) should rely on efficient refilling mechanisms to recover from embolism formation and therefore have high parenchyma amount. This would allow them to store and utilise non-structural carbohydrates more effectively throughout the xylem. By contrast, species that are more resistant are expected to have a lower parenchyma amount, as they would rely on a robust xylem structure, therefore minimizing the embolism formation and the need of activating refilling processes.

2. Materials and methods

In order to investigate the relationships between anatomical structures and functional hydraulic properties of the xylem transport system, I built up a database composed of anatomical and hydraulic traits of different species.

Below I describe the compilation of this database, with the different bibliographic sources and the empirical measurements carried out to expand the number of analyzed species and the target variables.

These variables can be divided in three major groups. A first group includes qualitative variables, a second one considers hydraulic traits and the third regards xylem anatomy. In total, 13 are the variables taken into account (Table 2.1).

2.1 Variables description

2.1.1 Qualitative variables

Plant species were divided between angiosperms and gymnosperms (A/G) as these two plant groups have peculiar xylem anatomical differences (see chapter 1.2.1).

Moreover, the Deciduousness or Evergreenness of (D/E) overwintering strategy was considered. Deciduous species need to mobilise more sugars at the beginning of spring to build a new crown whereas evergreen species invest more carbon in producing hard long lasting leaves. These different strategies may have an impact on the vulnerability of xylem to embolism.

Species were also divided into climbers and self-supporting (C/S). Self-supporting species need to invest more carbon in building a structure capable of supporting the plant while climbers tend to take advantage of other plants or abiotic structures to grow. Moreover, climbers generally have a higher parenchyma amount (Morris et al. 2016).

2.1.2 Hydraulic variables

P_{50} was the only hydraulic variable considered. It indicates the xylem tension inducing a percentage loss of conductance due to embolism formation (Ennajeh et

al. 2011b) of 50% (PLC=50 %). The detailed description of the PLC pattern with increasing xylem tension (i.e., negative xylem water potential (Ψxyl)), commonly called vulnerability curve (VC) is reported in chapter 1.2.2.

2.1.3 Anatomical variables

Parenchyma volume was considered analyzing separately its two main elements present in the wood: the axial parenchyma (PA_A) and the radial parenchyma (PA_R) (Figure 1.16). The sum of these two elements (PA_{AR}), was also estimated. The bark was not considered in this study.

The area of xylem (X_a) was measured. This area is divided in three main elements that were also estimated: the previously discussed parenchyma fractions (PA_A, PA_R), the volume of wood occupied by fibres (F_a) and the volume of wood occupied by vessels (V_a). Regarding the conduits, both the mean area of the conduit elements (MC_a) and the conduit density (C_d) were estimated. In angiosperms for "conduits" we refer to the vessel elements while in gymnosperms the tracheids were considered.

Furthermore, the xylem-specific potential hydraulic conductivity (K_s) was calculated.

Variable Type		Variable	Measure unit
Qualitative	A/G	Angiosperm/Gymnosperm	
	D/E	Deciduous/Evergreen	
	C/S	Climbers/Self-supporting	
Hydraulics		P_{50}	MPa
Xylem anatomy	PA_A	Axial parenchyma	%
	PA_R	Radial parenchyma	
	PA_{AR}	Total parenchyma	
	F_a	Fibres area	
	X_a	Xylem area	mm^2
	MC_a	Mean Vessels area	μm^2
	C_d	Vessels density	$n^{\circ} mm^{-2}$
	V_a	Area Of Vessels	%
	K_S	Xylem-specific potential hydraulic conductivity	$m^2 s^{-1} MPa^{-1}$

Table 2.1: Variables (N=13) considered for each species in the dataset.

2.2 Dataset construction

The final dataset is composed of three different subset of data, as described below.

A preliminary research of data from literature was carried out. Data were collected from Choat et al. 2012 and Morris et al. 2016. For 107 species both hydraulic (P_{50}) and parenchima fraction estimations (PA_A, PA_R, PA_{AR}) were available (group 1). For a major number of specimens only the value of P_{50} was known, and we provided the additional anatomical information by taking in-depth anatomycal measurements (PA_A, PA_R, PA_{AR}, F_a, X_a, MC_a, C_d, V_a, K_s) on available samples of these species (N=74) (group 2). In order to validate the dataset, for a minor number of species, both hydraulic and anatomical measurements were performed (N=14) (group 3).

Three main groups were therefore developed in my dataset: a first group (group 1) with data coming from literature, a second group (group 2) combining hydraulic data coming from literature with anatomical measurements made on our own and a third group (group 3) made of hydraulic and anatomical measurements made on our own.

2.3 Measurements

The material analysed was collected in different places defined as sampling sites (Table 2.2). Most of the samples (N=71) were collected in Botanical gardens (Bg) for the accessibility to a great variety of the plant material. Some specimens were collected inside the greenhouses (Table 2.3). A minor number of samples was collected in nature (N=22) in established locations where the research groups we collaborated with (University of Messina and University of Trieste) usually go and collect material.

Sampling site	n° of species	Coordinates	Altitude (m a.s.l)	Measurements carried out
Botanical garden - University of Padua	63	45.399° N, 11.881° E	12	Xylem anatomy
Messina	12	38.260° N, 15.598° E	51	Xylem anatomy
Botanical garden - University of Trieste	8	45.661° N, 13.795° E	125	Xylem anatomy (N=8), P_{50} (N=3)
Gabrovizza	6	45.732° N, 13.725° E	225	Xylem anatomy, P_{50}
Cernizza	2	45.780° N, 13.591° E	30	Xylem anatomy, P_{50}
Sgonico	2	45.738° N, 13.739° E	260	Xylem anatomy, P_{50}

Table 2.2: Number of species collected in each sampling site with spatial data. The values of altitude were estimated using Google Earth. For "Messina" we refer to some natural areas nearby the city. Gabrovizza, Cernizza and Sgonico represent different natural areas nearby the city of Trieste. In the column about the measurements that were carried out, by "xylem anatomy" we refer to all anatomical variables described in chapter 2.1.3.

Sampling site	Species
Botanical garden – University of Padua	- *Ceiba speciosa* (A.St.-Hil.) Ravenna - *Fouquieria splendens* Engelm. - *Olea europaea* L. - *Quercus suber* L. - *Rhizophora mangle* L. - *Tecoma capensis* (Thunb.) Lindl.
Botanical garden – University of Trieste	- *Fraxinus ornus* L.

Table 2.3: Species collected inside the greenhouses.

2.4 Anatomical analyses

2.4.1 Sampling methods and preparation of the material

For those species whose data on P_{50} were available from literature (group 2), one branch segment was collected. Instead, for those species whose P_{50} was measured by ourselves (group 3), a branch segment per replicate (up to 4 for each species) was collected. The segments were about 3 cm long and had a diameter ranging from 0.5 cm to 2.5 cm according to the species-specific branch characteristics. For

example, climbers like *Pueraria montana* (Lour.) Merr. has very thin branches whereas *Ficus carica* L. tend to grow with quite wide ones. When possible, the bark was carefully removed to simplify the following phases of sample preparation. Using a rotary microtome LEICA RM 2245 (Leica Biosystems, Nussloch, Germany) (Figure 2.1), for each segment from 3 to 5 transverse and tangential micro-sections at 25 μm were cut and placed on a single microscope slide for staining.

A preliminary observation with a microscope was done in order to evaluate the quality (i.e., absence of cracks and lining, homogenous section thickness) of the sections and to discard the less accurate ones. The material was than decolored with a solution of water and bleach (1% in distilled water) for 15 minutes. The section was cleaned with fresh water and stained with a solution of Safranin and AstraBlue (1% and 0.5% in distilled water respectively) for 30 minutes. Later on, the exceeding stain was removed in three steps using fresh water, a solution of 50% ethanol and ethanol 100%. After drying the sample with highly absorbing papers, the material was permanently fixed on microscope slides with Eukitt (BiOptica, Milano, Italy) and covered by a glass cover. The majority of the air bubbles were immediately manually pushed away by gently applying a light pressure on the cover glass. The sections were left for 2 days under the pressure of magnets to force the remaining air bubbles to exit the sections and the exceeding dried Eukitt was carefully removed with a cutter's blade. Images from the micro-sections were acquired using a D-sight slide scanner (Menarini, Florence, Italy) (Figure 2.2). Images of the cross sections were taken at 100x magnification whereas images of the tangential sections were acquired at 40x magnification. These steps, from the preparation of the micro-sections to the acquisition of the images are of crucial importance for the following manual and automatic analyses that will be discussed in the next chapters (2.4.2, 2.4.3). For this reason, very much attention was paid in order to acquire detailed images of intact and well-stained micro-sections (Figure 2.3).

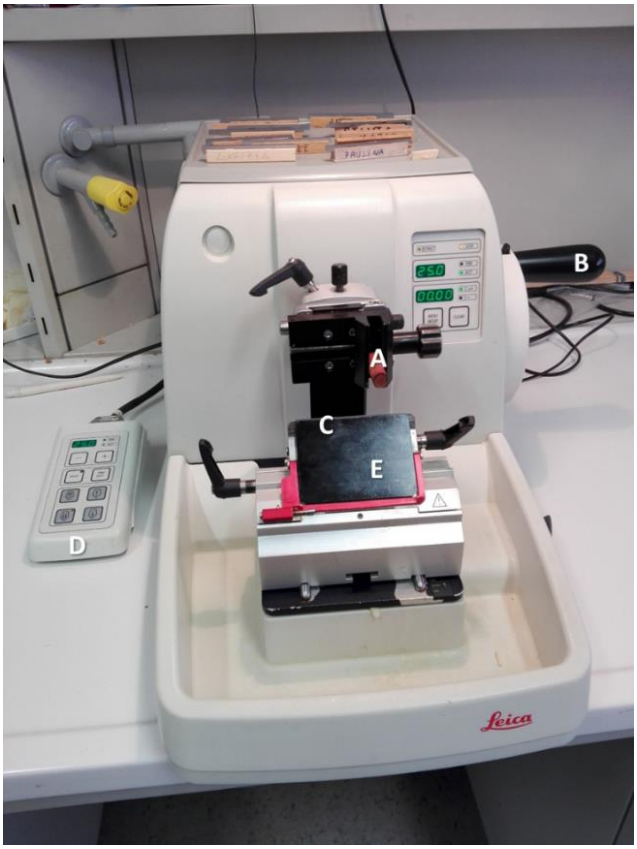

Figure 2.1: Rotary microtome Leica RM 2245 (Leica Biosystems, Nussloch, Germany). The debarked sample (A), by rotating the handle (B), is cut in micro-sections by the blade (C) at a pre-determined thickness (D) and collected from the designated surface (E).

Figure 2.2: D-sight slide scanner (Menarini, Florence, Italy).

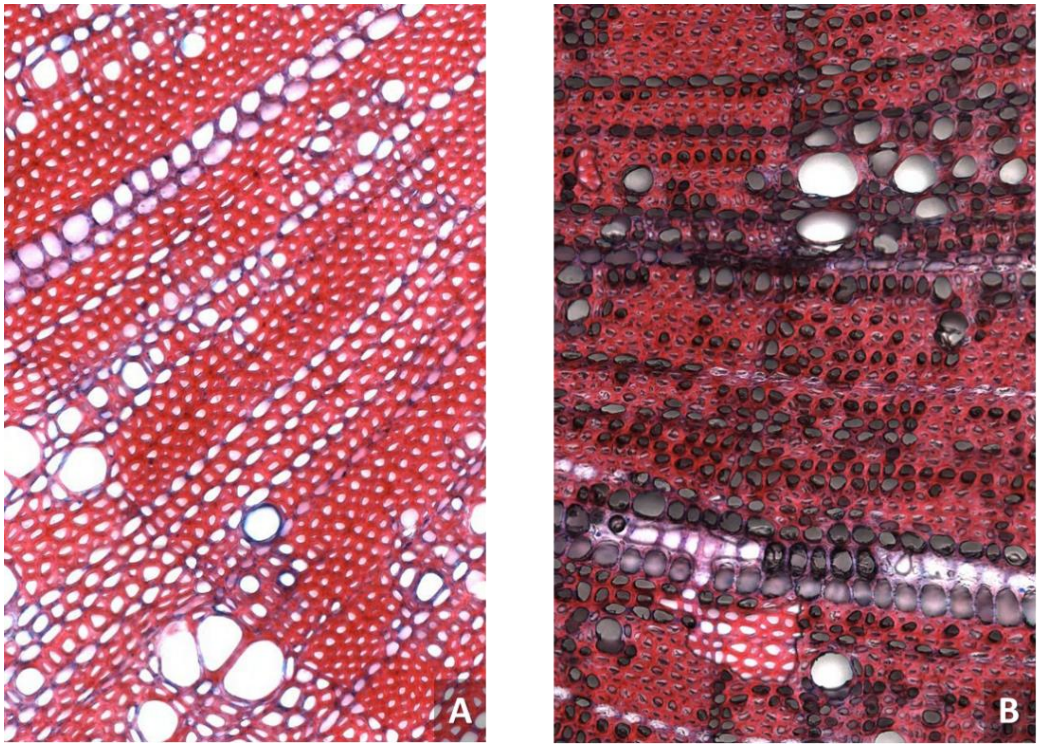

Figure 2.3: Well stained (A) and badly stained (B) cross-sections of *Rosmarinus officinalis* L. (100x).

2.4.2 Analysis of parenchyma fractions

The estimate of parenchyma fraction was performed by analysing images with Fiji Is Just ImageJ version 2.0.0 (Schneider et al. 2012) doing manual editing with an intuos Pen & Touch Tablet, Wacom. In each image, a rectangular area showing representative sample features of the wood was selected. Only well stained areas with intact tissues (i.e., not affected by artificial cracks caused by cutting), were selected (Figure 2.3). In transverse images, as a rule, the innermost annual ring was not considered and an area of minimum 1 ring including both early and latewood was analysed (Figure 2.4).

The axial parenchyma (PA_A) amount was estimated in cross-sections as the percentage area occupied by axial parenchyma cells over the total analysed area. Both apotracheal and paratracheal (Figure 2.5) cells were considered. Where possible, the area was including a rectangular portion of 2 or 3 rings, again from the beginning of early wood to the end of the latewood.

The radial parenchyma (PA_R) amount was estimated in tangential sections as the percentage area occupied by radial parenchyma cells (i.e., rays) over the total analysed area. In each image, a rectangular portion in the central region was analysed (Figure 2.6) in order to avoid blurred areas often occurring towards the lateral portions of the images (Figure 1.9).

The total parenchyma volume (PA_{AR}) was the result of the sum the two previously mentioned parenchyma fractions ($PA_{AR} = PA_A + PA_R$).

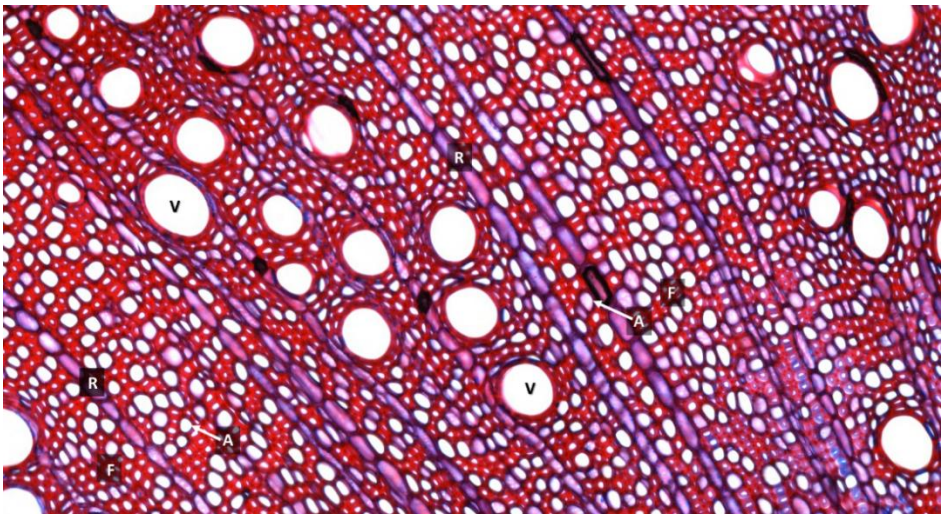

Figure 2.4: Cross-section area analysed in *Quercus ilex* L. (100x). See: axial parenchyma (A), radial parenchyma (R), vessels (V), fibres (F).

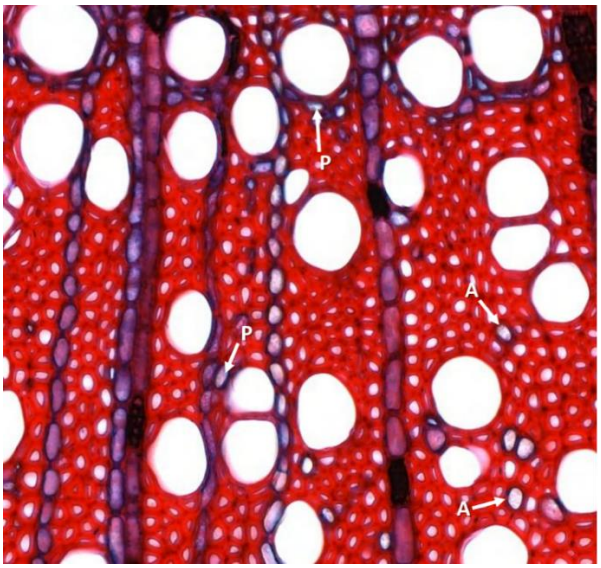

Figure 2.5: Cross-section showing apotracheal (A) and paratracheal (P) axial parenchyma in *Prunus mahaleb* L. (100x)

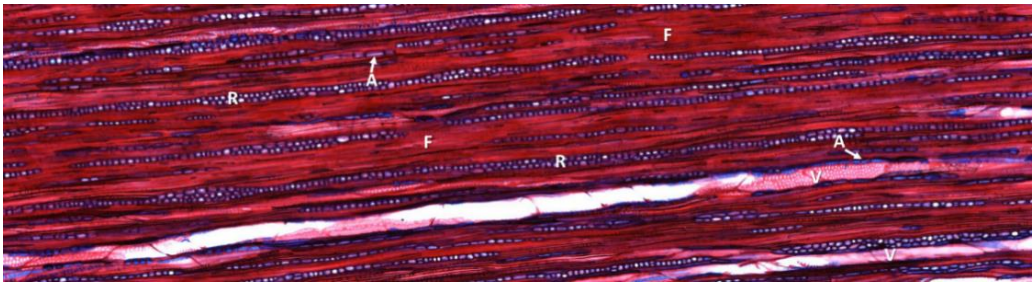

Figure 2.6: Tangential section area analysed in *Pistacia terebinthus* L. (40x). See: axial parenchyma (A), radial parenchyma (R), vessels (V), fibres (F).

2.4.3 Analysis of other anatomical features

The same cross-sectional images were also analysed with ROXAS 3.0.139 ® (von Arx and Carrer 2014) for the estimate of other anatomical traits. For each sample, a rectangular section containing the wood from the pith to the bark was analysed (Figure 2.7). Images were calibrated meaning that the image was centred to the pith and a wedge of 40° called "area of interest" was selected, so that the analysis was run on this outlined area. Annual rings were manually drawn and the analysed images were then checked and manually edited for correcting potential mistakes in the recognition of ring boundaries and cells' outlines. The obtained output file contained a broad range of variables' estimates, including the following of my interest:

- F_a: Fibres area;
- X_a: Xylem area;
- MC_a: Mean Vessels area;
- C_d: Vessels density;
- V_a: Area of Vessels;
- K_s: Xylem-specific potential hydraulic conductivity;

K_s was assessed as the sum of each single vessel conductivity, estimated with Hagen-Poiseuille law (Figure 1.24), divided by the analyzed xylem area (X_a) analyzed (Melcher et al. 2012).

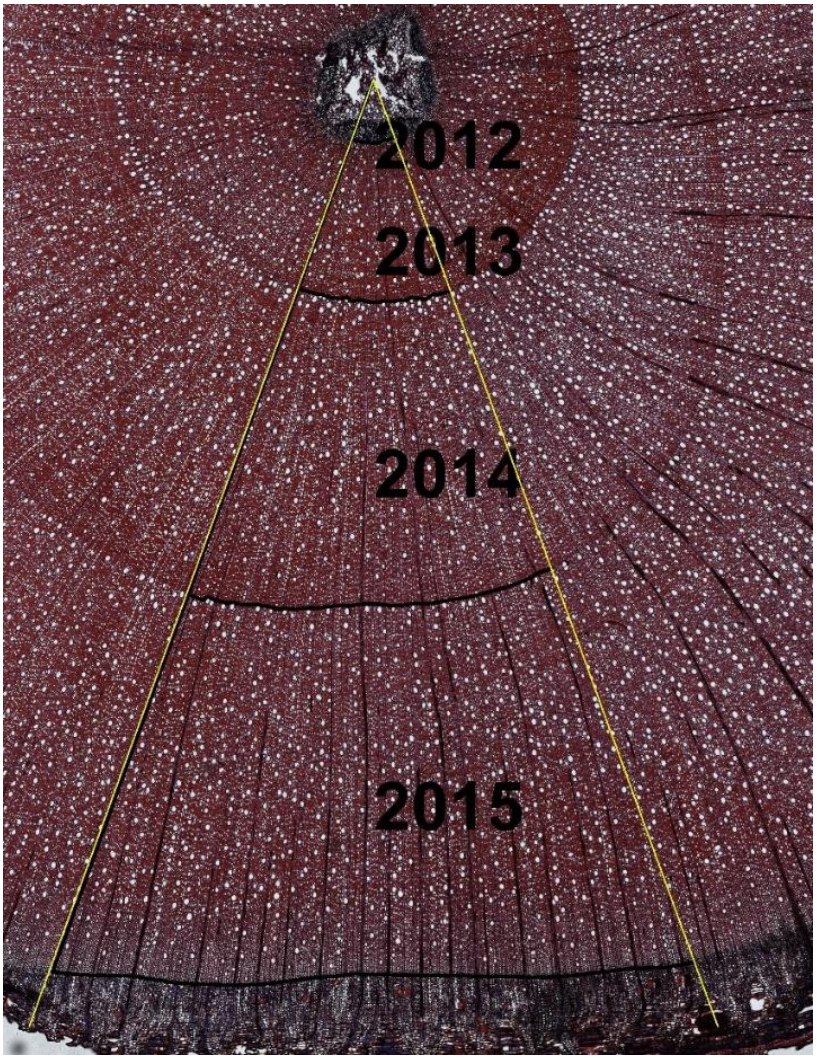

Figure 2.7: Cross section area analysed of *Myrtus communis* L. (100x) using ROXAS 3.0.139 ® by Georg von Arx (von Arx and Carrer 2014). The yellow lines indicate the wedge of 40° where the analyses were performed. The different growth rings were also defined (black lines and years). The oldest year (2012) as a rule of the software corresponds to the pith. The bark was not analysed.

2.5 Hydraulic analyses

2.5.1 Sampling methods

Branches were excised at predawn, before the onset of photosynthesis. This allowed vessels that experienced cavitation during the previous day to refill with water during night-time when the soil is more hydrated. The samples were therefore water saturated, that is the ideal condition for performing the experiments. Branches were immediately re-cut 3 times under water shortening

them 1 cm each time and placed in a bucket with the cut end immersed in water. This procedure is carried out to reduce the tension inside the vessels caused by the first excision done in open air. The branches were also covered with a black plastic bag to inhibit photosynthesis and favour refilling of embolised conduits (Trifilò et al. 2014). For each species, 6 to 10 branches coming from different specimens of the same species were collected to avoid pseudo-replicates. As a rule, to have more reliable results in measuring the P_{50} (see chapter 2.5.3), the branches were chosen 100-150 cm long, growing straight, with a main growing branch and just few lateral branches. As much as possible, branches growing in a sunny position were collected to avoid the potential shade effects (Salter et al. 2003). Samples were carried to the lab and the experiments were performed on that same day on fresh material.

2.5.2 Vessel length estimation

The maximum vessel length (VL_{max}) (see chapter 1.2.1) was estimated with the air injection method (Jacobsen et al. 2012). For each species, 3 to 5 replicates were analyzed and the mean value was calculated. The apical part of each branch was cut about 4 cm below the beginning of the current year's growth and 1 cm of bark was carefully removed. The cut section was trimmed three times and connected to a tubing system (Figure 2.8). Air was perfused from the apical end at a pressure of $10\ kPa$ while the basal end was immersed in a water tank and observed with a magnifying lens for the presence of air bubbles coming out from the cut surface. The basal end of the branch was progressively shortened by $1-2\ cm$ cuts, until 1-2 evident streams of air bubbles were observed. The remaining sample length was measured and recorded as VL_{max}. This measurement is of great importance for making proper pressure collar experiments (see chapter 2.5.3).

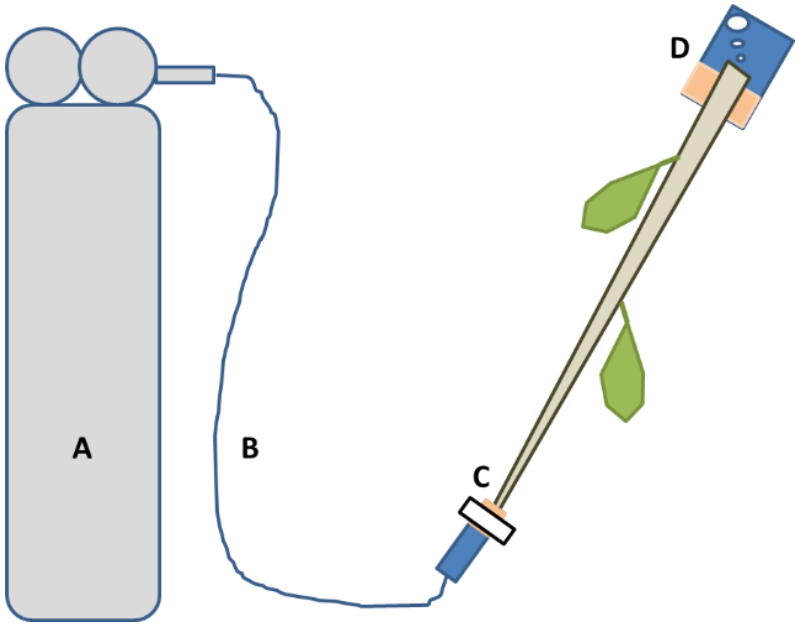

Figure 2.8: Vessel length estimation method (modified from Jacobsen et al. 2012): The air coming from thank (A) is pushed into the stem (B) at 10 KPa from the apical part (C). The sample is progressively shortened under water until bubbles (D) are seen emerging from the base. The sample length (C-D) is recorded.

2.5.3 Pressure collar experiments for the assessment of vulnerability curves

The experiments were performed with the pressure collar method. This technique is based on the use of a double-ended pressure sleeve (PMS Instruments, OR, USA) capable of simulating in a branch different levels of xylem tension by forcing air inside the xylem (Figure 2.11). Air, by flowing towards both ends to exit the sample, reduces the water flowing through the vessels from the base to the apex by filling xylem conduits with air and thus making them impermeable to water.

For each species, branch segments at least longer than the maximum vessel length were chosen (Ennajeh et al. 2011a). To do so, the length of the sample was kept at least at 1.5 × VL_{max}. Branches were progressively re-cut under water with scissors to release the tension in the vessels. At both ends, the branch was trimmed 3 times under water with a razor blade and carefully debarked for about 2 cm. The remaining segment (about 25-100 cm long depending on the species VL_{max}) was connected to a hydraulic apparatus (Xyl'em, Bronkhorst, France). Samples were perfused with a filtered poly-ionic solution enriched with 10 $mmolL^{-1}$ KCl (Savi

et al. 2017) and flushed for 30 minutes. The branch was defoliated cutting the stalk under water. After the flush, a central portion of the segment, about 8 cm, equal to the length of the pressure collar, was debarked while immersed in water. The sample was mounted on a double-ended pressure sleeve (PMS Instruments, OR, USA) and both samples' ends were trimmed under water again. The basal end of the sample was connected to a 1 m long plastic transparent tube filled in with water kept at a defined height (Figure 2.9). Due to gravity, water started flowing through the sample from the basal-end to the upper-end at a low pressure ($4.8\ kPa$). After waiting 3 minutes for flow stabilization with the applied low pressure, the maximum hydraulic conductance (K_{max}) was measured. This measurement was developed by collecting the sap from the upper-end with pre-weighted vials for 30 seconds or 1 minute interval according to the abundance of the sap flow inside the sample. 5 measurements were performed each time. Step by step, according to the expected vulnerability to embolism of the species, the pressure in the sleeve (P_{xyl}) was increased progressively by 0.2, 0.5 or 1.0 MPa, applied again for 3 minutes to allow water flow stabilization inside the sample and the conductance was re-measured (K) as previously described. By forcing air inside the sample, the water amount flowing throw it progressively decreases according to the effect of increasing number of air filled conduits due to air injection under pressure (P_{xyl}). The applied positive pressure is assumed to simulates the effect of the tension of same magnitude in the xylem (i.e., a negative pressure equal to P_{xyl}) causing embolism formation (see chapter 1.2.3), and thus reducing the xylem water conductance (K). The air can be seen emerging from both ends of the sample. The plastic tube connected to the basal end of the sample is wide enough to allow the escape of water bubbles from the sample (upstream) without interrupting the water flow inside the sample (downstream) (Figure 2.9). For each step of applied pressure (P_{xyl}), the percentage loss of conductance (PLC) was calculated as:

$$\mathrm{PLC} = \frac{1 - K}{K_{max}} * 100 \qquad \text{Eq. 2.3}$$

These measurements were carried on until reaching about 70-80% of PLC when no further increase was seeing applying higher P_{xyl}.

In order to estimate the P_{50} it was necessary to draw a vulnerability curve out of our measurements. This was done using RStudio version 1.1.423 and the packages Rcmdr version 2.2-4 and fitplc version 1.1-7 (Duursma and Choat 2017). For each replicate, an excel file was created where the data about PLC and relative P_{xyl} were summarized. Pairwise association of PLC vs P_{xyl} data were fitted with a sigmodal curve (S-shaped) drawn using R-software and the P_{50} (see chapter 1.2.3). Exponential-type curves (R-shaped) were discarded as they likely indicate the presence of some mistakes during the experiments like the presence of open vessels (i.e., sample length shorter than VL_{max}) causing a misleading estimation of the P_{50} (Ennajeh et al. 2011b) (Figure 2.10). P_{50} was estimated as the inflection point of the vulnerability curve.

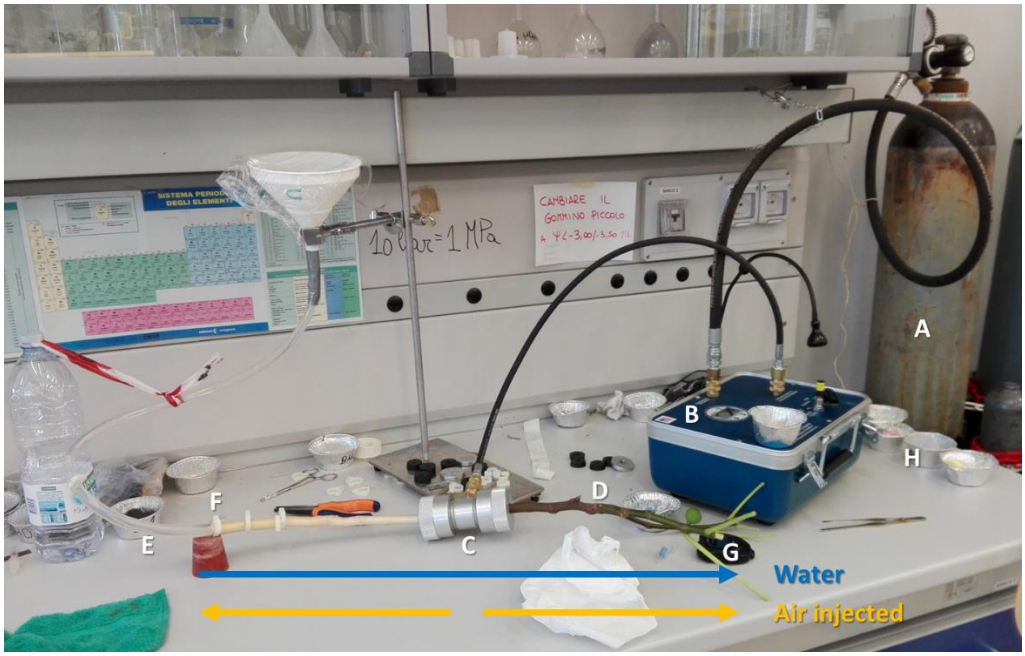

Figure 2.9: Double-ended pressure sleeve (PMS Instruments, OR, USA) with mounted sample of *Ficus carica* L. . The air coming from the tank (A) is forced at progressively higher pressures (B) into the pressure chamber (C) and therefore inside the vessel elements of the sample (D). While the air injected can exit the vessels at both ends (F, G) water at low pressure (E) flows inside the vessels from the basal end (F) to the upper end (G). The plastic tube (E) is wide enough for air bubbles to escape from the sample without reducing the water flux. Sap is collected with pre-weighted vials (H). See also the flow directions of the water and the air injected through the sample: the first one from the base to the apex and the second from the pressure chamber (C) towards both ends.

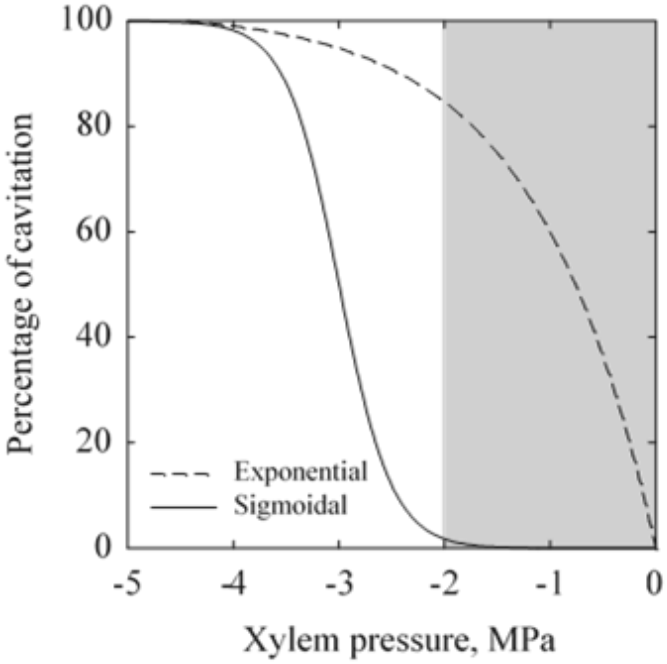

Figure 2.10: S-shaped curves and R-shaped curves (from Cochard et al. 2013). The P_{50} extracted from the Sigmodal curve is $-3.0\ MPa$ whereas the P_{50} of the Exponential curve is $-1.0\ MPa$.

The 14 assessed vulnerability curves are shown and discussed in the annexes (see chapter 8.1).

2.6 Statistical analyses

The dataset groups (i.e., group 1, group 2 and group 3) are composed of data collected with different methodologies. Therefore, as first step, the relationships between different variables (i.e., P_{50} and PA_{AR}) were analyzed separately for each dataset group. Then, if the same variables were present in different dataset groups, the comparability of the slopes (β) of the found linear regressions for the same relationships between variables in different dataset groups, was verified with One-way ANOVA tests. If no significant difference was found for a specific relationship, and therefore different dataset groups were showing a comparable trend for a given relationship, the regressions were fitted considering together the data coming from the tested dataset groups (i.e., group 2 and group 3) as to work on a bigger sample size. These statistical analyses are available in the annexes (see chapter 8.2).

After validating their comparability between different dataset groups, the relationships between P_{50} and PA_{AR}, P_{50} and F_a, P_{50} and MC_a, C_d and MC_a were assessed with log_{10}-transformed data to comply with assumptions of normality and homoscedasticity (Zar 1999; Zuur et al. 2010). The relationships between P_{50} and C_d, P_{50} and V_a, F_a and PA_{AR}, were fitted using linear regressions.

The statistical difference of the data distribution of P_{50}, PA_A, PA_R, PA_{AR}, F_a, MC_a, C_d and K_s between different functional groups (i.e., angiosperms and gymnosperms) was tested with the Mann-Whitney Rank Sum Test as it doesn't require the normality distribution of the input dataset. For these comparisons, data coming from all the three dataset groups (i.e., group 1, group 2, group 3) where considered. These statistical analyses are available in the annexes (see chapter 8.3).

Normality tests, linear regressions fitting and one-way ANOVA tests were performed using RStudio version 1.1.423. Mann-Whitney Rank Sum tests were run using SigmaPlot version 12.0.

3. Results

3.1 Statistical validation of the relationships between variables across dataset groups

A dataset composed of three data groups was assessed. Group 1 is made of data coming from literature, group 2 combines xylem vulnerability measurements coming from literature, with anatomical analyses made on our own while group 3 contains species whose measurements were all made from us. The data of this last group are the result of 3-4 replicates per species, therefore compensating for the low sample size (N=14) (see chapter 2.2). The compiled dataset was used to assess the relationships between embolism vulnerability and xylem anatomical characteristics.

The comparability of all the tested relationships between variables across different dataset groups (i.e., group 1, group 2 and group 3 for PA_{AR}~P_{50} relationship) was checked. All these relationships between variables resulted comparable across the different dataset groups. Therefore, in order to work on a bigger sample size, data coming from different dataset groups were considered together.

An in-detail description of the statistical tests assessed for validating the relationships between variables across different dataset groups is available in the annexes (see chapter 8.2).

3.2 Relationships between hydraulic and anatomical traits

3.2.1 PA_{AR} ~ P_{50}

Our working hypothesis was to test if more vulnerable species to cavitation were presenting a higher parenchyma amount, allowing them to storage and utilise non-structural carbohydrates more effectively throughout the xylem and therefore presenting more efficient refilling mechanisms (see chapter 1.3). The relationship between the total parenchyma amount (PA_{AR}) and the xylem vulnerability to embolism (P_{50}) was assessed. Angiosperms and gymnosperms species were considered separately, as they present different anatomical features (i.e., vessels and tracheids respectively), and different hydraulic safety margins (i.e., narrower

in angiosperms and wider in gymnosperms), thus influencing their behaviour under drought conditions (see chapter 1.2.3).

A significant ($p < 0.001$) (Table 3.1) positive trend was found for angiosperms (Figure 3.1) with species being more vulnerable to cavitation (i.e., less negative P_{50}) presenting a higher total parenchyma amount. No clear trend ($p > 0.05$) (Table 3.1) was found for the PA_{AR}~P_{50} relationship in gymnosperms (Figure 3.1) showing no increase in PA_{AR} in parallel with an increased xylem vulnerability (i.e., less negative P_{50}). For this reason, further analyses were focused only on angiosperms.

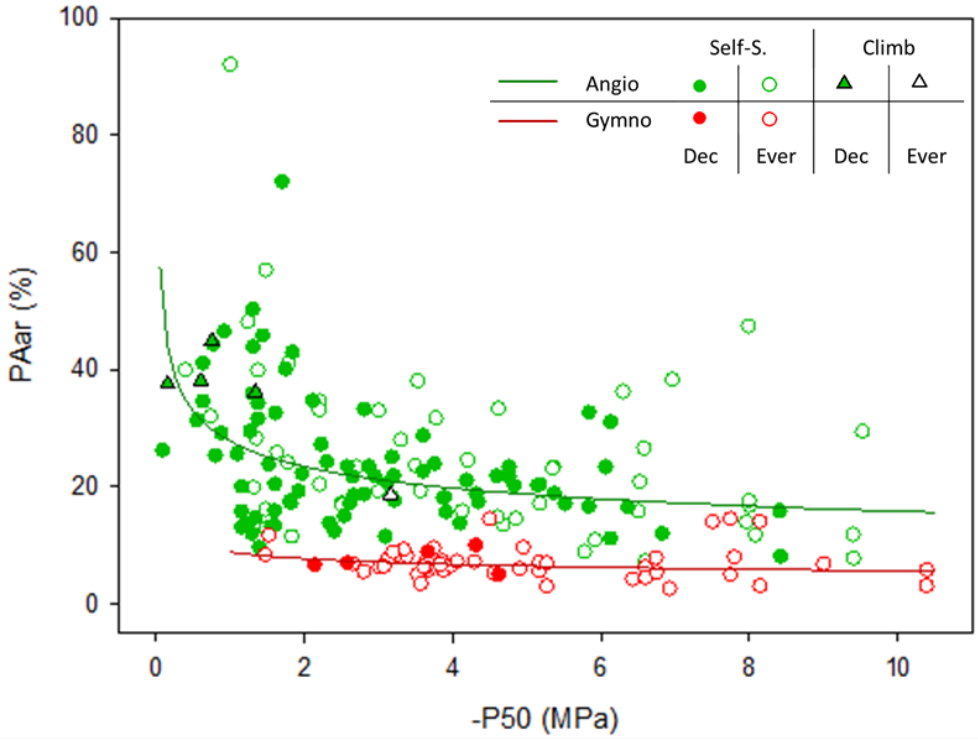

Figure 3.1: Scatterplot of the relationship between PA_{AR} and P_{50} for angiosperms ("Angio", green) and gymnosperms ("Gymno", red). See also the distribution of deciduous ("Dec", filled symbols) and evergreen ("Ever", empty symbols) species and the distribution of climbers ("Climb", triangles) and self-supporting ("Self-S.", circles) species. Fitted power regressions are also shown.

		R^2	F	DF	p-value
PA_{AR}~P_{50}	A	0.17	29.39	139	< 0.001
PA_{AR}~P_{50}	G	0.030	2.606	51	> 0.05

Table 3.1: Indices describing the PA_{AR}~P_{50} regression for angiosperms (A) and gymnosperms (G). In order to obtain linear regression models, data were Log_{10}-transformed.

3.2.2 PA_{AR} ~ P_{50}, F_a ~ P_{50}, V_a ~ P_{50}

Angiosperms' xylem is composed of three main functional structures: parenchyma cells (PA_{AR}) accounting for metabolically active processes, fibres (F_a) conferring elasticity and structural support and vessels (V_a) transporting water (see chapter 1.2.1). In response to an increase of PA_{AR} with an increased xylem vulnerability to embolism (i.e., P_{50} less negative), a variation of F_a and V_a in the wood are expected.

A significant ($p < 0.001$) negative trend between F_a and P_{50} was found (Figure 3.2, Table 3.2) with species being more vulnerable to cavitation presenting a lower amount of F_a. No clear trend ($p > 0.05$) was found for V_a~P_{50} relationship (Figure 3.2, Table 3.2).

Instead, the volume of wood occupied by vessels (V_a) was rather similar across species and its total variability (~$10 - 25\%$ of the total wood volume) was not related to xylem vulnerability to embolism (P_{50}) (Fig. 3.2).

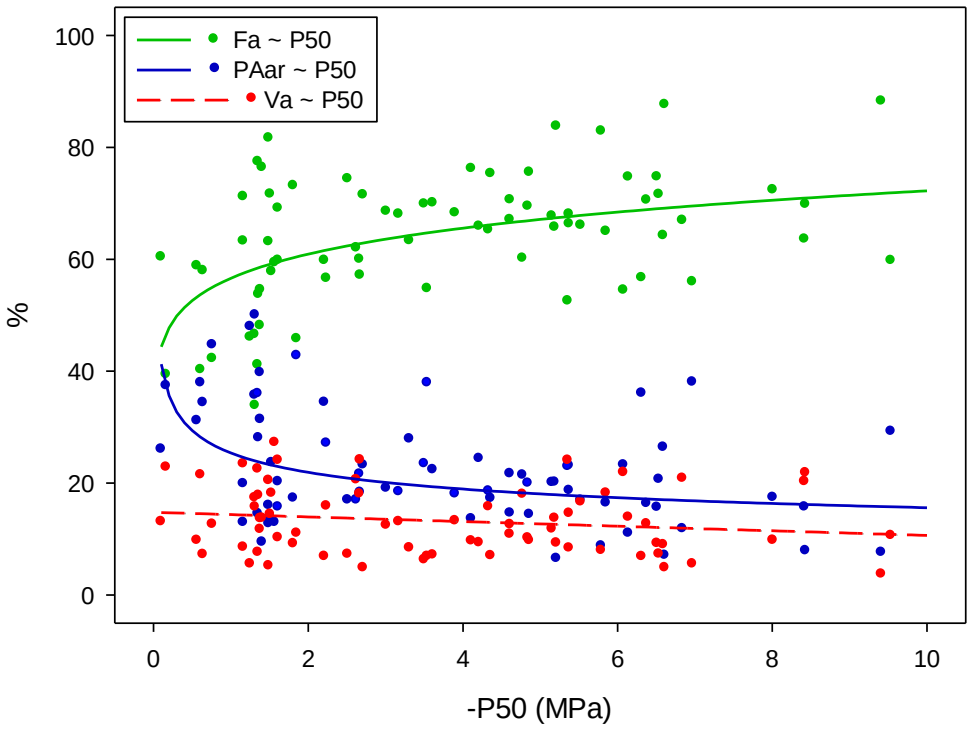

Figure 3.2: Scatterplot of the relationship between F_a and P_{50} (green), PA_{AR} and P_{50} (blue) and between V_a and P_{50} (red) for angiosperms. Fitted power regression for $F_a \sim P_{50}$ and $PA_{AR} \sim P_{50}$ relationships and fitted linear regression for $V_a \sim P_{50}$ relationship are also shown.

	R^2	F	DF	p-value
$F_a \sim P_{50}$	0.24	23.4	71	< 0.001
$PA_{AR} \sim P_{50}$	0.16	15.27	72	< 0.001
$V_a \sim P_{50}$	0.015	2.101	71	> 0.05

Table 3.2: Indices describing the $F_a \sim P_{50}$, $PA_{AR} \sim P_{50}$ and $V_a \sim P_{50}$ regressions. In order to obtain linear regression models, data of the $F_a \sim P_{50}$ and $PA_{AR} \sim P_{50}$ relationships were Log_{10}-transformed.

3.2.3 F_a ~ PA_{AR}

According to the findings of the previous paragraph (see chapter 3.2.2) and figure 3.2 itself, we found an inverse relationship between F_a (i.e., the overall amount of fibres in the wood) and PA_{AR} (i.e., the overall amount of parenchyma cells in the wood). An increase of parenchyma volume seems to be associated with a

reduction in fibres volume. Therefore, a significant ($p < 0.001$) negative relationship, explaining most of the variability ($R^2 = 0.73$) between F_a and PA_{AR} was found (Figure 3.3, Table 3.3) indicating that F_a and PA_{AR} are inversely related. If a species has a greater volume of parenchyma cells in the wood, it will produce a lower amount of fibres.

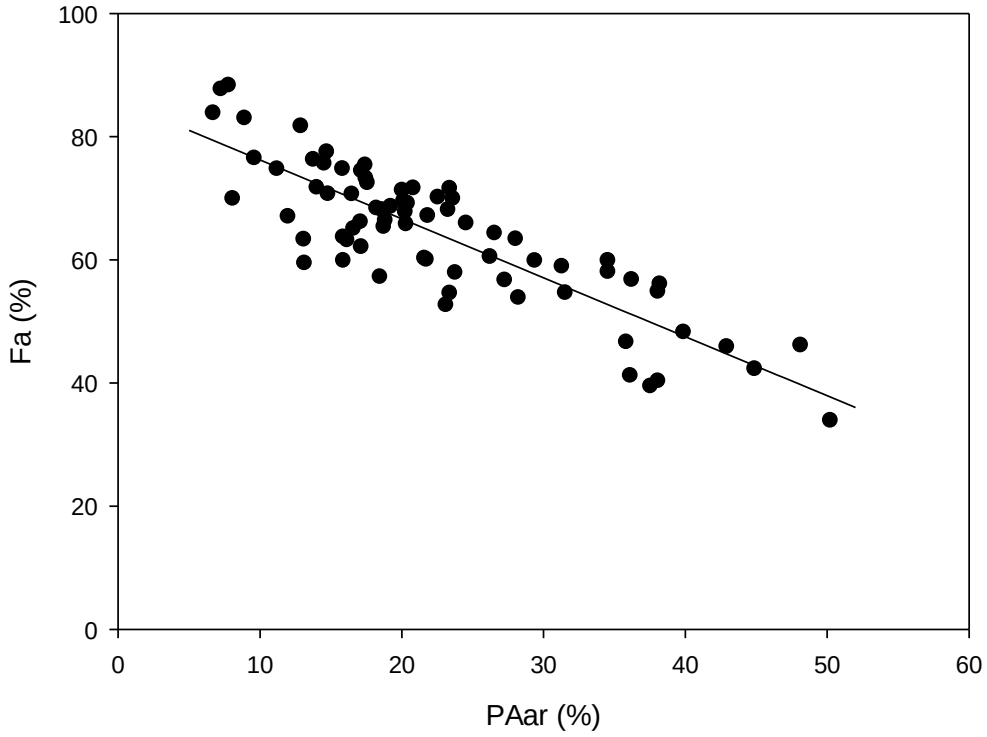

Figure 3.3: Scatterplot of the relationship between F_a and PA_{AR} for angiosperms. Fitted linear regression is also shown.

	R^2	F	DF	p-value
$F_a \sim PA_{AR}$	0.73	193.3	71	< 0.001

Table 3.3: Indices describing the $F_a \sim PA_{AR}$ linear regression.

3.2.4 C_d ~ MC_a

As it was previously shown (see chapter 3.2.2), the total volume of wood occupied by vessels (V_a) seems to vary within a short range ($10 - 25\%$) of total

wood volume irrespectively to the variation of the vulnerability to cavitation of the xylem (P_{50}). From an anatomical point of view, the size of the vessels, expressed by the mean conduit area (MC_a), and the number of vessels per unit area, described by the conduit density (C_d), are known to influence xylem vulnerability to embolism (P_{50}) (see chapter 1.2.3). The conduits occupying this given wood volume (V_a) are therefore expected to vary in size and frequency. The $C_d \sim MC_a$ relationship was tested.

A significant ($p < 0.001$) negative relationship, explaining most of the variability ($R^2 = 0.79$) between C_d and MC_a was found (Figure 3.4, Table 3.4) showing that C_d and MC_a are inversely related. An increase of conduit size is therefore associated with a reduction in conduit density.

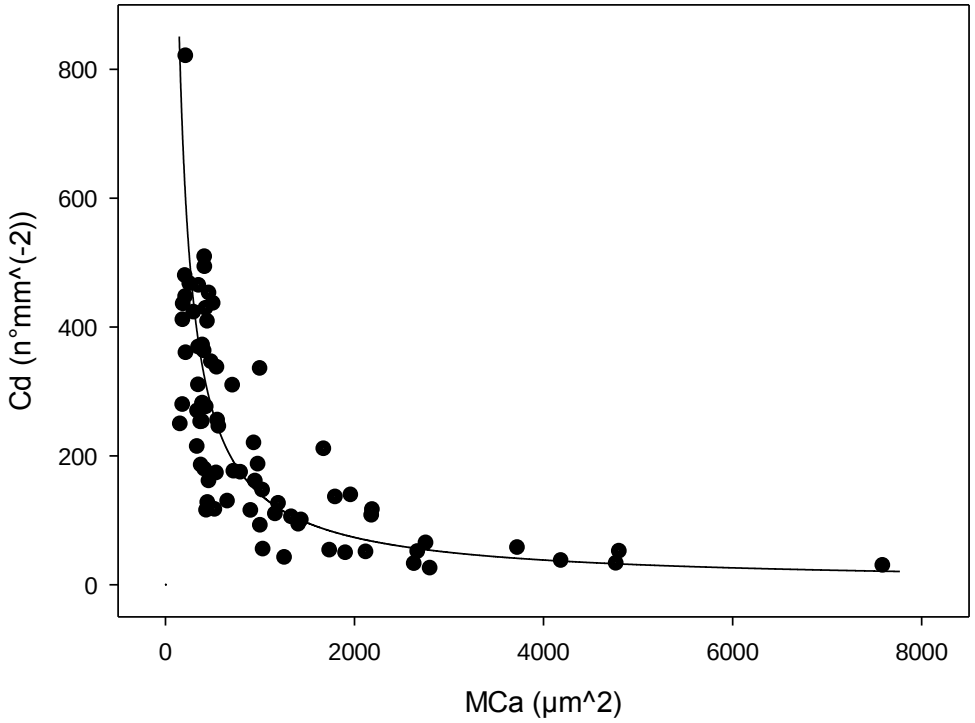

Figure 3.4: Scatterplot of the relationship between C_d and MC_a for angiosperms. Fitted power regression is also shown.

	R^2	F	DF	p-value
$C_d \sim MC_a$	0.79	261.5	69	< 0.001

Table 3.4: Indices describing the $C_d \sim MC_a$ regression. In order to obtain a linear regression model, data were Log_{10}-transformed.

3.2.5 $C_d \sim P_{50}$, $MC_a \sim P_{50}$

As it is shown in the previous paragraph (see chapter 3.2.4), C_d (i.e., the frequency of conduit for a given wood area) and MC_a (i.e., the mean area of xylem conduits) are inversely related. Both parameters are known to influence xylem vulnerability to embolism, expressed by P_{50} (i.e., the water potential at which 50% of the total xylem conductivity is lost). In fact, wider and less dense vessels are usually associated with a higher xylem vulnerability to embolism (see chapter 1.2.3). The $C_d \sim P_{50}$ and $MC_a \sim P_{50}$ relationships were therefore tested.

Both $C_d \sim P_{50}$ and $MC_a \sim P_{50}$ relationships were significant ($p < 0.001$) (Table 3.5). A negative trend was found between C_d and P_{50} (Figure 3.5a), with species more vulnerable to cavitation (i.e., less negative P50) presenting a lower number of conduits for a given wood volume (C_d). A positive trend was found between MC_a and P_{50} (Figure 3.5b), with species more vulnerable to cavitation presenting larger vessels.

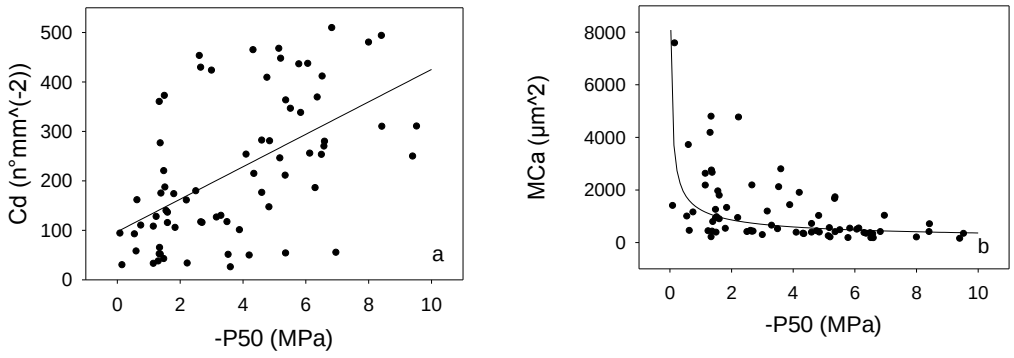

Figure 3.5: Scatterplot of the relationship between C_d and P_{50} (a) and between MC_a and P_{50} (b) for angiosperms. Fitted linear regression for $C_d \sim P_{50}$ relationship (a) and fitted power regression for $MC_a \sim P_{50}$ relationship (b) are also shown.

	R^2	F	DF	p-value
$C_d \sim P_{50}$	0.29	30.2	70	< 0.001
$MC_a \sim P_{50}$	0.25	24.22	68	< 0.001

Table 3.5: Indices describing the $C_d \sim P_{50}$ and $MC_a \sim P_{50}$ regressions. In order to obtain a linear regression model, data of the $MC_a \sim P_{50}$ relationship were Log_{10}-transformed.

3.3 Anatomical and hydraulic variability between functional groups

The variability of anatomical traits (percentage area of axial parenchyma (PA_A), percentage area of radial parenchyma (PA_R), total parenchyma (PA_{AR}) and fibres area (F_a), mean conduit area (MC_a), conduit density (C_d, expressing the number of vessels per unit area), theoretical hydraulic conductivity (K_S, that is the sum of each single vessel conductivity, estimated with Hagen-Poiseuille low, divided by the xylem area), and the hydraulic vulnerability to cavitation (P_{50}), was also compared between different functional groups: angiosperms (*A*) vs. gymnosperms (*G*), deciduous (*D*) vs. evergreen (*E*) species, climbers (*C*) vs. self-supporting (*S*) species. This comparison was carried out both (i) to test for differences in anatomical and hydraulic parameters between different functional groups, and (ii) to verify if these differences were in accordance with the findings on the general trends between hydraulic and anatomical traits (see chapter 3.2). The statistical analyses performed and the boxplots showing the differences in anatomical and hydraulic parameters between different functional groups are available in the annexes (see chapter 8.3).

Differences in most of the anatomical and hydraulic parameters were found in different functional groups (i).

The differences in anatomical and hydraulic parameters between different functional groups are in accordance with the findings on the general trends between hydraulic and anatomical traits previously discussed (ii) (see chapter 3.2). Angiosperm, deciduous and climbers species generally are more vulnerable to cavitation (i.e., they present a less negative P_{50}) than gymnosperms, evergreen ans self-supporting species respectively. Functional groups more vulnerable to cavitation (i.e., less negative P_{50}) were found to have a higher amount of

parenchyma fractions (axial (PA_A) and radial (PA_R)) and therefore also total parenchyma amount (PA_{AR}), a lower amount of fibres in the wood (F_a), a lower number of conduits per unit volume (C_d) and larger conduits (MC_a), in agreement with the findings explained in the previous chapter 3.2.

In addition, more hydraulically vulnerable functional groups (i.e., generally presenting a less negative P_{50}), were showing greater xylem specific hydraulic conductivity (K_s) therefore presenting a more efficient water transport system.

4. Discussion

4.1 Wood anatomy and cavitation resistance

In angiosperms, a significant trend between the xylem vulnerability to embolism (P_{50}) and the overall parenchyma volume (PA_{AR}) was found (Figure 3.1). The species presenting a higher vulnerability to embolism have a higher percentage of parenchyma cells in the xylem. It was shown that angiosperms generally operate at very narrow hydraulic safety margins (HSM), allowing transpiration when soil water availability is reduced and therefore soil water potential (ψ_{soil}) decreases, being highly exposed to xylem embolism formation (Choat et al. 2012), causing a reduction in productivity and therefore facing the risk of hydraulic failure and ultimately death (see chapter 1.2.3). In such a context, angiosperms are expected to possess a metabolically active embolism reversal mechanism (Nardini et al. 2011) based on the translocation of solutes and non-structural carbohydrates (NSC) (De Baerdemaeker et al. 2017) from parenchyma cells to the cavitated vessels (Zwieniecki and Holbrook 2009) (see chapter 1.2.3). The results suggest, in accordance with our working hypothesis (see chapter 1.3), that more vulnerable species would rely on a more efficient xylem refilling mechanism by producing a higher parenchyma amount in the wood. The greater xylem parenchyma volume would allow to both exchange NSC more efficiently (Plavcová and Jansen 2015) and storage a greater NSC amount (Plavcová et al. 2016) throughout the xylem, supporting the proposed metabolism-based embolism refilling scenario

(Zwieniecki and Holbrook 2009) whose energy is provided by parenchyma cells (Secchi and Zwieniecki 2011).

In gymnosperms, instead, non-significant trend was found between the xylem vulnerability to embolism (P_{50}) and the overall parenchyma volume (PA_{AR}) (figure 3.1). Gymnosperms generally have a higher HSM than angiosperms (Choat et al. 2012) and tend to close their stomata as already at a relatively poorly dehydrated soil, i.e. characterized by relatively high (i.e., not much negative) ψ_{soil} as angiosperms, reducing embolism formation and cavitation risk. Earlier stomata closure reduces carbon uptake and therefore the carbon available for producing and maintaining living tissues. The low production of living tissues in the wood (i.e., low xylem parenchyma amount) would allow reducing maintenance costs. As the PA_{AR}~P_{50} relationship for gymnosperms was not significant, parenchyma tissues do not seem to have an important role in xylem embolism reversal. It was shown that gymnosperms present a great parenchyma amount at leaf level therefore suggesting a preferential priority of xylem embolism repair in the distal portions (Johnson et al. 2012), where tension is highest (Petit et al. 2018), thus preventing the exposure of the remaining xylem to embolism formation. Moreover, smaller conduits such as tracheids can better cope with the water tensile metastable status due to greater adhesive forces for a unit of water volume (Hacke et al. 2017), facing lower risk of hydraulic failure. In addition, gymnosperms may replace embolized conduits with new growth (Brodribb et al. 2010; Brodersen and McElrone 2013).

As our major interest was to investigate the anatomical features linked to the tolerance of cavitation, further analyses were performed on angiosperms only. Angiosperms' wood is composed by three main elements: living and metabolically active tissues (i.e., parenchyma cells), fibres that confer mechanical support and storage water, and vessels accounting for water transport (Ziemińska et al. 2015). The percentage area occupied by fibres (F_a) and the percentage area occupied by parenchyma (PA_{AR}) resulted of similar significance for the variation in P_{50} (i.e., the water potential at which 50% of the total xylem conductivity is lost) (Figure 3.2), with species with higher vulnerability having higher amount of parenchyma cells, as to possess more living tissues and more efficient metabolic

processes. Species presenting a lower vulnerability to embolism have a higher amount of fibres, therefore accounting for more structural support and water storage. According to these findings, F_a and PA_{AR} were shown to be strongly negatively related (Figure 3.3). This result provides a functional explanation to the widely reported observation (Hacke and Sperry 2001; Jacobsen et al. 2005; Lens et al. 2013; Rosner 2017) of species that are less vulnerable to cavitation having a higher wood density (i.e., that is mainly due to the high amount of fibres), a parameter not directly linked to plant hydraulic functioning (Lachenbruch and McCulloh 2014).

While no trend emerged between the overall volume of wood occupied by fibres (V_a) and the P_{50} (Figure 3.2), a clear inverse relationship emerged between C_d (i.e., the frequency of conduit for a given wood area) and MC_a (i.e., the mean area of xylem conduits) (Figure 3.4). This finding is in agreement with the widely described geometrical constraint of the conduits packing limit (Martinez-Vilalta et al. 2012) suggesting that a plant, in a given wood volume, can either produce few big conduits or many small ones. Smaller conduits are more resistant to xylem embolism formation (see chapter 1.2.3) and are therefore safer than big vessels from a hydraulic point of view. By contrast, small vessels are less efficient in transporting water (i.e., low xylem specific hydraulic conductivity (K_s)) than relatively bigger ones, for the Heagen-Poiseuille law (Zimmermann 1983; Tyree and Ewers 1991) (see chapter 1.2.3).

As to confirm these concepts, species with narrower and denser vessels were found to have a lower vulnerability to embolism (Figure 3.5), in line with many other studies (Sperry and Tyree 1988; Tyree and Sperry 1989; Cochard and Tyree 1990; Hacke et al. 2006; Martinez-Cabrera et al. 2009; Christman et al. 2012).

This may be the reason why evolution has favoured, in dry environments, plants producing narrower vessels (von Arx et al. 2012; Pfautsch et al. 2016; Larter et al. 2017), reducing growth rate (Wheeler et al. 2005), and accounting for different sapwood rings to maintain a sufficient sapwood conductivity (Petit et al. 2016).

Nevertheless, apart from the two discussed inverse relationships ($C_d \sim MC_a$ and $F_a \sim PA_{AR}$), the other trends found are only partially explaining the observed

variability (low R^2) (see chapter 3.3). This may be related to the fact that a major part of our data is coming from literature, therefore increasing the factors influencing data variability (i.e., different measuring methods, different operators). In addition, the anatomical and hydraulic measurements were not related to tree size (Rosell et al. 2017; Petit et al. 2018; Prendin et al. 2018b) lowering data comparability for the presence of anatomical (Bettiati et al. 2012) and hydraulic (Mencuccini and Comstock 1997) adjustments to different positions within the crown.

It would be interesting to enrich the dataset with measurements of both stomatal sensitivity to leaf water potential (Bhaskar et al. 2007), therefore measuring the relatively isohydric and anisohidric water use strategy of plants, and the carbon investments in relation to hydraulic properties, as both are strongly related to xylem characteristics (Nardini et al. 2012; Klein 2014). Moreover, as phloem also plays key functions in the parenchyma network (Nardini et al. 2011), further analyses may be including measurements of phloem parenchyma volume as well.

4.2 Variability of anatomical and hydraulic traits between functional groups

The found differences of anatomical and hydraulic traits between different functional groups (angiosperms (*A*) vs. gymnosperms (*G*), deciduous (*D*) vs. evergreen (*E*) species, climbers (*C*) vs. self-supporting (*S*) species) are in accordance with the previously discussed findings on wood anatomy and cavitation resistance (see chapter 4.1). A description of the differences found between functional groups and the relative ecological implications follow. The graphs and the statistical analyses performed are available in the annexes (see chapter 8.3).

4.2.1 Angiosperms vs. gymnosperms

Angiosperms (*A*) and gymnosperms (*G*) present peculiar anatomical and hydraulic differences (Johnson et al. 2012)(see chapter 1.2.1): *A* rely on vessels for long distance water transport, while *G* have tracheids. This difference is reflected in the different mean conduit area (MC_a) and conduit density (C_d) between *A* and *G*, being probably also related to the known different vessel length (see chapter

1.2.1). *G* have more numerous but smaller conduits than *A*, also explaining both the lower hydraulic vulnerability (P_{50}) and the lower xylem specific hydraulic conductivity (K_s). Moreover, *A* tend to have an overall higher parenchyma volume (PA_{AR}), that is also shown for both parenchyma fractions (PA_A, PA_R).

4.2.2 Deciduous vs. evergreen

The findings on deciduous (*D*) and evergreen (*E*) are also complying the expectances (see chapter 2.1.1). Deciduous species need to mobilise more sugars at the beginning of spring to build a new crown, while evergreen species produce hard long lasting leaves. This ecological difference is reflected in a general higher amount of parenchyma cells (PA_{AR}) in *D*. This the higher parenchyma amount is also associated in *D* with a lower number of vessels per unit area (C_d) and a higher mean conduit area (MC_a), relying on a more efficient refilling mechanism to compensate for the hydraulic vulnerability of the xylem system (i.e., less negative P_{50}) thus being more efficient (i.e., higher xylem hydraulic conductivity (K_s)). *E* species would rely on a relatively more conservative strategy, presenting a generally higher resistance to xylem embolism (P_{50}), counting on safer but less efficient vessels (lower MC_a and K_s, higher C_d), and therefore requiring a less efficient refilling mechanism. In fact, they generally have lower parenchyma amount (PA_{AR}, PA_A, PA_R).

4.2.3 Climbers vs. self-supporting

The found differences between climbers (*C*) and self-supporting species (*S*) are weak due to very low *C* group size ($N = 4$) but indicative. Climbers, usually fast growing plants that take advantage of other plants for growing. They therefore present a higher conductivity (K_s) and a more efficient (higher MC_a, lower C_d) but more vulnerable xylem system (P_{50} less negative) than self-supporting that rely on a more conservative strategy for preserving the xylem functionality (Johnson et al. 2013). *C* therefore generally have a higher parenchyma amount than *S*, in accordance with other published papers (Morris et al. 2016), as to comply with

low safety of the water transport system. S would invest relatively more in F_a production as to build a structure capable of supporting the plant.

4.3 Hydraulic experiments

The hydraulic analyses performed proved the technique of the pressure collar for measuring the hydraulic vulnerability of plants. The assessed vulnerability curves (VCs) provided an extracted value of P_{50} that is quite reliable (95% confidence interval $\leq 1\ MPa$), despite few cases (i.e., *Quercus ilex* L., *Quercus pubescens* Willd.). The developed VCs are the results of 3-4 different replicates, such as plant branches that, despite the great attention paid in choosing and preparing the samples to make hydraulic experiments on (see chapter 2.5), present an intraspecific variability for the resistance to xylem embolism (Anderegg 2015). Moreover, even if the double-ended pressure sleeve was located all the times at mid-length of the branches while performing the experiments, no standardisation for the distance from the apex (Anfodillo et al. 2013; Prendin et al. 2018b) and for the effect of longitudinal growth (Carrer et al. 2015) was made. The measured P_{50} may therefore be influenced by its natural variability from the stem apex towards the base (Hacke et al. 2006; Hacke et al. 2017), thus resulting less accurate for some species (i.e., *Quercus ilex* L., *Quercus pubescens* Willd.). Moreover, for getting clearer results, these measurements should have been carried out on the apical part of the branches, where tension is highest (Petit et al, 2018). All these aspects, with the low sample size, may explain the weak trends between P_{50} and other anatomical variables for species in dataset group 3, despite the anatomical and hydraulic measurements are the results of the mean of 3-4 replicates.

A limit of the pressure collar technique is related to the total pressure that the system can apply to the branch under examination. In fact, this constraints the plants whose VCs can be generated and relative P_{50} extracted by that species showing a PLC of about 70-80% within 12 MPa of applied pressure and therefore theoretically having a P_{50} ranging from 0 to about 10 MPa. For these species, xylem vulnerability must be assessed with other techniques (Cochard et al. 2013).

5. Conclusions

The hydraulic vulnerability to embolism (P_{50}) is strongly related with xylem anatomical structures and is determined in particular by the anatomical and hydraulic properties of the conduits. Wider and therefore less dense vessels determine a higher vulnerability of xylem to embolism (i.e., P_{50} less negative), thus indicating a more efficient water transport system. In these conditions, angiosperms tend to produce a greater amount of living cells that would allow to both storage a greater amount of non-structural carbohydrates and utilize them more efficiently throughout the xylem, therefore relying on more efficient refilling mechanisms as to compensate for the low safety of the water transport system.

6. Acknowledgements

I thank all the gardeners of the botanic garden of the University of Padua for helping me in finding and collecting the braches from the different species cultivated in the botanic garden. I warmly thank Natasa Kiorapostolou, who supervised me diligently and kindly throughout my internship period in TeSAF department (University of Padua), and PhD Tadeja Savi, who enthusiastically assisted me during the hydraulic experiments at the "Scienze della Vita" department (University of Trieste). I want also to thank Francesco Petruzzellis and Prof. Chiara Romualdi for supporting me in making the statistical analyses on my dataset. I finally want to thank my supervisors, who gave me the opportunity to carry out this research project and gently mentored me.

7. References

Adams, H. D., Zeppel, M. J. B., Anderegg, W. R. L., Hartmann, H., Landhäusser, S. M., Tissue, D. T., … McDowell, N. G. (2017). A multi-species synthesis of physiological mechanisms in drought-induced tree mortality. *Nature Ecology & Evolution*, *1*(9), 1285–1291. https://doi.org/10.1038/s41559-017-0248-x

Akkemik, U., & Yaman, B. (2012). Wood anatomy of Eastern Mediterranean species. Kessel.

Allen, C. D., Macalady, A. K., Chenchouni, H., Bachelet, D., McDowell, N., Vennetier, M., … Cobb, N. (2010). A global overview of drought and heat-induced tree mortality reveals emerging climate change risks for forests. *Forest Ecology and Management*, *259*(4), 660–684. https://doi.org/10.1016/j.foreco.2009.09.001

Almeida-Rodriguez, A. M., Cooke, J. E. K., Yeh, F., & Zwiazek, J. J. (2010). Functional characterization of drought-responsive aquaporins in Populus balsamifera and Populus simonii×balsamifera clones with different drought resistance strategies. *Physiologia Plantarum*, *140*(4), 321–333. https://doi.org/10.1111/j.1399-3054.2010.01405.x

Anderegg, W. R. L. (2015). Spatial and temporal variation in plant hydraulic traits and their relevance for climate change impacts on vegetation. *New Phytologist*, *205*(3), 1008–1014. https://doi.org/10.1111/nph.12907

Anderegg, W. R. L., Kane, J. M., & Anderegg, L. D. L. (2013). Consequences of widespread tree mortality triggered by drought and temperature stress. *Nature Climate Change*, *3*(1), 30–36. https://doi.org/10.1038/nclimate1635

Anfodillo, T., Petit, G., & Crivellaro, A. (2013). Axial conduit widening in woody species: a still neglected anatomical pattern. *IAWA Journal*, *34*(4), 352–364. https://doi.org/10.1163/22941932-00000030

Angyalossy, V., Pace, M. R., Evert, R. F., Marcati, C. R., Oskolski, A. A., Terrazas, T., … Baas, P. (2016). IAWA List of Microscopic Bark Features. *IAWA Journal*, *37*(4), 517–615. https://doi.org/10.1163/22941932-20160151

Arend, M., & Fromm, J. (2007). Seasonal change in the drought response of wood cell development in poplar. *Tree Physiology*, *27*(7), 985–992. https://doi.org/10.1093/treephys/27.7.985

Attia, Z., Domec, J., Oren, R., Way, D. A., & Moshelion, M. (2015). Growth and physiological responses of isohydric and anisohydric poplars to drought. *Journal of Experimental Botany*, *66*(14), 4373–4381. https://doi.org/10.1093/jxb/erv195

Becker, P., Gribben, R. J., & Lim, C. M. (2000). Tapered conduits can buffer hydraulic conductance from path-length effects. *Tree Physiology*, *20*(14), 965–967. https://doi.org/10.1093/treephys/20.14.965

Bennett, A. C., McDowell, N. G., Allen, C. D., & Anderson-Teixeira, K. J. (2015). Larger trees suffer most during drought in forests worldwide. *Nature Plants*, *1*(10), 15139. https://doi.org/10.1038/nplants.2015.139

Bettiati, D., Petit, G., & Anfodillo, T. (2012). Testing the equi-resistance principle of the

xylem transport system in a small ash tree: empirical support from anatomical analyses. *Tree Physiology*, *32*(2), 171–177. https://doi.org/10.1093/treephys/tpr137

Bhaskar, R., Valiente-Banuet, A., & Ackerly, D. D. (2007). Evolution of hydraulic traits in closely related species pairs from mediterranean and nonmediterranean environments of North America. *New Phytologist*, *176*(3), 718–726. https://doi.org/10.1111/j.1469-8137.2007.02208.x

Birdsey, R., & Pan, Y. (2011). Drought and dead trees. *Nature Climate Change*, *1*(9), 444–445. https://doi.org/10.1038/nclimate1298

Boisvenue, C., & Running, S. W. (2006). Impacts of climate change on natural forest productivity - evidence since the middle of the 20th century. *Global Change Biology*, *12*(5), 862–882. https://doi.org/10.1111/j.1365-2486.2006.01134.x

Bonan, G. B. (2008). Forests and Climate Change: Forcings, Feedbacks, and the Climate Benefits of Forests. *Science*, *320*(5882), 1444–1449. https://doi.org/10.1126/science.1155121

Brienen, R. J. W., Lebrija-Trejos, E., Zuidema, P. A., & Martìnez-Ramos, M. (2010). Climate-growth analysis for a Mexican dry forest tree shows strong impact of sea surface temperatures and predicts future growth declines. *Global Change Biology*, *16*(7), 2001–2012. https://doi.org/10.1111/j.1365-2486.2009.02059.x

Brodersen, C. R., & McElrone, A. J. (2013). Maintenance of xylem Network Transport Capacity: A Review of Embolism Repair in Vascular Plants. *Frontiers in Plant Science*, *4*(April), 1–11. https://doi.org/10.3389/fpls.2013.00108

Brodersen, C. R., McElrone, A. J., Choat, B., Matthews, M. A., & Shackel, K. A. (2010). The Dynamics of Embolism Repair in Xylem: In Vivo Visualizations Using High-Resolution Computed Tomography. *Plant Physiology*, *154*(3), 1088–1095. https://doi.org/10.1104/pp.110.162396

Brodribb, T. J. (2009). Xylem hydraulic physiology: The functional backbone of terrestrial plant productivity. *Plant Science*, *177*(4), 245–251. https://doi.org/10.1016/j.plantsci.2009.06.001

Brodribb, T. J., Bowman, D. J. M. S., Nichols, S., Delzon, S., & Burlett, R. (2010). Xylem function and growth rate interact to determine recovery rates after exposure to extreme water deficit. *New Phytologist*, *188*(2), 533–542. https://doi.org/10.1111/j.1469-8137.2010.03393.x

Bryden, H. L., King, B. A., McCarthy, G. D., & McDonagh, E. L. (2014). Impact of a 30% reduction in Atlantic meridional overturning during 2009–2010. *Ocean Science*, *10*(4), 683–691. https://doi.org/10.5194/os-10-683-2014

Bryden, H. L., Longworth, H. R., & Cunningham, S. A. (2005). Slowing of the Atlantic meridional overturning circulation at 25° N. *Nature*, *438*(7068), 655–657. https://doi.org/10.1038/nature04385

Canny, M. (1995). A New Theory for the Ascent of Sap—Cohesion Supported by Tissue Pressure. *Annals of Botany*, *75*(4), 343–357. https://doi.org/10.1006/anbo.1995.1032

Carrer, M., von Arx, G., Castagneri, D., & Petit, G. (2015). Distilling allometric and environmental information from time series of conduit size: the standardization issue and its relationship to tree hydraulic architecture. *Tree Physiology*, *35*(1), 27–33. https://doi.org/10.1093/treephys/tpu108

Choat, B., Jansen, S., Brodribb, T. J., Cochard, H., Delzon, S., Bhaskar, R., … Zanne, A. E. (2012). Global convergence in the vulnerability of forests to drought. *Nature*, *491*(7426), 752–755. https://doi.org/10.1038/nature11688

Christman, M. A., Sperry, J. S., & Smith, D. D. (2012). Rare pits, large vessels and extreme vulnerability to cavitation in a ring-porous tree species. *New Phytologist*, *193*(3), 713–720. https://doi.org/10.1111/j.1469-8137.2011.03984.x

Clearwater, M. J., & Clark, C. J. (2003). In vivo magnetic resonance imaging of xylem vessel contents in woody lianas. *Plant, Cell and Environment*, *26*(8), 1205–1214. https://doi.org/10.1046/j.1365-3040.2003.01042.x

Cochard, H., Badel, E., Herbette, S., Delzon, S., Choat, B., & Jansen, S. (2013). Methods for measuring plant vulnerability to cavitation: a critical review. *Journal of Experimental Botany*, *64*(15), 4779–4791. https://doi.org/10.1093/jxb/ert193

Cochard, H., & Tyree, M. T. (1990). Xylem dysfunction in Quercus: vessel sizes, tyloses, cavitation and seasonal changes in embolism. *Tree Physiology*, *6*(4), 393–407. https://doi.org/10.1093/treephys/6.4.393

Crivellaro, A., & Schweingruber, F. (2015). Stem anatomical features of Dicotyledons. Kessel, Norbert.

Cunningham, S. a, Kanzow, T., Rayner, D., Baringer, M. O., Johns, W. E., Marotzke, J., … Bryden, H. L. (2007). Temporal Variability of the Atlantic Meridional Overturning Circulation at 26.5 N. *Science*, *317*(5840), 935–938. https://doi.org/10.1126/science.1141304

Davis, S. D., Sperry, J. S., & Hacke, U. G. (1999). The Relationship between Xylem Conduit Diameter and Cavitation Caused by Freezing. *American Journal of Botany*, *86*(10), 1367. https://doi.org/10.2307/2656919

De Baerdemaeker, N. J. F., Salomón, R. L., De Roo, L., & Steppe, K. (2017). Sugars from woody tissue photosynthesis reduce xylem vulnerability to cavitation. *New Phytologist*, *216*(3), 720–727. https://doi.org/10.1111/nph.14787

De Micco, V., & Aronne, G. (2012). Morpho-anatomical traits for plant adaptation to drought. In Plant responses to drought stress (pp. 37-61). Springer, Berlin, Heidelberg.

Delzon, S., Douthe, C., Sala, A., & Cochard, H. (2010). Mechanism of water-stress induced cavitation in conifers: bordered pit structure and function support the hypothesis of seal capillary-seeding. *Plant, Cell & Environment*, *33*(12), 2101–2111. https://doi.org/10.1111/j.1365-3040.2010.02208.x

Dixon, H. H., & Joly, J. (1894). On the ascent of sap. Proceedings of the Royal Society of London, 57, 3-5.

Domec, J.-C., Scholz, F. G., Bucci, S. J., Meinzer, F. C., Goldstein, G., & Villalobos-Vega, R.

(2006). Diurnal and seasonal variation in root xylem embolism in neotropical savanna woody species: impact on stomatal control of plant water status. *Plant, Cell and Environment*, *29*(1), 26–35. https://doi.org/10.1111/j.1365-3040.2005.01397.x

Duursma, R., & Choat, B. (2017). fitplc - an R package to fit hydraulic vulnerability curves. *Journal of Plant Hydraulics*, *4*, 2. https://doi.org/10.20870/jph.2017.e002

Ennajeh, M., Nouiri, M., Khemira, H., & Cochard, H. (2011b). Improvement to the air-injection technique to estimate xylem vulnerability to cavitation. *Trees*, *25*(4), 705–710. https://doi.org/10.1007/s00468-011-0548-8

Ennajeh, M., Simões, F., Khemira, H., & Cochard, H. (2011a). How reliable is the double-ended pressure sleeve technique for assessing xylem vulnerability to cavitation in woody angiosperms? *Physiologia Plantarum*, *142*(3), 205–210. https://doi.org/10.1111/j.1399-3054.2011.01470.x

Ernakovich, J. G., Hopping, K. A., Berdanier, A. B., Simpson, R. T., Kachergis, E. J., Steltzer, H., & Wallenstein, M. D. (2014). Predicted responses of arctic and alpine ecosystems to altered seasonality under climate change. *Global Change Biology*, *20*(10), 3256–3269. https://doi.org/10.1111/gcb.12568

Fitter, A. H., & Hay, R. K. (2012). Environmental physiology of plants. Academic press.

Franks, P. J., Dracke, P. L., & Froend, R. H. (2007). Anisohydric but isohydrodynamic: seasonally constant plant water potential gradient explained by a stomatal control mechanism incorporating variable plant hydraulic conductance. *Plant, Cell and Environment*, *30*(1), 19–30. https://doi.org/10.1111/j.1365-3040.2006.01600.x

Friedrichs, D. A., Buntgen, U., Frank, D. C., Esper, J., Neuwirth, B., & Loffler, J. (2008). Complex climate controls on 20th century oak growth in Central-West Germany. *Tree Physiology*, *29*(1), 39–51. https://doi.org/10.1093/treephys/tpn003

Gleason, S. M., Westoby, M., Jansen, S., Choat, B., Hacke, U. G., Pratt, R. B., … Zanne, A. E. (2016). Weak tradeoff between xylem safety and xylem-specific hydraulic efficiency across the world's woody plant species. *New Phytologist*, *209*(1), 123–136. https://doi.org/10.1111/nph.13646

Hacke, U. G., & Sperry, J. S. (2001). Functional and ecological xylem anatomy. *Perspectives in Plant Ecology, Evolution and Systematics*, *4*(2), 97–115. https://doi.org/10.1078/1433-8319-00017

Hacke, U. G., & Sperry, J. S. (2003). Limits to xylem refilling under negative pressure in Laurus nobilis and Acer negundo. *Plant, Cell and Environment*, *26*(2), 303–311. https://doi.org/10.1046/j.1365-3040.2003.00962.x

Hacke, U. G., Sperry, J. S., Wheeler, J. K., & Castro, L. (2006). Scaling of angiosperm xylem structure with safety and efficiency. *Tree Physiology*, *26*(6), 689–701. https://doi.org/10.1093/treephys/26.6.689

Hacke, U. G., Spicer, R., Schreiber, S. G., & Plavcová, L. (2017). An ecophysiological and developmental perspective on variation in vessel diameter. *Plant, Cell & Environment*, *40*(6), 831–845. https://doi.org/10.1111/pce.12777

Hanewinkel, M., Cullmann, D. A., Schelhaas, M.-J., Nabuurs, G.-J., & Zimmermann, N. E. (2013). Climate change may cause severe loss in the economic value of European forest land. *Nature Climate Change*, *3*(3), 203–207. https://doi.org/10.1038/nclimate1687

Hansen, J., Ruedy, R., Sato, M., & Lo, K. (2010). Global Surface Temperature Change. *Reviews of Geophysics*, *48*(4), RG4004. https://doi.org/10.1029/2010RG000345

Hansen, M. C., Potapov, P. V., Moore, R., Hancher, M., Turubanova, S. A., Tyukavina, A., … Townshend, J. R. G. (2013). High-Resolution Global Maps of 21st-Century Forest Cover Change. *Science*, *342*(6160), 850–853. https://doi.org/10.1126/science.1244693

Hemp, A., Zimmermann, R., Remmele, S., Pommer, U., Berauer, B., Hemp, C., & Fischer, M. (2017). Africa's highest mountain harbours Africa's tallest trees. *Biodiversity and Conservation*, *26*(1), 103–113. https://doi.org/10.1007/s10531-016-1226-3

Hilaire, E., Young, S. a, Willard, L. H., McGee, J. D., Sweat, T., Chittoor, J. M., … Leach, J. E. (2001). Vascular Defense Responses in Rice: Peroxidase Accumulation in Xylem Parenchyma Cells and Xylem Wall Thickening. *Molecular Plant-Microbe Interactions*, *14*(12), 1411–1419. https://doi.org/10.1094/MPMI.2001.14.12.1411

IPCC (2014). Climate change 2014—impacts, adaptation, and vulnerability: regional aspects. Cambridge University Press, Cambridge.

Jacobsen, A. L., Ewers, F. W., Pratt, R. B., Paddock III, W. A., & Davis, S. D. (2005). Do Xylem Fibers Affect Vessel Cavitation Resistance? *Plant Physiology*, *139*(1), 546–556. https://doi.org/10.1104/pp.104.058404

Jacobsen, A. L., Pratt, R. B., Tobin, M. F., Hacke, U. G., Ewers, W., Plants, W., … Ewers, F. W. (2012). A global analysis of xylem vessel length in woody plants, *99*(10), 1583–1591. https://doi.org/10.3732/ajb.l200140

Jacobsen, A. L., Rodriguez-Zaccaro, F. D., Lee, T. F., Valdovinos, J., Toschi, H. S., Martinez, J. A., & Pratt, R. B. (2015). Grapevine Xylem Development, Architecture, and Function. In U. Hacke (Ed.), *Functional and Ecological Xylem Anatomy* (pp. 133–162). Cham: Springer International Publishing. https://doi.org/10.1007/978-3-319-15783-2_5

Johnson, D. M., Domec, J.-C., Woodruff, D. R., McCulloh, K. A., & Meinzer, F. C. (2013). Contrasting hydraulic strategies in two tropical lianas and their host trees. *American Journal of Botany*, *100*(2), 374–383. https://doi.org/10.3732/ajb.1200590

Johnson, D. M., McCulloh, K. A., Woodruff, D. R., & Meinzer, F. C. (2012). Hydraulic safety margins and embolism reversal in stems and leaves: Why are conifers and angiosperms so different? *Plant Science*, *195*, 48–53. https://doi.org/10.1016/j.plantsci.2012.06.010

Jump, A. S., & Penuelas, J. (2005). Running to stand still: adaptation and the response of plants to rapid climate change. *Ecology Letters*, *8*(9), 1010–1020. https://doi.org/10.1111/j.1461-0248.2005.00796.x

Kiorapostolou, N., Galiano-Pérez, L., von Arx, G., Gessler, A., & Petit, G. (2018). Structural

and anatomical responses of Pinus sylvestris and Tilia platyphyllos seedlings exposed to water shortage. *Trees*, *0*(0), 0. https://doi.org/10.1007/s00468-018-1703-2

Klein, T. (2014). The variability of stomatal sensitivity to leaf water potential across tree species indicates a continuum between isohydric and anisohydric behaviours. *Functional Ecology*, *28*(6), 1313–1320. https://doi.org/10.1111/1365-2435.12289

Koch, G. W., Sillett, S. C., Jennings, G. M., & Davis, S. D. (2004a). The limits to tree height. *Nature*, *428*(6985), 851–854. https://doi.org/10.1038/nature02417

Kozlowski, T. T., Kramer, P. J., Pallardy, S.G. (1991). The physiological ecology of woody plants. Academic press. 24-28 Oval Road, London.

Kumagai, T., & Porporato, A. (2012). Strategies of a Bornean tropical rainforest water use as a function of rainfall regime: isohydric or anisohydric? *Plant, Cell & Environment*, *35*(1), 61–71. https://doi.org/10.1111/j.1365-3040.2011.02428.x

Lachenbruch, B., & McCulloh, K. A. (2014). Traits, properties, and performance: how woody plants combine hydraulic and mechanical functions in a cell, tissue, or whole plant. *New Phytologist*, *204*(4), 747–764. https://doi.org/10.1111/nph.13035

Lack, A. J., & Evans, D. E. (2001). Plant biology. Instant notes.

Larcher, W. (1983). Physiological plant ecology. Springer-Verlag.

Larter, M., Pfautsch, S., Domec, J., Trueba, S., Nagalingum, N., & Delzon, S. (2017). Aridity drove the evolution of extreme embolism resistance and the radiation of conifer genus Callitris. *New Phytologist*, *215*(1), 97–112. https://doi.org/10.1111/nph.14545

Lens, F., Tixier, A., Cochard, H., Sperry, J. S., Jansen, S., & Herbette, S. (2013). Embolism resistance as a key mechanism to understand adaptive plant strategies. *Current Opinion in Plant Biology*, *16*(3), 287–292. https://doi.org/10.1016/j.pbi.2013.02.005

Maherali, H., Moura, C. F., Caldeira, M. C., Willson, C. J., & Jackson, R. B. (2006). Functional coordination between leaf gas exchange and vulnerability to xylem cavitation in temperate forest trees. *Plant, Cell and Environment*, *29*(4), 571–583. https://doi.org/10.1111/j.1365-3040.2005.01433.x

Maherali, H., Pockman, W. T., & Jackson, R. B. (2004). Adaptive variation in the vulnerability of woody plants to xylem cavitation. *Ecology*, *85*(8), 2184–2199. https://doi.org/10.1890/02-0538

Martinez-Cabrera, H. I., Jones, C. S., Espino, S., & Schenk, H. J. (2009). Wood anatomy and wood density in shrubs: Responses to varying aridity along transcontinental transects. *American Journal of Botany*, *96*(8), 1388–1398. https://doi.org/10.3732/ajb.0800237

Martinez-Cabrera, H. I., Schenk, H. J., Cevallos-Ferriz, S. R. S., & Jones, C. S. (2011). Integration of vessel traits, wood density, and height in angiosperm shrubs and trees. *American Journal of Botany*, *98*(5), 915–922.

https://doi.org/10.3732/ajb.1000335

Martínez-Vilalta, J., & Garcia-Forner, N. (2017). Water potential regulation, stomatal behaviour and hydraulic transport under drought: deconstructing the iso/anisohydric concept. *Plant, Cell & Environment*, *40*(6), 962–976. https://doi.org/10.1111/pce.12846

Martinez-Vilalta, J., Mencuccini, M., Alvarez, X., Camacho, J., Loepfe, L., & Pinol, J. (2012). Spatial distribution and packing of xylem conduits. *American Journal of Botany*, *99*(7), 1189–1196. https://doi.org/10.3732/ajb.1100384

Martínez-Vilalta, J., Poyatos, R., Aguadé, D., Retana, J., & Mencuccini, M. (2014). A new look at water transport regulation in plants. *New Phytologist*, *204*(1), 105–115. https://doi.org/10.1111/nph.12912

Mauseth, J. D., Aducci, P., Della Mea, M., & Fracassini, D. S. (2006). Botanica: parte generale. Idelson-Gnocchi.

McCulloh, K. A., Johnson, D. M., Meinzer, F. C., Voelker, S. L., Lachenbruch, B., & Domec, J.-C. (2012). Hydraulic architecture of two species differing in wood density: opposing strategies in co-occurring tropical pioneer trees. *Plant, Cell & Environment*, *35*(1), 116–125. https://doi.org/10.1111/j.1365-3040.2011.02421.x

McDowell, N. G. (2011). Mechanisms Linking Drought, Hydraulics, Carbon Metabolism, and Vegetation Mortality. *Plant Physiology*, *155*(3), 1051–1059. https://doi.org/10.1104/pp.110.170704

McDowell, N. G., Fisher, R. A., Xu, C., Domec, J. C., Hölttä, T., Mackay, D. S., … Pockman, W. T. (2013). Evaluating theories of drought-induced vegetation mortality using a multimodel-experiment framework. *New Phytologist*, *200*(2), 304–321. https://doi.org/10.1111/nph.12465

McDowell, N., Pockman, W. T., Allen, C. D., Breshears, D. D., Cobb, N., Kolb, T., … Yepez, E. A. (2008). Mechanisms of plant survival and mortality during drought: why do some plants survive while others succumb to drought? *New Phytologist*, *178*(4), 719–739. https://doi.org/10.1111/j.1469-8137.2008.02436.x

Meinzer, F. C., Johnson, D. M., Lachenbruch, B., McCulloh, K. A., & Woodruff, D. R. (2009). Xylem hydraulic safety margins in woody plants: coordination of stomatal control of xylem tension with hydraulic capacitance. *Functional Ecology*, *23*(5), 922–930. https://doi.org/10.1111/j.1365-2435.2009.01577.x

Melcher, P. J., Michele Holbrook, N., Burns, M. J., Zwieniecki, M. A., Cobb, A. R., Brodribb, T. J., … Sack, L. (2012). Measurements of stem xylem hydraulic conductivity in the laboratory and field. *Methods in Ecology and Evolution*, *3*(4), 685–694. https://doi.org/10.1111/j.2041-210X.2012.00204.x

Mencuccini, M. (2014). Temporal scales for the coordination of tree carbon and water economies during droughts. *Tree Physiology*, *34*(5), 439–442. https://doi.org/10.1093/treephys/tpu029

Mencuccini, M., & Comstock, J. (1997). Vulnerability to cavitation in populations of two desert species, Hymenoclea salsola and Ambrosia dumosa , from different climatic regions. *Journal of Experimental Botany*, *48*(6), 1323–1334.

https://doi.org/10.1093/jxb/48.6.1323

Mencuccini, M., & Comstock, J. (1999). Variability in hydraulic architecture and gas exchange of common bean (Phaseolus vulgaris) cultivars under well-watered conditions: interactions with leaf size. *Australian Journal of Plant Physiology*, *26*(2), 115. https://doi.org/10.1071/PP98137

Menzel, A., & Fabian, P. (1999). Growing season extended in Europe. *Nature*, *397*(6721), 659–659. https://doi.org/10.1038/17709

Mitchell, P. J., O'Grady, A. P., Tissue, D. T., White, D. A., Ottenschlaeger, M. L., & Pinkard, E. A. (2013). Drought response strategies define the relative contributions of hydraulic dysfunction and carbohydrate depletion during tree mortality. *New Phytologist*, *197*(3), 862–872. https://doi.org/10.1111/nph.12064

Mitchell, P. J., O'Grady, A. P., Tissue, D. T., Worledge, D., & Pinkard, E. A. (2014). Co-ordination of growth, gas exchange and hydraulics define the carbon safety margin in tree species with contrasting drought strategies. *Tree Physiology*, *34*(5), 443–458. https://doi.org/10.1093/treephys/tpu014

Morris, H., Plavcová, L., Cvecko, P., Fichtler, E., Gillingham, M. A. F., Martínez-Cabrera, H. I., … Jansen, S. (2016). A global analysis of parenchyma tissue fractions in secondary xylem of seed plants. *New Phytologist*, *209*(4), 1553–1565. https://doi.org/10.1111/nph.13737

Nardini, A., Battistuzzo, M., & Savi, T. (2013). Shoot desiccation and hydraulic failure in temperate woody angiosperms during an extreme summer drought. *New Phytologist*, *200*(2), 322–329. https://doi.org/10.1111/nph.12288

Nardini, A., Casolo, V., Dal Borgo, A., Savi, T., Stenni, B., Bertoncin, P., … McDowell, N. G. (2016). Rooting depth, water relations and non-structural carbohydrate dynamics in three woody angiosperms differentially affected by an extreme summer drought. *Plant, Cell & Environment*, *39*(3), 618–627. https://doi.org/10.1111/pce.12646

Nardini, A., Lo Gullo, M. A., & Salleo, S. (2011). Refilling embolized xylem conduits: Is it a matter of phloem unloading? *Plant Science*, *180*(4), 604–611. https://doi.org/10.1016/j.plantsci.2010.12.011

Nardini, A., & Luglio, J. (2014). Leaf hydraulic capacity and drought vulnerability: possible trade-offs and correlations with climate across three major biomes. *Functional Ecology*, *28*(4), 810–818. https://doi.org/10.1111/1365-2435.12246

Nardini, A., Pedà, G., & Rocca, N. La. (2012). Trade-offs between leaf hydraulic capacity and drought vulnerability: morpho-anatomical bases, carbon costs and ecological consequences. *New Phytologist*, *196*(3), 788–798. https://doi.org/10.1111/j.1469-8137.2012.04294.x

Nardini, A., Savi, T., Losso, A., Petit, G., Pacilè, S., Tromba, G., … Salleo, S. (2017a). X-ray microtomography observations of xylem embolism in stems of Laurus nobilis are consistent with hydraulic measurements of percentage loss of conductance. *New Phytologist*, *213*(3), 1068–1075. https://doi.org/10.1111/nph.14245

Nardini, A., Savi, T., Trifilò, P., & Lo Gullo, M. A. (2017b). Drought Stress and the

Recovery from Xylem Embolism in Woody Plants (pp. 197–231). https://doi.org/10.1007/124_2017_11

O'Brien, M. J., Engelbrecht, B. M. J., Joswig, J., Pereyra, G., Schuldt, B., Jansen, S., … Macinnis-Ng, C. (2017). A synthesis of tree functional traits related to drought-induced mortality in forests across climatic zones. *Journal of Applied Ecology*, *54*(6), 1669–1686. https://doi.org/10.1111/1365-2664.12874

Pellizzari, E., Camarero, J. J., Gazol, A., Sangüesa-Barreda, G., & Carrer, M. (2016). Wood anatomy and carbon-isotope discrimination support long-term hydraulic deterioration as a major cause of drought-induced dieback. *Global Change Biology*, *22*(6), 2125–2137. https://doi.org/10.1111/gcb.13227

Peng, C., Ma, Z., Lei, X., Zhu, Q., Chen, H., Wang, W., … Zhou, X. (2011). A drought-induced pervasive increase in tree mortality across Canada's boreal forests. *Nature Climate Change*, *1*(9), 467–471. https://doi.org/10.1038/nclimate1293

Petit, G., & Anfodillo, T. (2009). Plant physiology in theory and practice: An analysis of the WBE model for vascular plants. *Journal of Theoretical Biology*, *259*(1), 1–4. https://doi.org/10.1016/j.jtbi.2009.03.007

Petit, G., Anfodillo, T., Carraro, V., Grani, F., & Carrer, M. (2011). Hydraulic constraints limit height growth in trees at high altitude. *New Phytologist*, *189*(1), 241–252. https://doi.org/10.1111/j.1469-8137.2010.03455.x

Petit, G., Pfautsch, S., Anfodillo, T., & Adams, M. A. (2010). The challenge of tree height in Eucalyptus regnans: when xylem tapering overcomes hydraulic resistance. *New Phytologist*, *187*(4), 1146–1153. https://doi.org/10.1111/j.1469-8137.2010.03304.x

Petit, G., Savi, T., Consolini, M., Anfodillo, T., & Nardini, A. (2016). Interplay of growth rate and xylem plasticity for optimal coordination of carbon and hydraulic economies in Fraxinus ornus trees. *Tree Physiology*, 1–10. https://doi.org/10.1093/treephys/tpw069

Petit, G., von Arx, G., Kiorapostolou, N., Lechthaler, S., Prendin, A. L., Anfodillo, T., … Sterck, F. (2018). Tree differences in primary and secondary growth drive convergent scaling in leaf area to sapwood area across Europe. *New Phytologist*, *218*(4), 1383–1392. https://doi.org/10.1111/nph.15118

Pfautsch, S., Harbusch, M., Wesolowski, A., Smith, R., Macfarlane, C., Tjoelker, M. G., … Adams, M. A. (2016). Climate determines vascular traits in the ecologically diverse genus Eucalyptus. *Ecology Letters*, *19*(3), 240–248. https://doi.org/10.1111/ele.12559

Plavcová, L., Hoch, G., Morris, H., Ghiasi, S., & Jansen, S. (2016). The amount of parenchyma and living fibers affects storage of nonstructural carbohydrates in young stems and roots of temperate trees. *American Journal of Botany*, *103*(4), 603–612. https://doi.org/10.3732/ajb.1500489

Plavcová, L., & Jansen, S. (2015). The Role of Xylem Parenchyma in the Storage and Utilization of Nonstructural Carbohydrates. In U. Hacke (Ed.), *Functional and Ecological Xylem Anatomy* (pp. 209–234). Cham: Springer International Publishing. https://doi.org/10.1007/978-3-319-15783-2_8

Pockman, W. T., & Sperry, J. S. (2000). Vulnerability to Xylem Cavitation and the Distribution of Sonoran Desert Vegetation. *American Journal of Botany*, *87*(9), 1287. https://doi.org/10.2307/2656722

Pratt, R. B., & Jacobsen, A. L. (2017). Conflicting demands on angiosperm xylem: Tradeoffs among storage, transport and biomechanics. *Plant, Cell & Environment*, *40*(6), 897–913. https://doi.org/10.1111/pce.12862

Prendin, A. L., Mayr, S., Beikircher, B., von Arx, G., & Petit, G. (2018b). Xylem anatomical adjustments prioritize hydraulic efficiency over safety as Norway spruce trees grow taller. *Tree Physiology*, (June). https://doi.org/10.1093/treephys/tpy065

Prendin, A. L., Petit, G., Fonti, P., Rixen, C., Dawes, M. A., & von Arx, G. (2018a). Axial xylem architecture of Larix decidua exposed to CO 2 enrichment and soil warming at the tree line. *Functional Ecology*, *32*(2), 273–287. https://doi.org/10.1111/1365-2435.12986

Price, C. A., Wright, I. J., Ackerly, D. D., Niinemets, Ü., Reich, P. B., & Veneklaas, E. J. (2014). Are leaf functional traits "invariant" with plant size and what is "invariance" anyway? *Functional Ecology*, *28*(6), 1330–1343. https://doi.org/10.1111/1365-2435.12298

Rascio N., Carfagna S., Esposito S., La Rocca N., Lo Gullo M. A., Trost P., Vona V. (2012). Elementi di fisiologia vegetale. I edizione. EdiSES, Napoli.

Rascio N., Carfagna S., Esposito S., La Rocca N., Lo Gullo M. A., Trost P., Vona V. (2017). Elementi di fisiologia vegetale. II edizione. EdiSES, Napoli.

Rece, J. B., Urry, L. A., Cain, M. L., Wasserman, S. A., Minorsky, P. V., & Jackson, R.B. (2014). *Campbell biology*. Pearson.

Reichstein, M., Bahn, M., Ciais, P., Frank, D., Mahecha, M. D., Seneviratne, S. I., … Wattenbach, M. (2013). Climate extremes and the carbon cycle. *Nature*, *500*(7462), 287–295. https://doi.org/10.1038/nature12350

Rosell, J. A., Olson, M. E., & Anfodillo, T. (2017). Scaling of Xylem Vessel Diameter with Plant Size: Causes, Predictions, and Outstanding Questions. *Current Forestry Reports*, *3*(1), 46–59. https://doi.org/10.1007/s40725-017-0049-0

Rosner, S. (2017). Wood density as a proxy for vulnerability to cavitation: Size matters. *Journal of Plant Hydraulics*, *4*, 1. https://doi.org/10.20870/jph.2017.e001

Sade, N., Gebremedhin, A., & Moshelion, M. (2012). Risk-taking plants. *Plant Signaling & Behavior*, *7*(7), 767–770. https://doi.org/10.4161/psb.20505

Salleo, S., Lo Gullo, M. A., Trifilò, P., & Nardini, A. (2004). New evidence for a role of vessel-associated cells and phloem in the rapid xylem refilling of cavitated stems of Laurus nobilis L. *Plant, Cell and Environment*, *27*(8), 1065–1076. https://doi.org/10.1111/j.1365-3040.2004.01211.x

Salter, M. G., Franklin, K. A., & Whitelam, G. C. (2003). Gating of the rapid shade-avoidance response by the circadian clock in plants. *Nature*, *426*(6967), 680–683. https://doi.org/10.1038/nature02174

Salzmann, N., Huggel, C., Rohrer, M., & Stoffel, M. (2014). Data and knowledge gaps in glacier, snow and related runoff research – A climate change adaptation perspective. *Journal of Hydrology*, *518*(PB), 225–234. https://doi.org/10.1016/j.jhydrol.2014.05.058

Savi, T., Love, V. L., Dal Borgo, A., Martellos, S., & Nardini, A. (2017). Morpho-anatomical and physiological traits in saplings of drought-tolerant Mediterranean woody species. *Trees*, *31*(4), 1137–1148. https://doi.org/10.1007/s00468-017-1533-7

Schneider, C. A., Rasband, W. S., & Eliceiri, K. W. (2012). NIH Image to ImageJ: 25 years of image analysis. *Nature Methods*, *9*(7), 671–675. https://doi.org/10.1038/nmeth.2089

Secchi, F., Pagliarani, C., & Zwieniecki, M. A. (2017). The functional role of xylem parenchyma cells and aquaporins during recovery from severe water stress. *Plant, Cell & Environment*, *40*(6), 858–871. https://doi.org/10.1111/pce.12831

Secchi, F., & Zwieniecki, M. A. (2011). Sensing embolism in xylem vessels: the role of sucrose as a trigger for refilling. *Plant, Cell & Environment*, *34*(3), 514–524. https://doi.org/10.1111/j.1365-3040.2010.02259.x

Slatyer, R. (1958). The Measurement of Diffusion Pressure Deficit in Plants by a Method of Vapour Equilibration. *Australian Journal of Biological Sciences*, *11*(3), 349. https://doi.org/10.1071/BI9580349

Slik, J. W. F., Paoli, G., McGuire, K., Amaral, I., Barroso, J., Bastian, M., … Zweifel, N. (2013). Large trees drive forest aboveground biomass variation in moist lowland forests across the tropics. *Global Ecology and Biogeography*, *22*(12), 1261–1271. https://doi.org/10.1111/geb.12092

Speranza, A., & Calzoni, G. L. (1996). Struttura delle piante in immagini. *Zanichelli Editore* SpA, Bologna.

Sperry, J. (2013). Cutting-edge research or cutting-edge artefact? An overdue control experiment complicates the xylem refilling story. *Plant, Cell & Environment*, *36*(11), n/a-n/a. https://doi.org/10.1111/pce.12148

Sperry, J. S., & Tyree, M. T. (1988). Mechanism of Water Stress-Induced Xylem Embolism. *Plant Physiology*, *88*(3), 581–587. https://doi.org/10.1104/pp.88.3.581

Sterck, F., & Zweifel, R. (2016). Trees maintain a similar conductance per leaf area through integrated responses in growth, allocation, architecture and anatomy. *Tree Physiology*, (June), 1307–1309. https://doi.org/10.1093/treephys/tpw100

Steudle, E. (2001). The Cohesion-Tension Mechanism and the Acquisition of Water by Plant Roots. *Annual Review of Plant Physiology and Plant Molecular Biology*, *52*(1), 847–875. https://doi.org/10.1146/annurev.arplant.52.1.847

Stute, M., Forster, M., Frischkorn, H., Serejo, A., Clark, J. F., Schlosser, P., … Bonani, G. (1995). Cooling of Tropical Brazil (5 C) During the Last Glacial Maximum. *Science*, *269*(5222), 379–383. https://doi.org/10.1126/science.269.5222.379

Taiz, L., & Zeiger, E. (2006). Plant physiology. 4th. *Sinauer Associate, Sunderland, Mass., EUA*.

Torres-Ruiz, J. M., Cochard, H., Fonseca, E., Badel, E., Gazarini, L., & Vaz, M. (2017). Differences in functional and xylem anatomical features allow Cistus species to co-occur and cope differently with drought in the Mediterranean region. *Tree Physiology*, *37*(6), 755–766. https://doi.org/10.1093/treephys/tpx013

Trifilò, P., Raimondo, F., Lo Gullo, M. A., Barbera, P. M., Salleo, S., & Nardini, A. (2014). Relax and refill: xylem rehydration prior to hydraulic measurements favours embolism repair in stems and generates artificially low PLC values. *Plant, Cell & Environment*, *37*(11), 2491–2499. https://doi.org/10.1111/pce.12313

Trueba, S., Pouteau, R., Lens, F., Feild, T. S., Isnard, S., Olson, M. E., & Delzon, S. (2017). Vulnerability to xylem embolism as a major correlate of the environmental distribution of rain forest species on a tropical island. *Plant, Cell & Environment*, *40*(2), 277–289. https://doi.org/10.1111/pce.12859

Tyree, M. T. (1997). The Cohesion-Tension theory of sap ascent: current controversies. *Journal of Experimental Botany*, *48*(10), 1753–1765. https://doi.org/10.1093/jxb/48.10.1753

Tyree, M. T., & Ewers, F. W. (1991). The hydraulic architecture of trees and other woody plants. *New Phytologist*, *119*(3), 345–360. https://doi.org/10.1111/j.1469-8137.1991.tb00035.x

Tyree, M. T., & Sperry, J. S. (1989). Vulnerability of Xylem to Cavitation and Embolism. *Annual Review of Plant Physiology and Plant Molecular Biology*, *40*(1), 19–36. https://doi.org/10.1146/annurev.pp.40.060189.000315

Venturas, M. D., Sperry, J. S., & Hacke, U. G. (2017). Plant xylem hydraulics: What we understand, current research, and future challenges. *Journal of Integrative Plant Biology*, *59*(6), 356–389. https://doi.org/10.1111/jipb.12534

Vilagrosa, A., Chirino, E., Peguero-Pina, J. J., Barigah, T. S., Cochard, H., & Gil-Pelegrín, E. (2012). Xylem Cavitation and Embolism in Plants Living in Water-Limited Ecosystems. In R. Aroca (Ed.), *Plant Responses to Drought Stress* (pp. 63–109). Berlin, Heidelberg: Springer Berlin Heidelberg. https://doi.org/10.1007/978-3-642-32653-0_3

von Arx, G., Archer, S. R., & Hughes, M. K. (2012). Long-term functional plasticity in plant hydraulic architecture in response to supplemental moisture. *Annals of Botany*, *109*(6), 1091–1100. https://doi.org/10.1093/aob/mcs030

von Arx, G., & Carrer, M. (2014). ROXAS – A new tool to build centuries-long tracheid-lumen chronologies in conifers. *Dendrochronologia*, *32*(3), 290–293. https://doi.org/10.1016/j.dendro.2013.12.001

Wang, R., Zhang, L., Zhang, S., Cai, J., & Tyree, M. T. (2014). Water relations of R obinia pseudoacacia L.: do vessels cavitate and refill diurnally or are R-shaped curves invalid in R obinia ? *Plant, Cell & Environment*, *37*(12), 2667–2678. https://doi.org/10.1111/pce.12315

Wheeler, J. K., Sperry, J. S., Hacke, U. G., & Hoang, N. (2005). Inter-vessel pitting and cavitation in woody Rosaceae and other vesselled plants: a basis for a safety versus efficiency trade-off in xylem transport. *Plant, Cell and Environment*, *28*(6), 800–

812. https://doi.org/10.1111/j.1365-3040.2005.01330.x

Wheeler, T. D., & Stroock, A. D. (2008). The transpiration of water at negative pressures in a synthetic tree. *Nature*, *455*(7210), 208–212. https://doi.org/10.1038/nature07226

Wiedenhoeft, A. (2012). Structure and Function of Wood. In *Handbook of Wood Chemistry and Wood Composites, Second Edition* (pp. 9–32). CRC Press. https://doi.org/10.1201/b12487-4

Yadeta, K. A., & J. Thomma, B. P. H. (2013). The xylem as battleground for plant hosts and vascular wilt pathogens. *Frontiers in Plant Science*, *4*(April), 1–12. https://doi.org/10.3389/fpls.2013.00097

Yang, S., & Tyree, M. T. (1993). Hydraulic resistance in Acer saccharum shoots and its influence on leaf water potential and transpiration. *Tree Physiology*, *12*(3), 231–242. https://doi.org/10.1093/treephys/12.3.231

Zar, J. H. (1999). Biostatistical analysis. Pearson Education India.

Ziemińska, K., Westoby, M., & Wright, I. J. (2015). Broad Anatomical Variation within a Narrow Wood Density Range—A Study of Twig Wood across 69 Australian Angiosperms. *PLOS ONE*, *10*(4), e0124892. https://doi.org/10.1371/journal.pone.0124892

Zimmermann, M. H. (1983). Xylem structure and the ascent of sap, Springer-V.

Zuur, A. F., Ieno, E. N., & Elphick, C. S. (2010). A protocol for data exploration to avoid common statistical problems. *Methods in Ecology and Evolution*, *1*(1), 3–14. https://doi.org/10.1111/j.2041-210X.2009.00001.x

Zwieniecki, M. a., & Holbrook, N. M. (1998). Diurnal variation in xylem hydraulic conductivity in white ash (Fraxinus americana L.), red maple (Acer rubrum L.) and red spruce (Picea rubens Sarg.). *Plant, Cell and Environment*, *21*(11), 1173–1180. https://doi.org/10.1046/j.1365-3040.1998.00342.x

Zwieniecki, M. A., & Holbrook, N. M. (2009). Confronting Maxwell's demon: biophysics of xylem embolism repair. *Trends in Plant Science*, *14*(10), 530–534. https://doi.org/10.1016/j.tplants.2009.07.002

8. Annexes

8.1 Hydraulic vulnerability curves

Vulnerability curves (VCs) assessed for 14 species (Figure 8.1a, 8.1b).

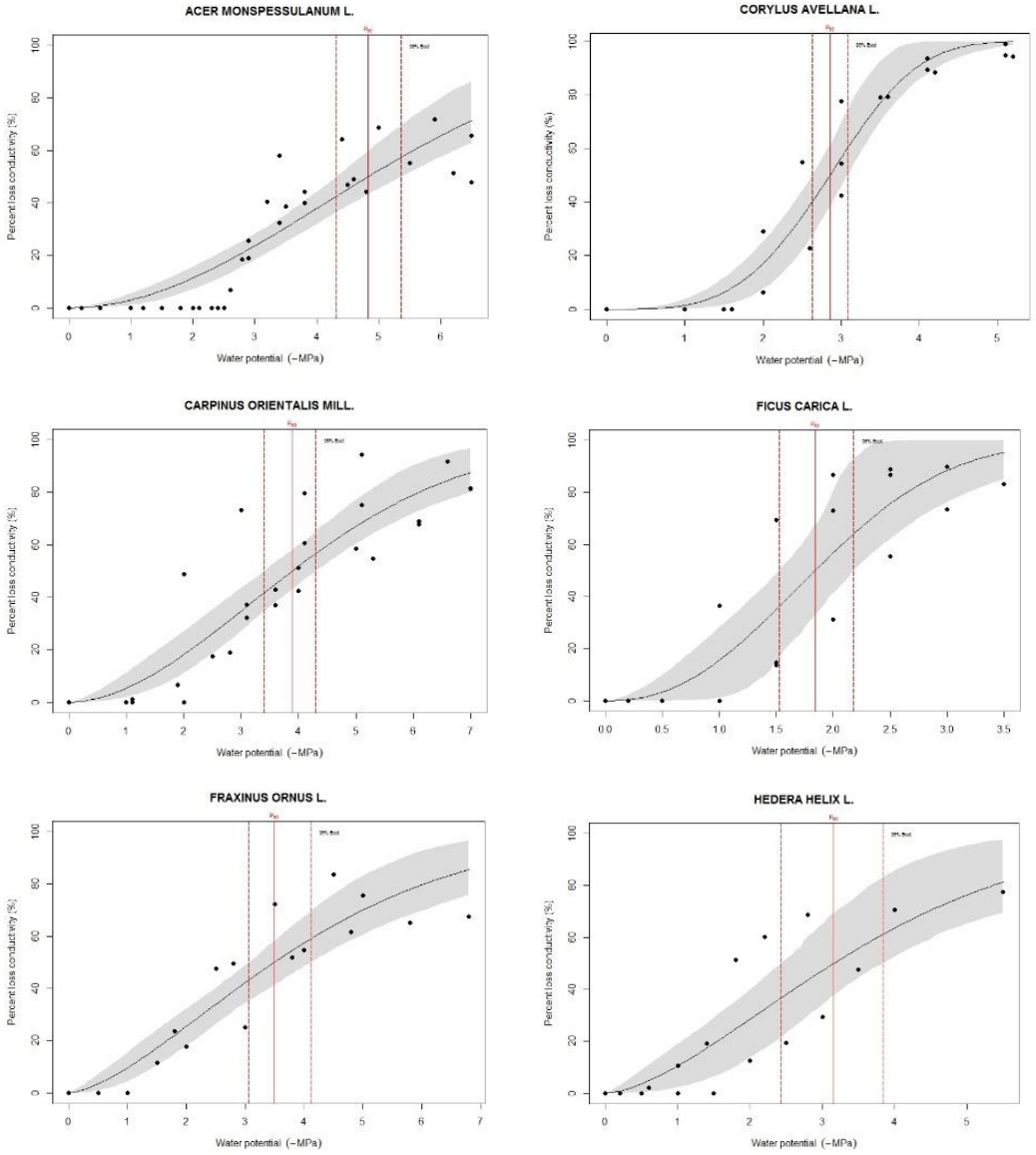

Figure 8.1a: Vulnerability curves assessed using R-package Fitplc (Duursma and Choat 2017). Shaded area represent the 95% confidence intervals of the sigmodal curve; Solid and dashed vertical lines represent the P_{50} and its 95% confidence intervals respectively.

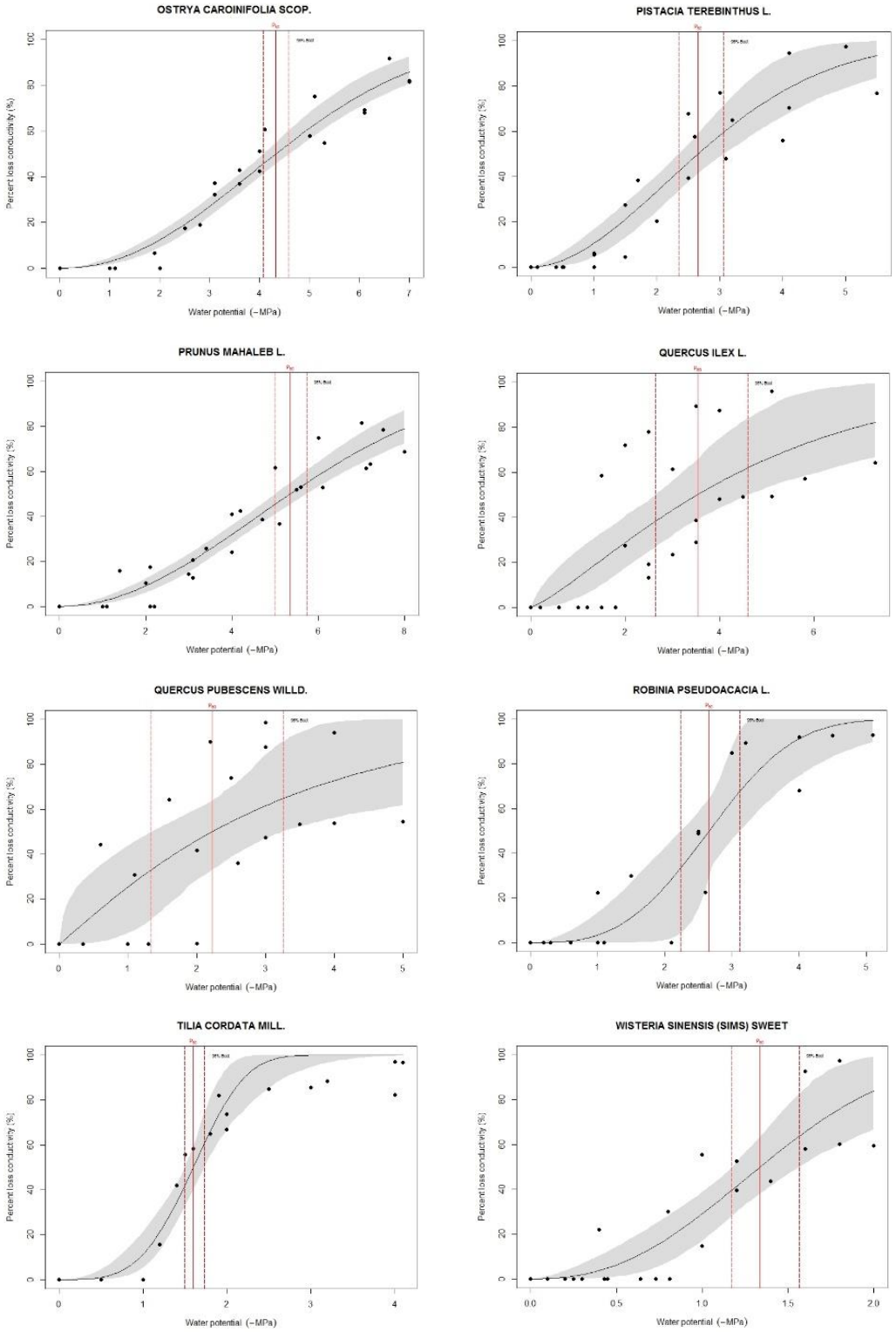

Figure 8.1b: Vulnerability curves assessed using R-package Fitplc (Duursma and Choat 2017). Shaded area represent the 95% confidence intervals of the sigmodal curve; Solid and dashed vertical lines represent the P_{50} and its 95% confidence intervals respectively.

The obtained values of P_{50} range from 1.34 (-MPa) of *Wisteria sinensis* (Sims) Sweet, to 5.34 (-MPa) of *Prunus mahaleb* L. (Table 8.1b). Therefore, within the species whose VCs were assessed, *Wisteria sinensis* (Sims) Sweet is the most vulnerable species while *Prunus mahaleb* L. is the most resistant species to cavitation. The 95% confidence intervals for the obtained P_{50} values ranged from a minimum of 0.23 MPa for *Tilia cordata* Mill. to 2.00 MPa for *Quercus ilex* L..

Species	P_{50} (-MPa)	2.5%	97.5%
Acer monspessulanum L.	4.83	4.36	5.40
Corylus avellana L.	2.86	2.60	3.08
Carpinus orientalis Mill.	3.89	3.39	4.33
Ficus carica L.	1.84	1.52	2.19
Fraxinus ornus L.	3.49	3.04	4.05
Hedera helix L.	3.16	2.46	3.87
Ostrya carpinifolia Scop.	4.32	4.08	4.59
Pistacia terebinthus L.	2.66	2.37	3.07
Prunus mahaleb L.	5.34	5.01	5.70
Quercus ilex L.	3.53	2.58	4.58
Quercus pubescens Willd.	2.23	1.37	3.22
Robinia pseudoacacia L.	2.66	2.25	3.09
Tilia cordata Mill.	1.60	1.51	1.74
Wisteria sinensis (Sims) Sweet	1.34	1.17	1.57

Table 8.1: Values of P_{50} extracted from the VCs. Lower (2.5%) and upper (97.5%) limits of the confidence interval (95%) are also shown.

8.2 Statistical tests assessed on the relationships between hydraulic and anatomical traits

8.2.1 PA_{AR} ~ P_{50}

The relationship between PA_{AR} (i.e., the total amount of parenchyma in the xylem) and P_{50} (i.e., the water potential at which 50% of the total xylem conductivity is lost) was checked for angiosperms in group 1, group 2 and group 3 separately. In all the three groups, negative trend between $log_{10}(PA_{AR})$ and $log_{10}(P_{50})$ was found, with species having a higher P_{50} (i.e., less negative) producing a bigger amount of parenchyma cells in the xylem (Figure 8.2, Table 8.2(ii)). This trend is comparable to all the three dataset groups (Figure 8.2, Table

8.2(i)) even if no clear results are emerging for group 3 due to low sample size ($N = 14$, $p > 0.05$) (Table 8.2(ii)). Same trend is shown in Figure 8.4, Table 8.4 and described in comparison to the other two tissues the wood is made of: F_a (i.e., the overall amount of fibres in the xylem) and V_a (i.e., the overall volume of wood occupied by vessels).

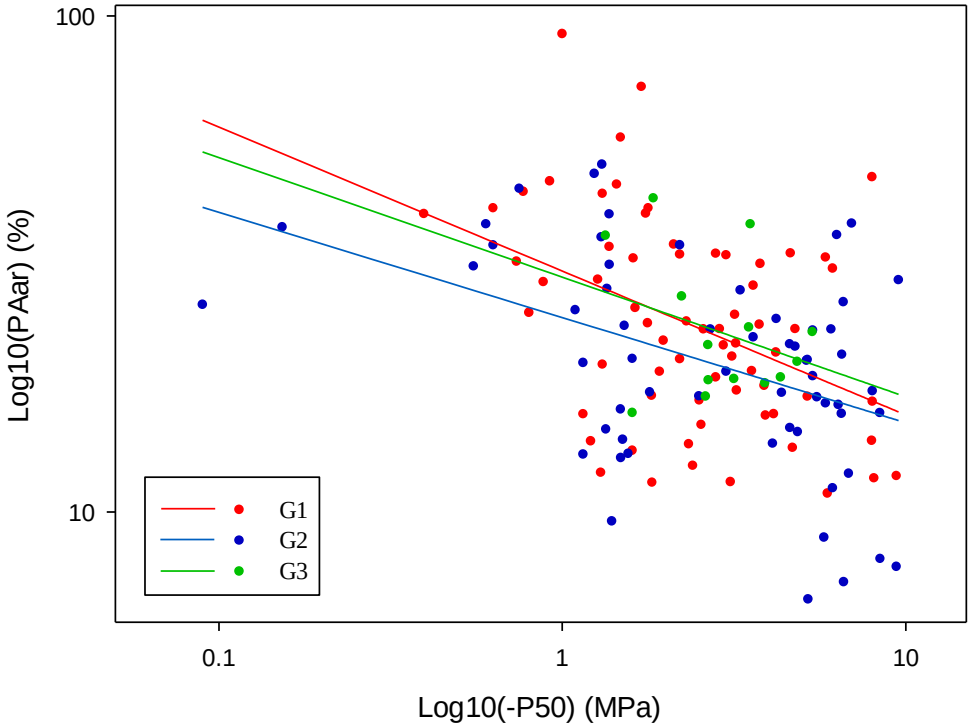

Figure 8.2: Relationship between PA_{AR} and P_{50} for angiosperms between the three data groups (G1 red, G2 blue, G3 green). Data are Log_{10}-transformed. Fitted linear regressions are shown.

(i)	group	F	DF	p-value
$PA_{AR} \sim P_{50}$	G1, G2, G3	1.1892	-4	> 0.05

(ii)	group	R^2	F	DF	p-value
$PA_{AR} \sim P_{50}$	G1	0.16	13.39	65	< 0.001
$PA_{AR} \sim P_{50}$	G2	0.18	13.53	58	< 0.001
$PA_{AR} \sim P_{50}$	G3	0.022	1.294	12	> 0.05

Table 8.2: (i) Indices of the One-way ANOVA Test assessed to test for differences in the slope of the $PA_{AR} \sim P_{50}$ regressions between angiosperms of group 1 (G1), group 2 (G2) and group 3 (G3); (ii) Indices describing the regressions lines obtained from Log_{10}-transformed data.

The relationship between PA_{AR} and P_{50} was checked for gymnosperms in group 1 and group 2 separately. The slope of the two fitted linear regressions is different (Figure 8.3, Table 8.3(i)). The two dataset groups are therefore not comparable for PA_{AR}~P_{50} relationship in gymnosperms. Anyway, no clear results are emerging for both groups (Table 8.3(ii)).

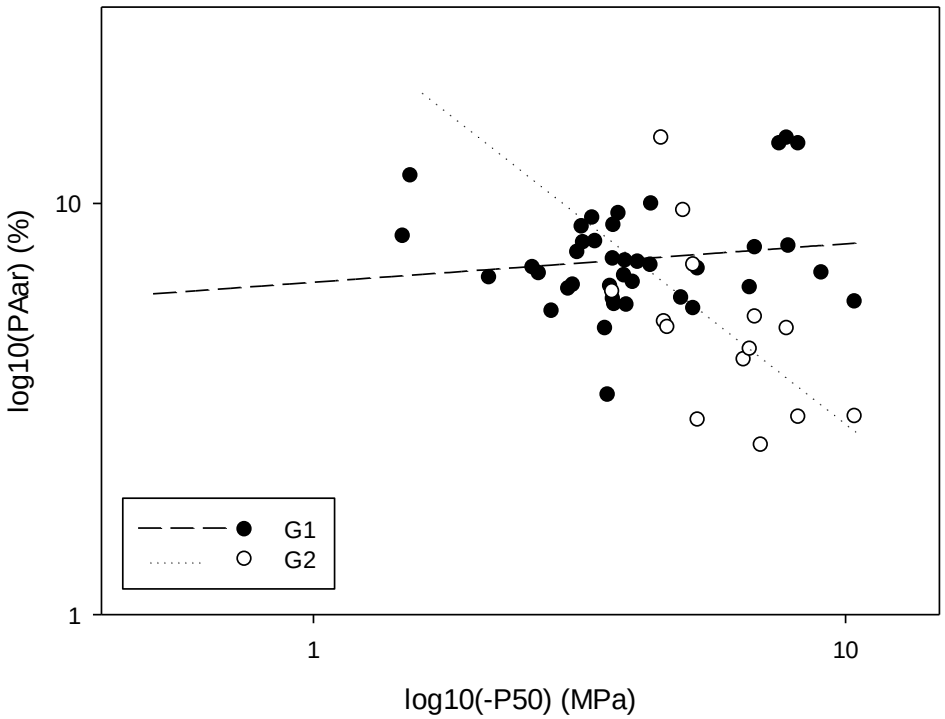

Figure 8.3: Relationship between PA_{AR} and P_{50} for gymnosperms between data group 1 (Filled circles, solid line) and group 2 (open circles, dashed line). Data are Log_{10}-transformed. Fitted linear regressions are shown.

(i)	group	F	DF	p-value
PA_{AR}~P_{50}	G1, G2	11.472	-2	<0.001

(ii)	group	R^2	F	DF	p-value
PA_{AR}~P_{50}	G1	-0.0062	0.7665	37	0.387
PA_{AR}~P_{50}	G2	0.31	6.85	12	0.0225

Table 8.3: (i) Indices of the One-way ANOVA Test assessed to test for differences in the slope of the PA_{AR}~P_{50} regressions between gymnosperms of group 1 (G1) and group 2 (G2); (ii) Indices describing the regressions lines obtained from Log_{10}-transformed data.

8.2.2 PA_{AR} ~ P_{50}, F_a ~ P_{50}, V_a ~ P_{50}

The relationship between F_a (i.e., the overall amount of fibres in the xylem) and P_{50} (i.e., the water potential at which 50% of the total xylem conductivity is lost) was checked for angiosperms in group 2 and 3 separately. A negative trend between F_a and P_{50} was found, with species having a higher P_{50} producing a lower amount of fibres in the xylem (Figure 8.4). This trend is comparable to the two dataset groups including F_a data (group 2 and group 3) (Table 8.4).

The relationship between V_a (i.e., the overall volume of wood occupied by vessels) and P_{50} was checked for angiosperms in group 2 and 3 separately. No significant trend between V_a and P_{50} was found (Figure 8.4). These findings are comparable to both dataset groups V_a data are available (group 2 and group 3) (Table 8.4). V_a range between $\sim 10 - 25\%$ of total wood volume.

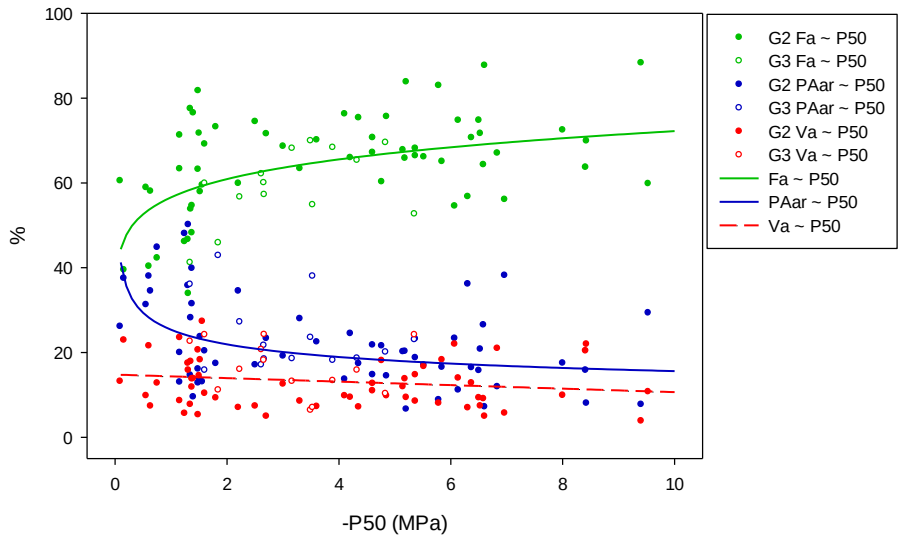

Figure 8.4: Scatterplot of the relationship between F_a and P_{50} (green), PA_{AR} and P_{50} (blue) and between V_a and P_{50} (red) for angiosperms. Filled and open circles represent data from group 2 and group 3 respectively. Fitted regressions were generated considering both groups together.

	group	F	DF	p-value
$F_a \sim P_{50}$	G2, G3	2.4423	-2	> 0.05
$PA_{AR} \sim P_{50}$	G2, G3	0.8076	-2	> 0.05
$V_a \sim P_{50}$	G2, G3	0.2098	-2	> 0.05

Table 8.4: Indices of the One-way ANOVA Test assessed to test for differences in the slope of the $F_a \sim P_{50}$, $PA_{AR} \sim P_{50}$, $V_a \sim P_{50}$ regressions between group 2 (G2) and group 3 (G3).

8.2.3 F_a ~ PA_{AR}

The relationship between F_a (i.e., the overall amount of fibres in the xylem) and PA_{AR} (i.e., the total amount of parenchyma in the xylem) was checked for angiosperms in group 2 and 3 separately. A very significant trend ($p < 0.001$) that is explaining most of the variability ($R^2 = 0.7276$) between F_a and PA_{AR} was found (Figure 8.5). Plants in the xylem either have a high fibres amount, therefore reducing the parenchyma volume or a high parenchyma amount and a reduced fibres volume that means PA_{AR} and F_a are inversely related. This trend is comparable to the two dataset groups including F_a data (group 2 and group 3) (Table 8.5).

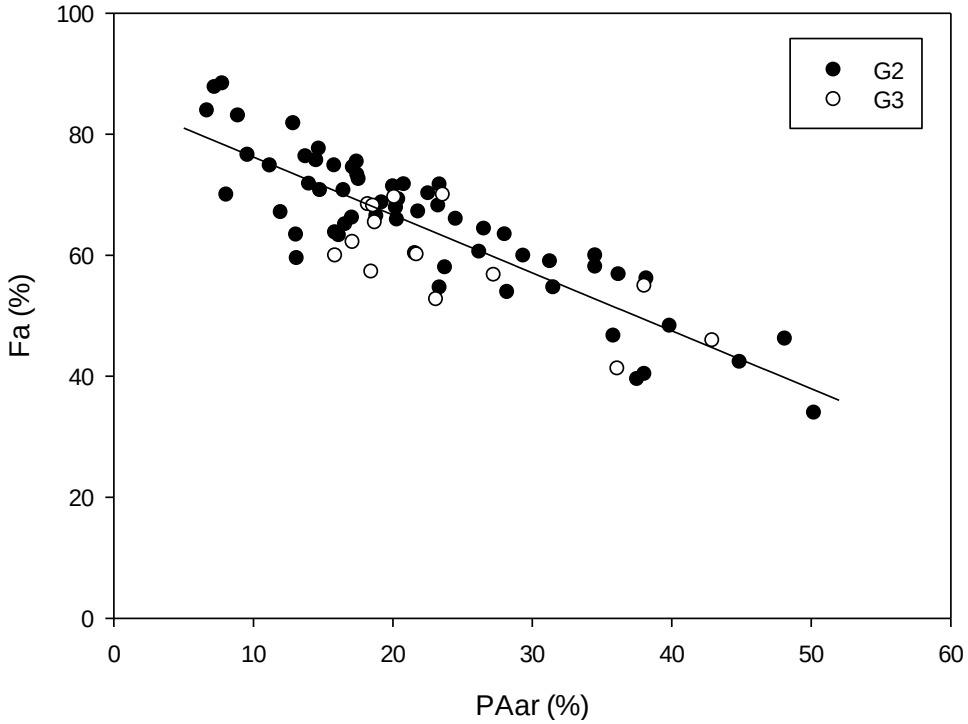

Figure 8.5: Scatterplot of the relationship between F_a and PA_{AR} for angiosperms. Filled and open circles represent data from group 2 and group 3 respectively. Fitted linear regression was generated considering both groups together.

	group	F	DF	p-value
$F_a \sim PA_{AR}$	G2, G3	0.6324	-2	> 0.05

Table 8.5: Indices of the One-way ANOVA Test assessed to test for differences in the slope of the $F_a \sim PA_{AR}$ regressions between group 2 (G2) and group 3 (G3).

8.2.4 $C_d \sim MC_a$

The relationship between C_d (i.e., the frequency of conduit for a given wood area) and MC_a (i.e., the mean area of xylem conduits) was checked for angiosperms in group 2 and 3 separately. A very significant trend ($p < 0.001$) that is explaining most of the variability ($R^2 = 0.7209$) between C_d and MC_a was found (Figure 8.6). Plants in the xylem either produce few big vessels or rely on many small ones. This means that C_d and MC_a are inversely related. This trend is comparable to the two dataset groups including data of C_d and MC_a (group 2 and group 3) (Table 8.6).

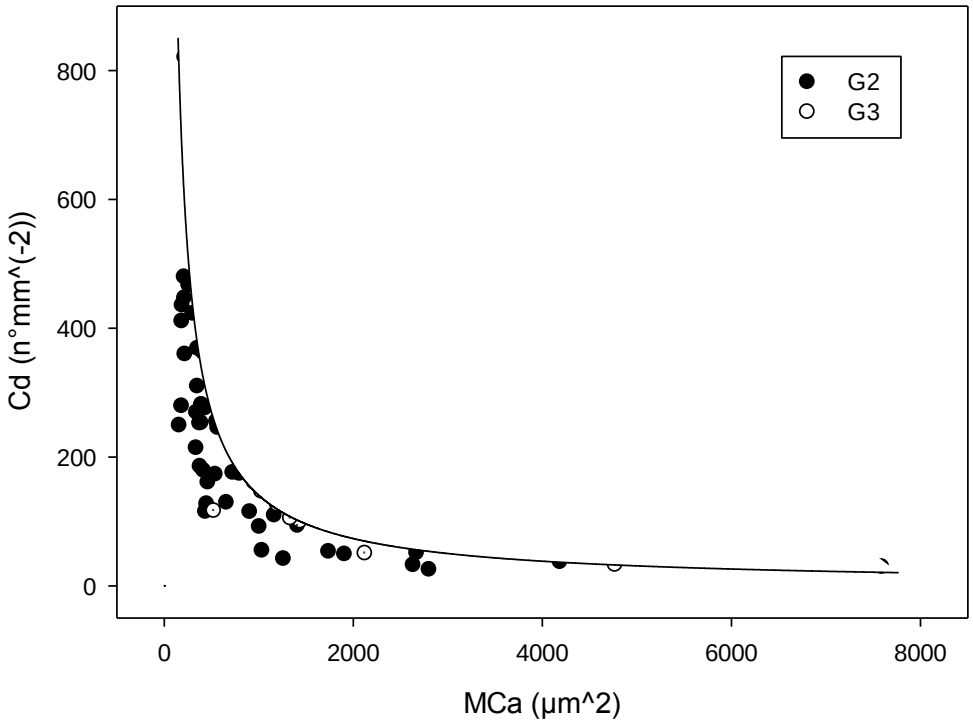

Figure 8.6 Scatterplot of the relationship between C_d and MC_a for angiosperms. Filled and open circles represent data from group 2 and group 3 respectively. Fitted power regression was generated considering both groups together.

	group	F	DF	p-value
$C_d \sim MC_a$	G2, G3	2.967	-2	> 0.05

Table 8.6: Indices of the One-way ANOVA Test assessed to test for differences in the slopes of the $C_d \sim MC_a$ regression between group 2 (G2) and group 3 (G3).

8.2.5 $C_d \sim P_{50}$, $MC_a \sim P_{50}$

The relationship between C_d (i.e., the frequency of conduit for a given wood area) and P_{50} (i.e., the water potential at which 50% of the total xylem conductivity is lost) was checked for angiosperms in group 2 and 3 separately. A negative trend between C_d and P_{50} was found, with species having a higher P_{50} (i.e., less negative) producing a lower number of vessels per unit area (Figure 8.7). This trend is comparable to the two dataset groups including data of C_d (group 2 and group 3) (Table 8.7).

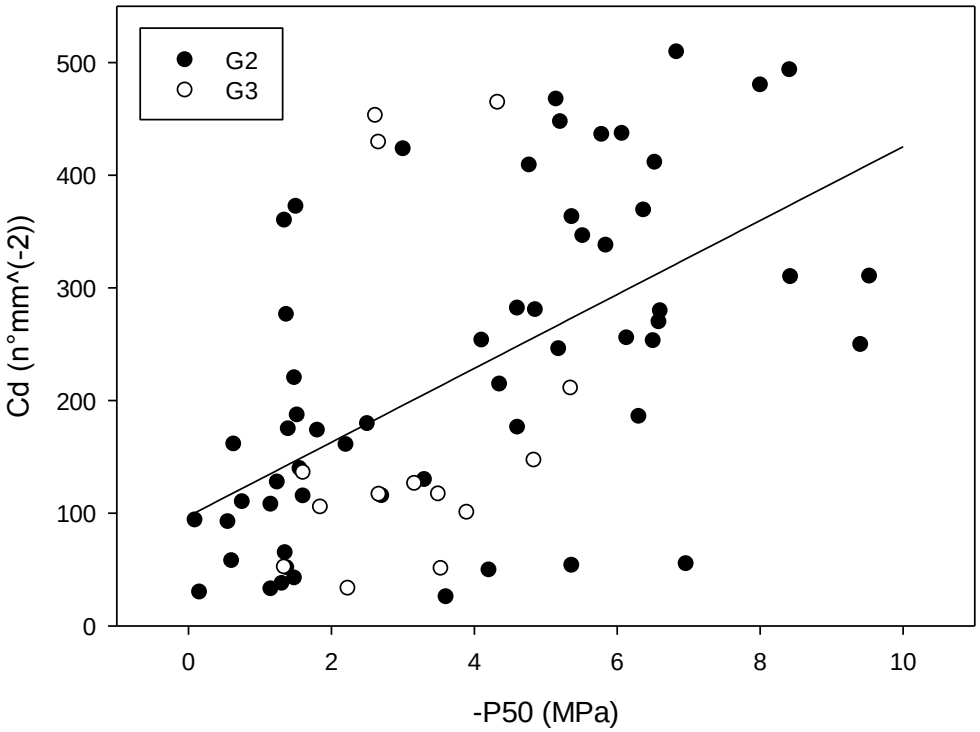

Figure 8.7: Scatterplot of the relationship between C_d and P_{50} for angiosperms. Filled and open circles represent data from group 2 and group 3 respectively. Fitted linear regression was generated considering both groups together.

	group	F	DF	p-value
$C_d \sim P_{50}$	G2, G3	1.1759	-2	> 0.05

Table 8.7: Indices of the One-way ANOVA Test assessed to test for differences in the slope of the $C_d \sim P_{50}$ regressions between group 2 (G2) and group 3 (G3).

The relationship between MC_a (i.e., the mean area of xylem conduits) and P_{50} was checked for angiosperms in group 2 and 3 separately. A positive trend between MC_a and P_{50} was found, with species having a higher P_{50} (i.e., less negative) producing bigger vessels (Figure 8.8, Table 8.8(ii)). The slope of the two fitted regression lines in log10-transformed data is different between the two dataset groups including MC_a (group 2 and group 3) (Table 8.8(i)) and no clear results are emerging for group 3 due to low sample size ($N = 14$, $p > 0.05$). Nevertheless, both groups are showing a substantial positive trend for $Log_{10}(MC_a) \sim Log_{10}(P_{50})$ (Figure 8.8 up-right box) and were therefore considered as comparable.

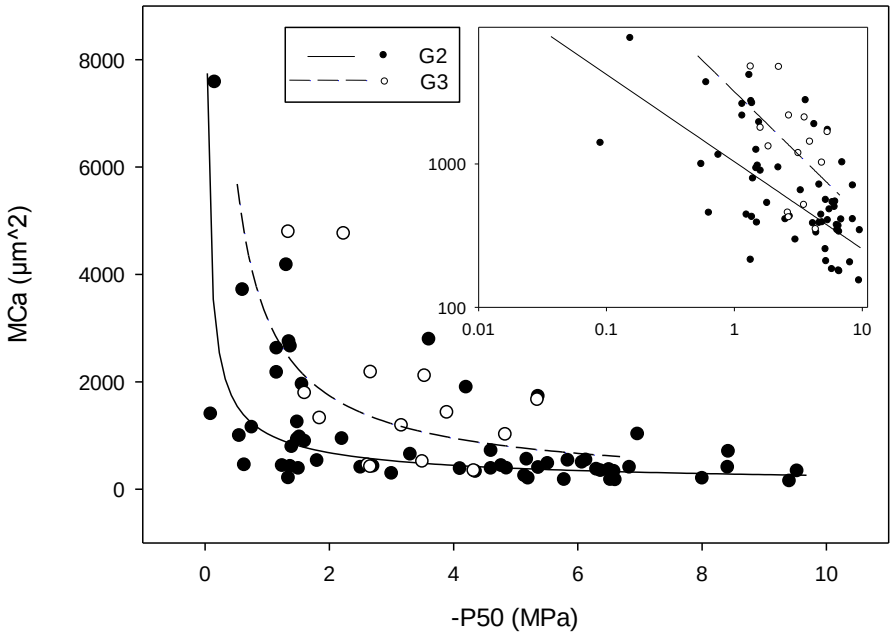

Figure 8.8: Scatterplot of the relationship between MC_a and P_{50} for angiosperms. Filled and open circles represent data from group 2 and group 3 respectively. Solid and dashed curves were generated with data from group 2 and group 3 respectively. Data Log_{10}-transformed are also shown.

(i)	group	F	DF	p-value
$MC_a \sim P_{50}$	G2, G3	5.4708	-2	< 0.01

(ii)	group	R^2	F	DF	p-value
$MC_a \sim P_{50}$	G2	0.33	29.06	57	< 0.001
$MC_a \sim P_{50}$	G3	0.12	2.766	12	> 0.05

Table 8.8: (i) Indices of the One-way ANOVA Test assessed to test for differences in the slope of the $MC_a \sim P_{50}$ regressions between group 2 (G2) and group 3 (G3); (ii) Indices describing the regressions lines obtained from Log_{10}-transformed data.

8.3 Anatomical and hydraulic variability between functional groups

In this paragraph, the relationships between the anatomical and hydraulic variables for the different functional groups (i.e. angiosperms and gymnosperms) are analysed and compared.

Hydraulic vulnerability

Differences in P_{50} (i.e., the water potential at which 50% of the total xylem conductivity is lost) between angiosperms (*A*) and gymnosperms (*G*), deciduous (*D*) and evergreen (*E*) species, climbers (*C*) and self-supporting (*S*) species, were all significant ($p < 0.05$) (Table 8.9). *A* have a higher (i.e., less negative) P_{50} than *G*, *D* have higher P_{50} than *E* and *C* have higher P_{50} than *S* (Figure 8.9). Therefore, *A* are more vulnerable to cavitation than *G*, *D* are more vulnerable to cavitation than *E* and *C* are more vulnerable to cavitation than *S*.

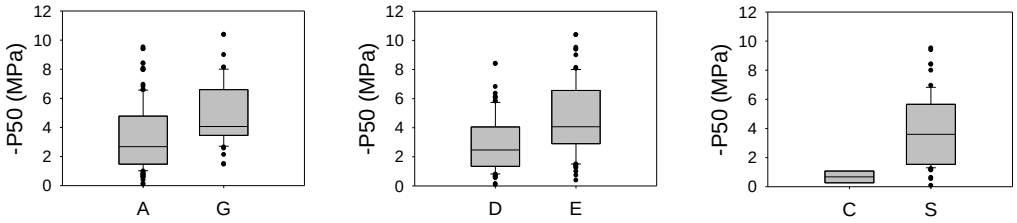

Figure 8.9: Boxplot showing the difference in P_{50} between functional groups. Significant difference was found between *A* and *G*, *D* and *E*, *C* and *S*.

	U-stat	T	n(small)	n(big)	p-value
A vs. *G*	2175	6782	53	142	<0.001
D vs. *E*	2399	6677	92	93	<0.001
C vs. *S*	11	21	4	69	0.002

Table 8.9: Output of the Mann-Whitney Rank Sum Test assessed to test for differences in P_{50} between functional groups.

Parenchyma

Differences in PA_A (i.e., the amount of axial parenchyma in the xylem) between angiosperms (*A*) and gymnosperms (*G*), deciduous (*D*) and evergreen (*E*) species, were significant ($p < 0.05$) (Table 8.10). Differences in PA_A values between climbers (*C*) and self-supporting (*S*) species are not significant ($p > 0.05$). *A* have a higher PA_A than *G*, *D* have higher PA_A than *E* (Figure 8.10). No differences in PA_A were found between *C* and *S*.

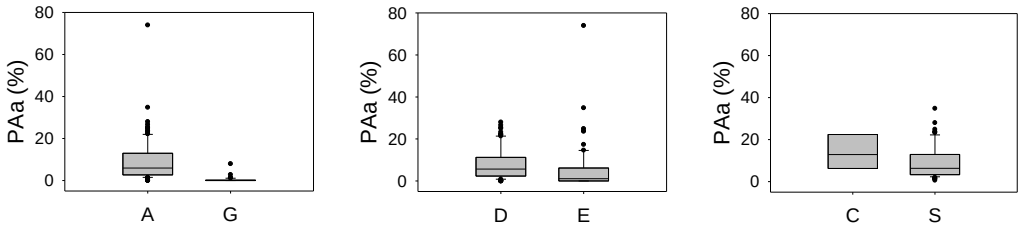

Figure 8.10: Boxplot showing the difference in PA_A between functional groups. Significant difference was found between *A* and *G*, *D* and *E*.

	U-stat	T	n(small)	n(big)	p-value
A vs. *G*	227.5	1658.5	53	127	<0.001
D vs. *E*	2188	5428	80	90	<0.001
C vs. *S*	81	205	4	69	0.171

Table 8.10: Output of the Mann-Whitney Rank Sum Test assessed to test for differences in PA_A between functional groups.

Differences in PA_R (i.e., the amount of radial parenchyma in the xylem) between angiosperms (*A*) and gymnosperms (*G*), deciduous (*D*) and evergreen (*E*) species, climbers (*C*) and self-supporting (*S*) species, were all significant ($p < 0.05$) (Table 8.11). *A* have a higher PA_R than *G*, *D* have higher PA_R than *E* and *C* have higher PA_R than *S* (Figure 8.11).

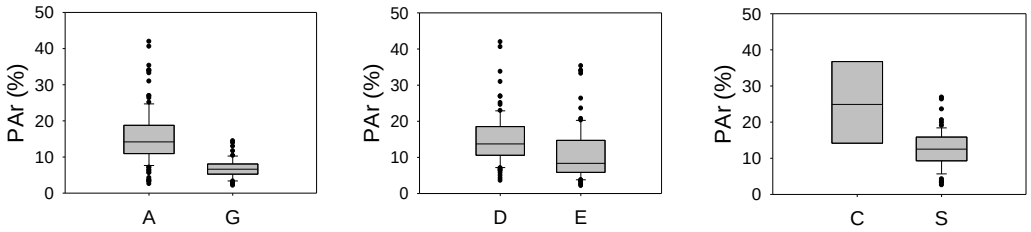

Figure 8.11: Boxplot showing the difference in PA_R between functional groups. Significant difference was found between *A* and *G*, *D* and *E*, *C* and *S*.

	U-stat	T	n(small)	n(big)	p-value
A vs. *G*	706.5	2137.5	53	128	<0.001
D vs. *E*	2231.5	5552.5	81	90	<0.001
C vs. *S*	51	235	4	69	0.036

Table 8.11: Output of the Mann-Whitney Rank Sum Test assessed to test for differences in PA_R between functional groups.

Differences in PA_{AR} (i.e., the total amount of parenchyma in the xylem) between angiosperms (*A*) and gymnosperms (*G*), deciduous (*D*) and evergreen (*E*) species, climbers (*C*) and self-supporting (*S*) species, were all significant ($p < 0.05$) (Table 8.12). *A* have a higher PA_{AR} than *G*, *D* have higher PA_{AR} than *E* and *C* have higher PA_{AR} than *S* (Figure 8.12).

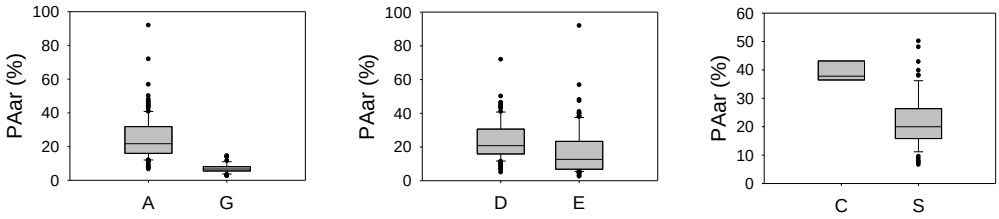

Figure 8.12: Boxplot showing the difference in PA_{AR} between functional groups. Significant difference was found between *A* and *G*, *D* and *E*, *C* and *S*.

	U-stat	T	n(small)	n(big)	p-value
A vs. *G*	172	1603	53	141	<0.001
D vs. *E*	2515.5	10226.5	92	92	<0.001
C vs. *S*	20	266	4	69	0.004

Table 8.12: Output of the Mann-Whitney Rank Sum Test assessed to test for differences in PA_{AR} between functional groups.

Fibres

Differences in F_a (i.e., the overall amount of fibres in the xylem) between climbers (*C*) and self supporting (*S*) species were significant ($p < 0.05$) (Table 8.13). Differences in F_a values between deciduous (*D*) and evergreen (*E*) species were not significant ($p > 0.05$). *C* have lower F_a than *S* (Figure 8.13). No differences in F_a were found between *D* and *E*. As gymnosperms do not have fibres, they were not taken into consideration in this section and the F_a comparison between *A* and *G* was not evaluated.

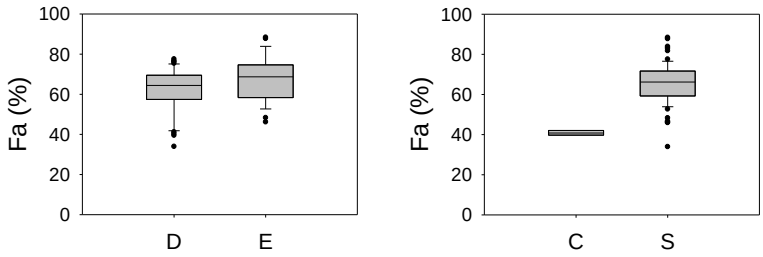

Figure 8.13: Boxplot showing the difference in F_a between functional groups. Significant difference was found between *C* and *S*.

	U-stat	T	n(small)	n(big)	p-value
D vs. *E*	450	1236	29	44	0.067
C vs. *S*	4	14	4	69	0.001

Table 8.13: Output of the Mann-Whitney Rank Sum Test assessed to test for differences in F_a between functional groups.

Conduit size and frequency

Differences in MC_a (i.e., the mean area of xylem conduits) between angiosperms (*A*) and gymnosperms (*G*), deciduous (*D*) and evergreen (*E*) species, climbers (*C*) and self-supporting (*S*) species, were all significant ($p < 0.05$) (Table 8.14). *A* have a higher MC_a than *G*, *D* have higher MC_a than *E* and *C* have higher MC_a than *S* (Figure 8.14). Therefore, *A* have bigger conduits than *G*, *D* have bigger conduits than *E* and *C* have bigger conduits than *S*.

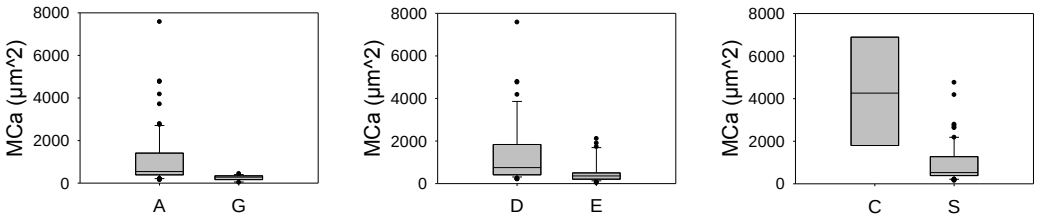

Figure 8.14: Boxplot showing the difference in MC_a between functional groups. Significant difference was found between *A* and *G*, *D* and *E*, *C* and *S*.

	U-stat	T	n(small)	n(big)	p-value
A vs. *G*	127	232	14	74	<0.001
D vs. *E*	390	1056	36	46	<0.001
C vs. *S*	21	269	4	70	0.005

Table 8.14: Output of the Mann-Whitney Rank Sum Test assessed to test for differences in MC_a between functional groups.

Differences in C_d (i.e., the frequency of conduit for a given wood area) between angiosperms (*A*) and gymnosperms (*G*), deciduous (*D*) and evergreen (*E*) species, climbers (*C*) and self-supporting (*S*) species, were all significant ($p < 0.05$) (Table 8.15). *A* have lower C_d than *G*, *D* have lower C_d than *E* and *C* have lower C_d than *S* (Figure 8.15). Therefore, *A* have less conduits per unit area than *G*, *D* have less conduits per unit area than *E* and *C* have less conduits per unit area than *S*.

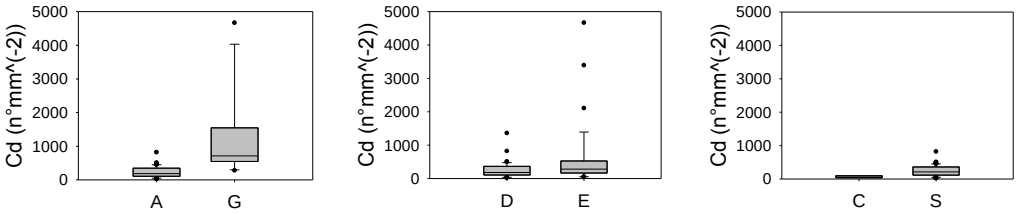

Figure 8.15: Boxplot showing the difference in C_d between functional groups. Significant difference was found between *A* and *G*, *D* and *E*, *C* and *S*.

	U-stat	T	n(small)	n(big)	p-value
A vs. *G*	50	1091	14	74	<0.001
D vs. *E*	597	1725	36	46	0.031
C vs. *S*	35	45	4	70	0.012

Table 8.15: Output of the Mann-Whitney Rank Sum Test assessed to test for differences in C_d between functional groups.

Xylem specific hydraulic conductivity

Differences in K_s (i.e., the overall conductivity of wood vascular elements in the xylem) between angiosperms (*A*) and gymnosperms (*G*), deciduous (*D*) and evergreen (*E*) species, climbers (*C*) and self-supporting (*S*) species, were all

significant ($p < 0.05$) (Table 8.16). *A* have a higher K_s than *G*, *D* have higher K_s than *E* and *C* have higher K_s than *S* (Figure 8.16). Therefore, *A* have a more efficient water transport system than *G*, *D* have a more efficient water transport system than *E* and *C* have a more efficient water transport system than *S*.

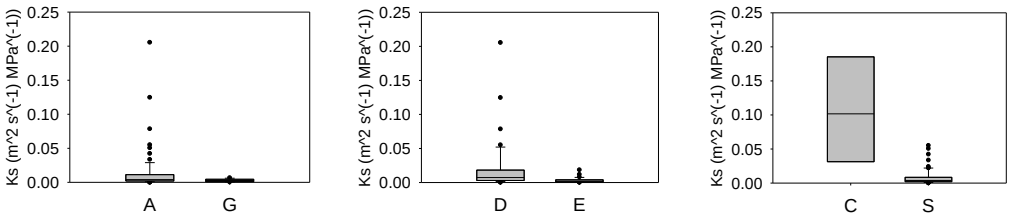

Figure 8.16: Boxplot showing the difference in K_s between functional groups. Significant difference was found between *A* and *G*, *B*, *D* and *E*, *C* and *S*.

	U-stat	T	n(small)	n(big)	p-value
A vs. *G*	127	232	14	74	<0.001
D vs. *E*	349	1015	36	46	<0.001
C vs. *S*	10	280	4	70	0.002

Table 8.16: Output of the Mann-Whitney Rank Sum Test assessed to test for differences in K_s between functional groups.